S-palmitoylation as a Regulatory Mechanism for Localization and Function of Neuronal Substrates Involved in Action Potential Initiation and Propagation

by

Julie Philippe Gupta

A dissertation submitted in partial fulfillment
of the requirements for the degree of
Doctor of Philosophy
(Pharmacology)
in the University of Michigan
2021

Doctoral Committee:

Assistant Professor Paul M. Jenkins, Chair
Assistant Professor Matthew Brody
Professor Yoichi Osawa
Professor Carole Parent
Professor Manoj Puthenveedu
Professor Kristen Verhey

Julie P. Gupta

jumariep@umich.edu

ORCID iD: 0000-0002-3517-4284

Dedication

To my beloved grandfather, Yves VENEC—you are my whole world.

Acknowledgements

First, I would like to thank my mentor, Dr. Paul Jenkins for believing in me throughout the last five years. Thank you Paul for sharing your scientific expertise and love of science, for instilling in me the importance of doing good science, and for always making lab a fun and productive environment. Most importantly, thank you for giving the space to explore my "other" passions through my career development work and science outreach and for always accepting that I didn't need to fit the mold to positively contribute to our dynamic pharmacology community. You always trusted I could handle my research while diving into other passions and you never held me back, something I will forever be grateful for. I am also thankful for the very genuine friendship we developed over the years. I would also like to thank additional members of my thesis committee: Drs. Manoj Puthenveedu, Carole Parent, Yoichi Osawa, Matthew Brody, and Kristen Verhey. The insight and advice you all provided during committee meetings steered my thesis project in the right direction and I am grateful for your commitments to help my project progress as well as help me progress as a scientist. You all showed incredible care and kindness, and helped me persevere through a technically difficult project. Special thanks to Dr. Carole Parent, who patiently sat through multiple individual meetings to listen and provide critical feedback that helped me reach this day. Carole, your unwavering dedication to help me advance over the years made every bit of difference, thank you.

I would also like to thank Dr. Matthew Brody for supporting me through all things palmitoylation-related. Thank you Matt for answering every question, no matter how small, no matter how silly, at any hour of the day; I am so grateful for your willingness to share your expertise, your reagents, and your passion for palmitoylation, and for letting me contribute to your journal clubs and your lab's written work. Next, I would like to thank all current and previous members of the Jenkins lab. To my two very special friends, Dr. Andrew Nelson and Amanda France, you both have impacted my life both as a scientist and as a person in more ways than I can describe. Thank you Andrew for fostering the kind and supportive environment that lead me to join this lab, and for your support even beyond your time in the Jenkins lab. Your passion for science inspired me and kept me motivated every day of graduate school. Amanda, thank you for your unconditional support and for your genuine friendship. I'm not sure how I got so lucky to meet you, but I count my blessings every day for you. Thank you for always being there, for the small things and the big things. Whether it was to talk through a failed experiment or to unpack the state of the world, I couldn't have reached this day without you by my side. Your presence in the Jenkins lab is thoroughly missed.

I would also like to thank the many collaborators who included me in their own work. To Dr. Alexandra Bouza, thank you for letting me contribute to the β1 palmitoylation chapter, it was a labor of love and the most fun and productive collaboration I have ever had the honor of contributing to. Thank you also for your friendship each and every day, I can't wait to walk our (not yet existent) small dogs in Boston Commons. Thank you to the numerous scientists on the β1 palmitoylation project who made it possible, as well as Dr. Lori Isom, who supported Allie and I through all the ups and downs of this project. I am so proud to have been a part of it. I would

also like to thank Dr. Arun Anantharam for allowing me to contribute to many of his lab's projects concerning synaptotagmin-7's roles in PNS synaptic plasticity. Thank you all for teaching me that science is more fruitful when it is collaborative and for making me feel part of something bigger and more important when given the opportunity to work on a team.

Next, I am incredibly thankful for the Pharmacology community. Thank you to the very dedicated team of administrators who keep the department and the labs running, as well as the trainees balanced and fed. Thank you for your help and support in all aspects of graduate school outside of the lab: Lisa Garber, Josh Daniels, Ingrid Shriner-Ward, Dar-Weia Liao, Chereen Mroz, Dennis Ondreyka, Audrey Morton-Dziekan, and Elizabeth Oxford. Special thanks to Elizabeth Oxford for your support, your friendship, and for letting me contribute to and lead many of the department's career development initiatives over the years. I am so grateful for all of you have done for students since your arrival, you have our best interest in mind and we are so lucky to have you as our advocate. Thank you to Dr. David Jones for putting on the "David show" every day in the lab and making sure we were always laughing even during the hardest days. You always believed in me and always had my back.

I would also like to express my gratitude for the funding sources that have so generously supported my graduate training over the years: the Program in Biomedical Sciences, the Rackham Merit Fellowship, the Bernard Maas Fellowship, the Pharmacological Sciences Training Grant (T-32-GM007767), the Charles W. Edmunds Predoctoral Fellowship, and the Rackham Predoctoral Fellowship, as well as all of the funding to Paul M. Jenkins: NINDS (R21 NS113022-01), Michigan Institute for Clinical & Health Research (MICHR), One Mind Rising Star Award,

and Simons Foundation Autism Research Initiative. I also want to thank the mentors who wrote numerous letters of recommendation on my behalf, which allowed me to receive these prestigious fellowships: Drs. Emily Jutkiewicz and Emily Scott. You both played important roles in my success at Michigan and I am so thankful for your mentorship and guidance over the years.

Special thanks to the community of wonderful professors and trainees I had the chance to meet at the Acylation meetings, who became such great friends over the years. Thank you all for sharing reagents, sharing "palmitoylation tricks", and for being a community I always felt safe and encouraged to present for and be myself at. I am forever indebted to Dr. Will Fuller who shared the world's last 5g of available thiopropyl sepharose beads that allowed me to finish my thesis. The palmitoylation community will always have a special place in my heart.

I would also like to thank my family and friends for their love and support throughout life, especially throughout my graduate training. Special thanks to my incredibly brilliant and caring mom, Laurence Philippe-Venec, who inspired me to become a scientist and has given me all the resources, love, strength, courage, and support a daughter could ever need. Maman, you moved us 6000 miles away to give us a better life and there is not a day I am not thankful for your sacrifices. To my sister Marion Philippe, who cheers me on every day with compassion and understanding, I cannot thank you enough for always believing in me more than I believe in myself, and thank you for never failing to show it through your actions. You are my source of inspiration and you have a heart of gold. To my beloved grandparents, Yves and Marie-France Venec, thank you for raising us to be good and work hard and love each other, you instilled in us the importance of finding passion and meaning in our work, and I wish you were here to see the

fruits of those lessons. To my parents-in-law, Utpal Gupta and Jaya Gautam, thank you for warmly welcoming me into your family and always treating me as if I was your own daughter. Your support during this time has been unwavering and I am so grateful to have role models like you to look up to and draw inspiration from. To my very best friend Andrea Pesch, there isn't anyone else I would want to go through graduate school with and I can't thank you enough for your ever constant presence during this time—your humor kept me going through the darkest of days. May we never stop co-leading everything, (over)-eating Indian food, blank slate ice cream, and reveling in each other's bad jokes for the rest of our lives. Finally, to my constant (and forever!) source of brightness, happiness, and understanding, Ankur Gupta, my husband, thank you for coming into my life 10 years ago and never leaving. Thank you for supporting and loving me through every moment, and simply just taking me as I am. Every day is brighter because of you.

Finally, I would like to thank every person who has ever partaken in my journey as an immigrant— 18 years ago, I stepped off the plane not knowing a single word of English. To the village of selfless and dedicated educators, mentors, and friends who helped me learn English, assimilate into the American culture, graduate from college as a first generation American, earn a PhD, and became my family away from my home country, thank you. Thank you for letting me experience the true American dream, I am forever indebted.

Table of Contents

List of Figures

Abstract

S-palmitoylation, the covalent addition of a 16-carbon fatty acid to cysteine residues of proteins, anchors proteins to membrane domains to regulate protein localization, trafficking, stability, and function, and plays broad roles in promoting, facilitating, and fine-tuning critical neuronal processes such as development, synaptic plasticity, axonal growth, dendritogenesis, neuronal transmission, and neuronal excitability. Understanding the role of palmitoylation for neuronal substrate function provides important insight into how normal processes may be regulated and in turn how pathophysiological processes may arise when palmitoylation goes awry. The goal of this thesis work was to explore the role of *S*-palmitoylation for proper localization, stability, and functions of two neuronal proteins, the voltage-gated sodium channel (VGSC) β1 subunit and ankyrin-B, both previously unknown to be palmitoylated but highly associated with neurological diseases such as Early Infantile-Developmental and Epileptic Encephalopathy (EIEE52) and autism spectrum disorder (ASD), respectively.

VGSC β1 subunits are multifunctional proteins that canonically modulate VGSC α subunit biophysical properties and cell surface localization, while also participating in cell-cell and cell-matrix adhesion, necessary for intracellular signal transduction, cell migration, and differentiation. Recently, VGSC β1 subunits were also shown to undergo proteolytic cleavage to generate a β1 intracellular C-terminal domain that translocates to the nucleus and participates in transcriptional regulation, a potentially important mechanism underlying EIEE52. However, the mechanisms that

regulate proteolysis of β1 were unknown. We demonstrate in this work that β1 subunit palmitoylation regulates β1 cell surface localization and subsequent β1 proteolytic cleavage at the plasma membrane of heterologous cells. This work provides important insight into a regulatory mechanism that regulates β1 cleavage, which has important consequences for downstream cellular excitability via alterations in gene transcription.

Ankyrins act as general adaptor proteins that localize membrane, cytoskeletal, and cytoplasmic proteins at specialized membrane domains, and promote cell polarity and function in many vertebrate tissues. One ankyrin family member, ankyrin-B, has recently been found to scaffold VGSC $Na_v1.2$ at the dendritic membrane of cortical pyramidal neurons to promote dendritic excitability and synaptic plasticity. How ankyrin-B itself targets to dendritic membranes to cluster VGSC $Na_v1.2$ there was previously unknown. We show here that ankyrin-B is modified by *S*-palmitoylation, and that palmitoylation of ankyrin-B is required for ankyrin-B localization at dendritic membranes necessary for subsequent Nav1.2 clustering at dendrites. We demonstrate that ankyrin-B palmitoylation is mediated by the palmitoyl acyl transferase enzyme zDHHC17. We also demonstrate that the axonal cargo transport of ankyrin-B is unaffected by palmitoylation, thereby highlighting two pools of ankyrin-B: a dendritic palmitoylation-dependent pool and a vesicular, axonal palmitoylation-independent pool. Targeting palmitoylation could represent an opportunity to specifically target the dendritic pool of ankyrin-B without affecting the axonal pool. These findings reveal an important regulatory mechanism underlying dendritic localization and function of ankyrin-B in neurons, which may have important implications in the etiology of ankyrin-B-associated autism spectrum disorders.

Given that VGSCs, β subunits, and ankyrins form macromolecular complexes essential for proper neuronal activity, and that disruption of any of these members in complex can lead to severe neurological diseases, this work provides a glimpse into a more mechanistic understanding of the regulatory mechanisms underlying proper localization and function of these substrates individually, so that future work can investigate the role palmitoylation plays for the formation and maintenance of ankyrin-B/Nav1.2/β1 macromolecular complexes under normal and pathophysiological conditions.

Chapter 1: General Introduction

(This chapter has been published in *Molecular Membrane Biology*. 2019;35(1): 60-75. doi: 10.1080/09687688.2019.1710274. Review. PMCID: PMC7031816)

Julie M. Philippe and Paul M. Jenkins, PhD

Summary

Protein palmitoylation is a critical posttranslational modification that regulates protein trafficking, localization, stability, sorting, and function. In mammals, addition of this lipid modification onto proteins is mediated by a family of 23 palmitoyl acyltransferases (PATs). PATs often palmitoylate substrates in a promiscuous manner, precluding our understanding of how these enzymes achieve specificity for their substrates. Despite generous efforts to identify consensus motifs defining PAT-substrate specificity, it remains to be determined whether additional factors beyond interaction motifs, such as local palmitoylation, participate in PAT-substrate selection. In this review, we emphasize the role of local palmitoylation, in which substrates are palmitoylated and trapped in the same subcellular compartments as their PATs, as a mechanism of enzyme-substrate specificity. We focus here on non-Golgi-localized PATs, as physical proximity to their substrates enables them to engage in local palmitoylation, compared to Golgi PATs, which often direct trafficking of their substrates elsewhere. PAT subcellular localization may be an under-recognized, yet important determinant of PAT-substrate specificity that may work in conjunction or completely independently of interaction motifs. We also discuss some current hypotheses about

protein motifs that contribute to localization of non-Golgi-localized PATs, important for the downstream targeting of their substrates.

Introduction

Lipid modifications facilitate sorting of both soluble and transmembrane proteins to specialized membrane domains [1, 2]. Normal signaling relies on the proper localization of lipid-modified substrates to discrete microenvironments, necessary for the formation, maintenance, and function of polarized cells [1-3]. For example, neurons rely heavily on the precise and regulated localization of proteins within axonal and dendritic membrane compartments. The polarized distribution of proteins within neuronal domains promotes axonal growth, anterograde and retrograde signaling, synaptic transmission, and proper neuronal excitability and synchronization. Similarly, cardiomyocytes depend on the proper organization of specific proteins along intercalated discs and T-tubules to ensure normal cell-to-cell communication and cardiac contractility. Epithelial cells rely on their polarized membranes to enable the directional transport of solutes, a process integral for their ability to absorb, secrete, and protect the intestinal lining. This asymmetrical, but precise organization of proteins within membrane domains is critical for normal physiological function of many diverse cell types, and more broadly contributes to the formation and synchronization of whole mammalian organs. Not surprisingly, many of these neuronal, cardiac, and epithelial proteins are lipidated to achieve proper targeting to specialized microdomains, necessary for downstream interactions and function.

One type of lipid modification is *S*-palmitoylation, which anchors proteins to specialized membrane domains. *S*-palmitoylation is a reversible lipid modification, acting as a dynamic molecular 'switch' to modulate protein functionality and physiological pathways within the cell. *S*-palmitoylation is predominantly characterized by the covalent addition of a 16-carbon fatty acid,

palmitate, onto cysteine residues of proteins. This dynamic lipid modification is mediated by a large family of 23 palmitoyl acyl transferases (PATs), which all share a core aspartate-histidine-histidine-cysteine (zDHHC) motif within the active site of the enzyme, located between transmembrane 2 and 3 [4, 5]. The highly conserved zDHHC motif is a cysteine rich domain (CR), which consists of ~50 amino acids, whose structure is a variant of the Cys4 zinc-finger-like metal ion binding site, followed by a complex Cys-His region [6, 7]. This CR domain contains the catalytic site of zDHHC proteins [6]. PATs have 4-6 transmembrane domains, with the N- and C-terminal regions and the zDHHC-CR domain oriented toward the cytoplasm, as determined by the transmembrane topology of the yeast PAT Akr1p [8].

A diverse set of transmembrane and soluble proteins are *S*-palmitoylated, to promote membrane targeting, protein-protein interactions, protein folding and stability, sorting, and function [1, 2, 9-12]. In fact, proteomics studies have estimated that over 10% of the proteome is palmitoylated [13, 14]. A number of palmitoylated proteins have been associated with numerous pathologies such as cancer, bacterial and viral infections, neurodegenerative diseases, intellectual disability, as well as neuropsychiatric diseases [13, 15-22]. Understanding basic mechanisms underlying protein palmitoylation and how palmitoylation mechanisms may become aberrant in disease may shed light on disease etiology.

Groundbreaking studies identified seven yeast zDHHC PATs and twenty-three mammalian zDHHC PATs, which palmitoylate yeast and mammalian proteins, respectively [23]. Although some PATs exhibit substrate specificity, the promiscuity and functional redundancy amongst the yeast and mammalian PATs have complicated our understanding of PAT-substrate specificity.

Studies in *Saccharomyces cerevisiae* identified Akr1 and Erf2p as PATs for casein kinase Yck2 and small GTPase Ras2, respectively [24-27], representing important single enzyme-substrate pairs. The yeast SNARE Tlg1 is palmitoylated by Swf1 [28], while Pf4a was shown to palmitoylate the yeast chitin synthase Chs3 [29]. In contrast, the guanine nucleotide-binding protein alpha-2 subunit Gpa2 is capable of being palmitoylated by four yeast proteins, Akr1, Pfa5, Pfa3, and Erf2, suggesting significant functional redundancy and substrate overlap between yeast PATs [30]. Similarly, the yeast vacuolar fusion factor Vac8 is palmitoylated predominantly by Pfa3 [31, 32], but can also be palmitoylated by Erf2, Pfa4, Pfa5, and Akr1 [33]. Individual deletion of Pfa3, Erf2, Pfa4, Pfa5, or Akr1 in yeast does not affect Vac8 localization, which is an important function of Vac8 palmitoylation. Only simultaneous genetic deletion of all five yeast PATs results in loss of Vac8 palmitoylation and mis-localization of Vac8, highlighting the overlapping substrate recognition by these yeast PATs [33]. Functional redundancy is also seen with mammalian PATs, such that depletion of a single PAT often results in residual levels of substrate palmitoylation. A common example is the scaffolding protein PSD95, whose palmitoylation is mediated by zDHHC-2, -3, -7, and -15 to regulate AMPAR integration and stability at the excitatory post-synaptic membrane [34, 35]. A dominant-negative designed against zDHHC2 and zDHHC15 inhibited only 40% of PSD95 palmitoylation, suggesting that residual PSD95 palmitoylation is mediated by its remaining PATs [36]. The stress-regulated exon (STREX) splice variant of large conductance calcium- and voltage-activated potassium (BK) channel is palmitoylated by zDHHC-3, -5, -7, -9, and -17 to govern STREX plasma-membrane association and determine channel regulation by protein kinase A phosphorylation [37]. Silencing zDHHC-3, -5, -7, -9, and -17 individually by siRNA resulted in significant reduction in STREX palmitoylation, but did not completely abolish STREX palmitoylation, highlighting PAT functional redundancy [37]. Similarly, endothelial nitric

oxide (eNOS), whose palmitoylation is critical for its subcellular targeting and nitric oxide production, is palmitoylated by zDHHC-2, -3, -7, -8, and -21 [38]. Individual knockdown of *ZDHHC21* only reduces [H]^3-palmitate incorporation into eNOS by 60%, with the remaining 40% of eNOS palmitoylation accounted for by the remaining zDHHC-2,-3,-7, and -8. [38]. Lastly, the scaffolding protein ankyrin-G is palmitoylated by zDHHC5 and zDHHC8 in a functionally redundant manner to achieve its specific targeting and function at the lateral membrane of epithelial cells [39]. These examples highlight only a few of many substrates palmitoylated by multiple PATs [40-43]. These data demonstrate the promiscuity of PATs in their palmitoylation of multiple substrates, as well as the conserved functional redundancy amongst both yeast and mammalian PATs. Although PAT redundancy has been hypothesized to be important for protein regulation at the level of zDHHC activity, it has also complicated the identification of specific substrate-enzyme pairs.

Elegant studies have shown that PAT enzymes exhibit some substrate specificity [42, 44-47], but no consensus sequences have been identified to accurately predict substrate profiles for each PAT. How PATs recognize their respective substrates remains a significant question in the acylation field. There are, however, some established characteristics shared amongst palmitoylated cysteines that likely contribute to a PAT's ability to select its substrate: (a) myristoylation or prenylation sites often flank the palmitoylated cysteine(s), (b) palmitoylated cysteine(s) are often surrounded by basic or hydrophobic amino acids, and (c) palmitoylated cysteine(s) are located in the cytoplasmic regions between or near the transmembrane domains [48]. Thus, regions surrounding the palmitoylated cysteine play important roles for PAT recognition. This is highlighted by Nadolski and Linder, who showed that the yeast vacuolar fusion protein Vac8, which possesses an SH4 domain containing the three palmitoylated cysteines, is predominantly

palmitoylated by Pfa3 *in vitro* [49]. However, isolated SH4 domain from Vac8 tagged to a fluorescent protein (SH4-GFP) is capable of being palmitoylated by all five yeast PATs, consistent with a previous study by Hou *et al* [33, 49]. Thus, the motif containing the palmitoylation site by itself, in this case the SH4 domain, is often not sufficient to confer PAT specificity. This highlights the importance of considering the full protein sequence to identify PAT recognition sequences, which may be distant from the palmitoylated cysteine. For Vac8, it was determined that the 11th armadillo repeat of Vac8 downstream of its SH4 domain contributes to the specific interaction between Pfa3 and Vac8 [49]. Given that PATs may need to interact with their substrates at the catalytic CR domain as well as a docking site further away from the active site, it may be that full length proteins possess multiple contact sites that confer PAT specificity [49]. In contrast, the short fusion protein, Vac8 SH4-GFP, likely only engages with the catalytic DHHC motif present in all PATs, without requiring interaction with any other contact site on the PAT in order to be palmitoylated [49].

Neuronal substrates such as huntingtin also exhibit distinct motifs that confer substrate-enzyme specificity. The mammalian PATs, zDHHC13 and zDHHC17 contain an N-terminal ankyrin repeat domain, which contributes significantly to their specificity for huntingtin. In COS cells, overexpressed huntingtin is a substrate for zDHHC17 and zDHHC13, but not for zDHHC3, a PAT which lacks ankyrin repeats. A chimera in which the ankyrin-repeat domain from zDHHC17 is fused to zDHHC3 allows zDHHC3 to interact with huntingtin and mediates huntingtin palmitoylation [45]. This suggests huntingtin relies on its binding to ankyrin repeats for palmitoylation. Thus, residues distant from the palmitoylation motif can provide important context for enzyme-substrate specificity.

Although there is clear evidence that PAT-substrate specificity is partially governed by the amino acid sequence flanking the palmitoylated cysteine [44, 46, 50, 51], some data argues a stochastic palmitoylation model, in which palmitoylation is governed by the accessibility of cysteine residues of membrane proteins located at a certain depth in the inner leaflet of the membrane, rather than by the local sequence motif [52]. The study demonstrates that genetically introduced cysteine residues in membrane proteins, even in prokaryotic membrane proteins, which are not usually palmitoylated, undergo generic palmitoylation so long as the cysteine residue is accessible to the catalytic center of the PAT, suggesting a lack of specificity for *S*-palmitoylation [52]. Although this model has yet to be studied in proteins in their native environment, it highlights the complexity underlying PAT-substrate recognition and palmitoylation dynamics that the acylation field is attempting to unravel. Nevertheless, this study reveals the importance of physical proximity between the PAT and its substrate, which in itself may be its own contributor of specificity.

A recent review by Ernst *et al* demonstrated the importance of accounting for the spatial context of PATs, specifically PAT localization within distinct Golgi domains, to better understand anterograde sorting of specific substrates en route to the cell surface [53]. With this in mind, we investigate in this review the possibility that PAT spatial context, or PAT subcellular localization, governs substrate targeting following substrate palmitoylation **(Figure 1.1).** We focus here on non-Golgi-localized PATs, as the localization of their substrates is often determined by the localization of their PATs **(Figure 1.1).** This hypothesis, known as local palmitoylation, in which substrates are palmitoylated and specifically targeted to the *same* subcellular compartments as that of their respective PATs, may be an important determinant of specificity between non-Golgi-localized PATs and their substrates [36, 54]. PAT subcellular localization and local palmitoylation of their

substrates may be an under-recognized, yet important predictor of substrate profiles and localization.

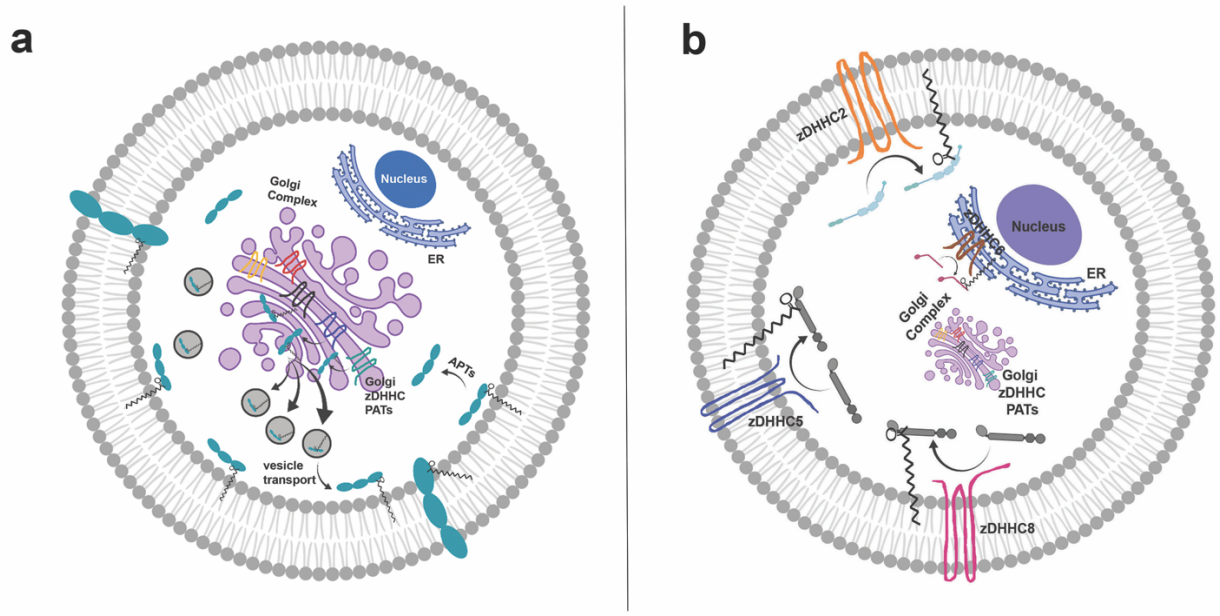

Figure 1.1. Palmitoylation and subcellular trafficking.

A. Golgi-targeted zDHHC PATs mediate the palmitoylation of substrates for substrate stabilization at Golgi membranes prior to their packaging into vesicles and forward-trafficking to the plasma membrane. **B.** Three main zDHHC PATs, zDHHC2, zDHHC5, and zDHHC8, are active PATs targeted to the plasma membrane (PM), while zDHHC6 is an active PAT present on ER membranes. These non-Golgi PATs are appropriately positioned to palmitoylate substrates locally, and govern substrate targeting to these same membranes. The precise localization of non-Golgi PATs is critical for the proper non-Golgi-membrane localization of their substrates following palmitoylation, and may be an important predictor of PAT-substrate specificity. Created with BioRender.com

Golgi-localized PATs promote the palmitoylation and forward trafficking of substrates to the plasma membrane.

In their important study investigating the subcellular localization of each individual zDHHC PAT by overexpression, Ohno *et al* observed that the majority of PATs localized exclusively to the Golgi [55]. Canonically, the Golgi is recognized as one of the main sorting centers of the secretory pathway [56]. Most palmitoylated substrates are first palmitoylated at the Golgi and are subsequently trafficked to other subcellular compartments, including the plasma membrane (PM) **(Figure 1.1)**. Recently, Ernst *et al.* demonstrated that protein palmitoylation promotes anterograde transport of proteins from the Golgi to the PM [57]. Addition of a palmitate onto proteins, mediated by PATs, promotes proteins' affinity for the highly curved cisternal regions of the Golgi membrane lipid bilayer, where transport occurs, thereby facilitating vesicle budding, sorting, and anterograde trafficking of substrates to the PM [57]. An elegant study by Rocks *et al* highlighted the role of Golgi-localized palmitoylation in directing anterograde trafficking of Ras to the PM [58]. Palmitoylation of farnesylated HRas and NRas in the Golgi targets Ras to the PM. Subsequent de-palmitoylation at the PM drives retrograde trafficking of HRas and NRas back to the Golgi, where Ras can be re-palmitoylated. These palmitoylation/depalmitoylation cycles tightly regulate Ras localization and sorting, as well as fine-tune Ras-dependent signaling [58]. Ras is palmitoylated by Golgi-localized zDHHC9-GCP16 [59]. The precise Golgi localization of zDHHC9 is likely beneficial for direct palmitoylation and subsequent stabilization of Ras at Golgi membranes, before Ras is packaged and trafficked to the PM.

Additionally, palmitoylation of GABA-synthesizing enzyme GAD65 is critical for proper trafficking of GAD65 from Golgi membranes to presynaptic clusters in axon termini [60]. Although palmitoylation is not necessary for membrane anchoring of GAD65, palmitoylation promotes sorting of GAD65 to the trans-Golgi network en route to axonal pre-synaptic membranes [61]. GAD65 palmitoylation is mediated by Golgi-localized zDHHC17, a Golgi-PAT well positioned to palmitoylate and stabilize GAD65 in the Golgi as it makes its way to the pre-synaptic membrane surface [62]. Additionally, Golgi-localized PATs such as zDHHC3, -7, and -17 have been shown to enhance endomembrane association of SNARE proteins SNAP25/23, to promote their trafficking to and function at the PM [41]. Given that Golgi localization of Golgi PAT enzymes play a critical role for Golgi-to-PM protein sorting, it is perhaps unsurprising that many zDHHC PATs reside in the Golgi [39, 55, 57, 63, 64] **(Figure 1.1).** However, in these cases the majority of their substrates are trafficked *away* from the subcellular compartment housing the Golgi PAT.

Plasma membrane PATs mediate local palmitoylation and drive PM-localization of their substrates.

Many studies have demonstrated that active PATs also exist in non-Golgi subcellular compartments, including the PM [39, 55, 65-67] **(Figure 1.1)**. In some cases, proteins are palmitoylated first at the Golgi and further palmitoylated in post-Golgi compartments for enhanced regulation and signaling. In other cases, substrates bypass Golgi palmitoylation and undergo palmitoylation in compartments independent of the Golgi to achieve their final destination [39]. In

either case, localization of the relevant PAT seems to play an important role in the ultimate localization of the target protein.

For example, two evolutionarily-related and functionally redundant zDHHC PATs, zDHHC5 and zDHHC8, were shown to localize to the PM in HEK293T cells and in polarized epithelial cells [39, 55], and to synaptic membranes in neurons [65, 66]. In hippocampal neurons, zDHHC8 was targeted to the synapse, while zDHHC5 predominantly targeted to dendritic shafts with occasional immunofluorescence signal detected in dendritic spines [66]. Although Thomas *et al* observed zDHHC5 only at dendritic shafts, Brigidi *et al* have observed zDHHC5 at postsynaptic membranes, likely due to application of pharmacological agents that induce changes in neuronal activity and result in re-localization of zDHHC5 to different neuronal domains, as well as different time-scales of detection [65, 66]. Nevertheless, the unique localization of zDHHC5 and zDHHC8 within neuronal dendritic domains likely contributes to the localization of their substrates following palmitoylation. Indeed, GRIP1b, a known substrate of zDHHC5, co-localizes with zDHHC5 in dendritic puncta in neurons [66]. Importantly, GRIP1b palmitoylation and localization at dendritic shafts is dependent on both expression as well as proper localization of zDHHC5 at dendritic shafts [66]. More specifically, zDHHC5-mediated palmitoylation of GRIP1b targets it to dendritic recycling endosomes (REs), where GRIP1b is able to bind to kinesin motor protein KIF5 to mediate the proper trafficking and recycling of GluA2 subunits of α-amino-3-hydroxy-5-methyl-4-isoxazolepropionic acid receptors (AMPARs) [68] **(Figure 1.2)**. Real-time tracking of zDHHC5 demonstrated that zDHHC5 moves on REs as it cycles from dendritic shafts to dendritic spines to palmitoylate its substrates [65], suggesting zDHHC5 may be locally palmitoylating GRIP1b at REs within dendritic shafts **(Figure 1.2)**. Although GRIP1b is predominantly palmitoylated by zDHHC5, it can also be palmitoylated by zDHHC8, albeit to a smaller degree

since an shRNA specific to *Zdhhc8* only slightly reduced GRIP1b palmitoylation in neurons [66]. Given that zDHHC8 is predominantly localized to dendritic spines, while GRIP1b and zDHHC5 are both predominantly localized to dendritic shafts, including dendritic endosomes, zDHHC5 is judiciously positioned to locally palmitoylate and drive GRIP1b targeting.

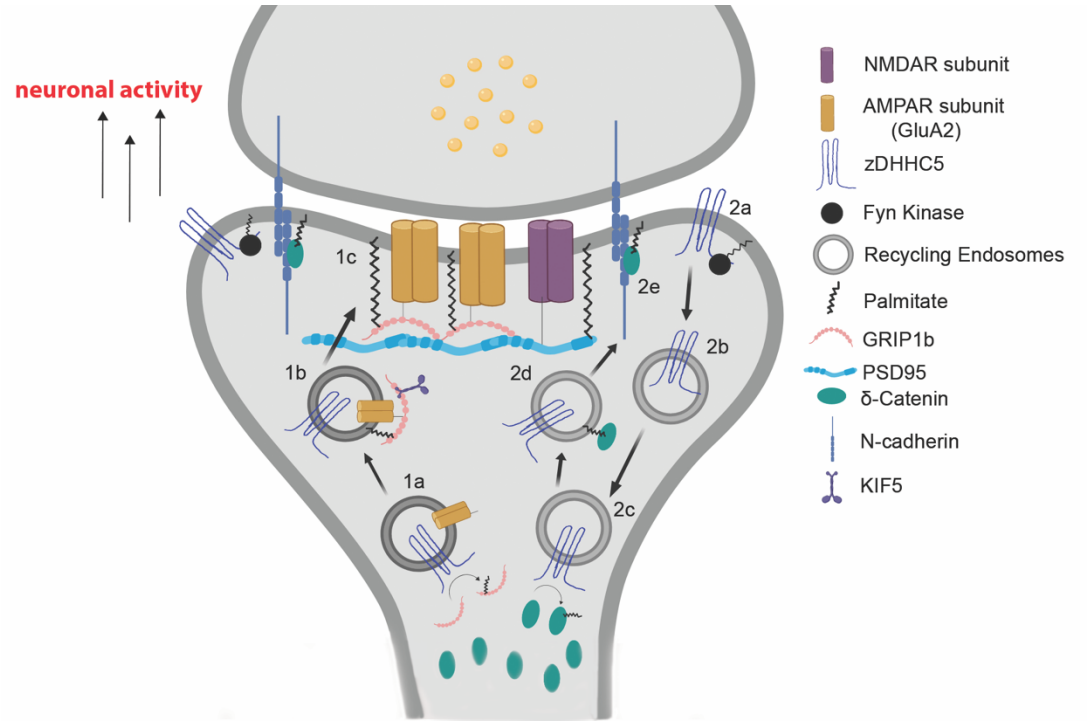

Figure 1.2. Neuronal activity-regulated translocation of zDHHC5 for local palmitoylation of its synaptic substrates

1A. zDHHC5 cycles from the dendritic shaft to dendritic spines on recycling endosomes (REs) to palmitoylate GRIP1b. **1B.** Palmitoylation of GRIP1b by RE-localized zDHHC5 targets GRIP1b to REs to enable GRIP1b binding to KIF5, which mediates the proper trafficking and stabilization of AMPAR GluA2 subunits to the PM **(1C)**. **2A.** Under basal conditions, zDHHC5 is stabilized at the post-synaptic membrane through Fyn-mediated phosphorylation, which prevents its association with endocytic machinery. **2B.** Upon increase in neuronal activity, zDHHC5 translocates from the post-synaptic membrane to dendritic shafts on REs to recruit its substrates. **2C.** Once arrived at the shaft, zDHHC5 palmitoylates its substrate δ-catenin. **2D.** Palmitoylated δ-catenin is trafficked to the post-synaptic membrane on REs with zDHHC5. **2E.** Palmitoylation-dependent δ-catenin recruitment at post-synaptic membranes binds and stabilizes N-cadherin, leading to enhanced synaptic plasticity. Created with BioRender.com

Synaptically-targeted zDHHC8 in the neuron is also appropriately positioned to palmitoylate its synaptic substrates in order to promote synaptic transmission and plasticity. Some groups have reported that zDHHC8 resides in vesicle-like clusters along the dendritic shafts in developing hippocampal neurons [15], while other groups only detect zDHHC8 at dendritic spines [66], perhaps due to species differences or different culture conditions. However, evidence demonstrating that overexpression of zDHHC8 increases spine density and spine stability supports zDHHC8 localization at dendritic spines, at least under overexpression conditions [69]. Synaptically-localized zDHHC8 enables the palmitoylation of the synaptic substrate cdc42. Cdc42 localization in dendritic spines is dependent on its palmitoylation, mediated by the synaptic PAT zDHHC8 [69]. The regulator of GluA trafficking PICK1 is also a substrate for zDHHC8. zDHHC8-mediated palmitoylation of PICK1 allows for proper cerebellar long-term depression (LTD) induction, a process that occurs in dendritic spines [70]. Synaptic targeting of zDHHC8 must confer some specificity for its synaptic substrates like PICK1, since zDHHC5, which is not predominantly localized to dendritic spines, did not mediate the palmitoylation of PICK1, despite the presence of the PDZ-binding motif in zDHHC5 and zDHHC8 and the PDZ-containing domain in PICK1 [70].

zDHHC5 and zDHHC8 have been shown to be functionally redundant in polarized epithelial cells, likely due to their overlapping localization at the lateral membrane. Ankyrin-G is a known substrate of both zDHHC5 and zDHHC8 in polarized epithelial cells. Of the 23 mammalian PATs, only zDHHC5 and zDHHC8 are specifically localized to the lateral membrane in epithelial cells, where they palmitoylate ankyrin-G to drive its targeting to the lateral membrane [39]. Proper lateral membrane targeting of ankyrin-G is required for ankyrin-G's ability to build

this membrane through recruitment and scaffolding of important binding partners, such as E-cadherin and βII-spectrin [39, 71, 72].

Another zDHHC5 substrate which relies on local palmitoylation is the sodium pump regulator phospholemman (PLM). PLM is known to accelerate massive endocytosis (MEND), a process of massive cell surface membrane endocytosis after calcium overload and reperfusion of anoxic cardiac muscle [73]. PLM is a substrate of zDHHC5 [67]. PLM palmitoylation inhibits the sodium pump, which has important implications for calcium homeostasis and cardiac contractility [74]. Interestingly, both zDHHC5 and PLM associate by co-immunoprecipitation and localize to caveolin-enriched microdomains at the PM of rat ventricular cardiomyocytes, supporting local palmitoylation of PLM by zDHHC5 at the PM [67]. Although zDHHC2 is also reported to be targeted to the cell surface of cardiac myocytes, it did not associate with PLM, which does not preclude the possibility that zDHHC2 may be capable of palmitoylating PLM [67]. A study demonstrated co-expression of zDHHC5 and zDHHC2 in a human fibroblast-derived cardiac myocyte cell line decreases sodium pump currents, implying increased palmitoylation of PLM, mediated by overexpressed zDHHC2 and zDHHC5. In contrast, dual knockdown of zDHHC2 and zDHHC5 resulted in a 90% increase in sodium pump currents, likely contributed to by loss of PLM palmitoylation as well as reduced MEND, which would recapitulate the ablated MEND phenotype observed in zDHHC5-knockout hearts [73]. These data would suggest zDHHC2 may also be capable of palmitoylating PLM. This is supported by demonstration that dual zDHHC2 and zDHHC5 expression as well as dual knockdown resulted in a significantly greater effect on sodium pump currents, compared to expression or knockdown of zDHHC5 alone [73]. The subcellular localization of the only two known PM-localized zDHHC PATs in cardiac myocytes, zDHHC2 and zDHHC5, is likely critical for specificity towards PLM, whose final destination is also the

PM. PLM palmitoylation affects PLM function, but does not affect its ability to associate with the cell surface [67]. Given that PLM is already cell-surface localized prior to its palmitoylation, having a PM-localized PAT like zDHHC5 or zDHHC2 in proximity to mediate local PLM palmitoylation may be favorable.

In neurons, zDHHC2 localizes to mobile dendritic vesicles, as well as the post-synaptic density (PSD) [35, 36, 54, 75] **(Figure 1.3)**. zDHHC2 palmitoylates PSD95, the critical scaffolding protein in the excitatory post-synaptic density (PSD) and regulator of synaptic strength and plasticity [76]. While Golgi-localized zDHHC3 and zDHHC15 palmitoylate PSD95 at the Golgi to promote its membrane trafficking, it is PSD-residing zDHHC2 that palmitoylates and targets PSD95 directly at the PSD, which is required for PSD95-scaffolding of AMPARs and NMDARs at the PSD [35] **(Figure 1.3)**. Given that zDHHC2 is localized to the PSD and that PSD95 must interact with zDHHC2 to be palmitoylated [35], PSD95 likely undergoes local palmitoylation at the PSD. Fukata *et al* also demonstrated that zDHHC2 puncta co-localize with an antibody that specifically recognizes palmitoylated PDS95 at postsynaptic regions in cultured neurons, providing additional rationale for local palmitoylation of PSD95 at postsynaptic membranes, to generate "PSD95 nanodomains" [54]. These data highlight the importance of proper zDHHC2 localization at the PSD for proper PSD95 palmitoylation and localization at the PSD, critical for the regulation of synaptic strength and plasticity **(Figure 1.3)**.

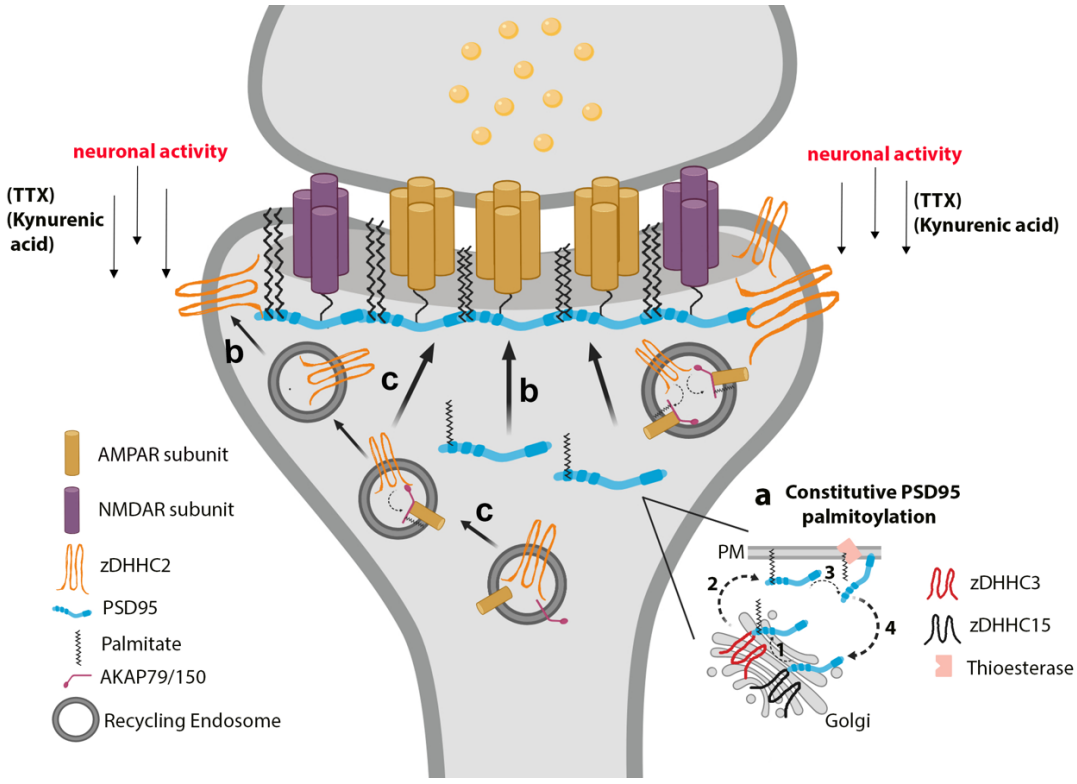

Figure 1.3. RE- and PSD-localized zDHHC2 locally palmitoylates and targets synaptic substrates to REs and the PSD.

A. PSD95 is constitutively palmitoylated by Golgi-localized zDHHC3 and zDHHC15, which promotes its forward trafficking to the PM. A thioesterase depalmitoylates PSD95 to drive its retrograde trafficking back to the Golgi. **B.** Under conditions of decreased neuronal activity, REs containing zDHHC2 deliver zDHHC2 to the PSD. PSD-localized zDHHC2 then interacts with PSD95 to palmitoylate and target PSD95 to the PSD. **C.** RE-localized zDHHC2 mediates the palmitoylation of AKAP79/150, to promote the proper delivery of AMPARs at the post-synaptic membrane during LTP. Created with BioRender.com

Plasma membrane PATs sense synaptic activity to drive their localization and substrate localization to specific subcellular compartments.

If proper surface membrane targeting of non-Golgi PATs determines their substrate's localization, then understanding how these PATs reach their sites of physiological function may highlight how substrates are selected and where substrates are localized. Some mechanisms regulating the cellular targeting of non-Golgi-associated PATs have been studied. One observed mechanism is the activity-sensing abilities of PATs, such as zDHHC2 and zDHHC5, which govern their specific subcellular localization in response to changing neuronal activity. Noritake *et al* demonstrated that zDHHC2 is activity-regulated in the brain: zDHHC2 translocates near the plasma membrane on dendritic vesicles upon decrease in neuronal activity, to increase palmitoylation, localization, and function of its synaptic substrates and maintain synaptic homeostasis [36, 77]. TIRF microscopy studies demonstrated zDHHC2 rapidly approaches the postsynaptic membrane in response to reduced neuronal activity by kynurenic acid or the voltage-gated sodium channel blocker tetrodotoxin, to increase the palmitoylation and synaptic accumulation of PSD95 at the PSD [36] **(Figure 1.3)**. Whether zDHHC2-containing vesicles fuse with the membrane or remains intracellular in neurons is unknown. In neuroendocrine PC12 cells, zDHHC2 cycles from recycling endosomes (REs) to the plasma membrane. Fluorescence recovery after photo-bleaching (FRAP) analysis of PC12 cells expressing HA-tagged zDHHC2 shows that zDHHC2 integrates into the plasma membrane, to regulate PSD95 palmitoylation at the PSD [75]. This is not due to increased enzymatic zDHHC2 activity, but rather from dynamic cycling of zDHHC2 between the PM and Rab11-recycling endosomes [75]. Thus, translocation of zDHHC2

between different subcellular compartments in response to activity is not restricted to neuronal cells, and likely contributes to mechanisms of local palmitoylation.

Given that zDHHC2 targeting to the plasma membrane has important implications for PSD95 palmitoylation, PSD formation and integrity, and synaptic strengthening, it would be expected that zDHHC2 targeting to REs would also have important physiological significance. Indeed, zDHHC2 localization at REs enables zDHHC2-mediated palmitoylation and localization of A-kinase anchoring protein (AKAP79/150) in REs [78-80] **(Figure 1.3)**. During long-term synaptic potentiation (LTP), or synapse strengthening, REs within dendritic spines carry synaptic cargo, such as AMPA receptors, and deliver them at synapses through RE exocytosis [81, 82] **(Figure 1.3)**. AKAP79/150 facilitates LTP/LTD signaling by regulating the phosphorylation, exocytosis, trafficking, and activity of AMPARs within REs [79, 83-86]. zDHHC2-mediated palmitoylation of AKAP79/150 is required for its function in regulating dendritic RE exocytosis of AMPA receptors and AMPA receptor-dependent synaptic potentiation [87] **(Figure 1.3)**. Consistent with local palmitoylation, zDHHC2 colocalizes with AKAP79/150 in dendritic REs of cultured hippocampal neurons, revealing that zDHHC2 is well positioned to palmitoylate AKAP79/150 in this specific compartment [87]. AMPARs themselves are palmitoylated [88]. Thus far, only Golgi-localized zDHHC3 has been shown to mediate palmitoylation of AMPA receptor subunits [88]. Whether zDHHC2 can palmitoylate AMPA receptors remains to be determined. Given that AMPARs and zDHHC2 cycle between the PM and REs, it may be that AMPA receptors cycle in conjunction with zDHHC2 cycling, in response to LTD/LTP, to regulate synaptic transmission.

Specific zDHHC5 localization is also highly driven by synaptic activity, which has important implications for dynamic localization of its substrates. At baseline, zDHHC5 resides in

dendritic spines of cultured hippocampal neurons, but cycles between postsynaptic membranes and dendritic shafts on recycling endosomes (REs) in an activity-dependent manner. Following a protocol of chemical LTP (cLTP), zDHHC5 moves from spines to dendritic shafts to recruit and palmitoylate δ-catenin, before translocating and trafficking both itself and palmitoylated δ-catenin back into spines on REs [65]. Palmitoylation-dependent δ-catenin recruitment in spines is critical for insertion and stabilization of AMPA receptors into the PSD and synaptic plasticity [65, 89] **(Figure 1.2)**. Thus, activity-driven translocation of zDHHC5 to dendritic shafts permits the local palmitoylation of δ-catenin in the dendritic shaft before both proteins cycle back into the spine to enhance synaptic strength and plasticity. This activity-dependent trafficking of zDHHC5 between dendritic spines and shafts is thought to depend on phosphorylation. Under baseline conditions, zDHHC5 is maintained at spine plasma membranes through tyrosine phosphorylation by Fyn kinase within a YxxL motif, thereby rendering zDHHC5 unable to associate with the endocytosis machinery. Upon cLTP activation, Fyn-mediated phosphorylation of zDHHC5 is inhibited through loss of Fyn activation, thereby triggering endocytosis of zDHHC5, and enabling its trafficking to dendritic shafts [65]. Thus, phosphorylation is an important regulator of zDHHC5 localization.

To date, there is no evidence demonstrating the activity-sensing capacities of zDHHC8 nor its ability to translocate according to changes in synaptic activity. Perhaps the inability for zDHHC8 to cycle between membrane compartments differentiates substrate specificity between zDHHC5 and zDHHC8. Although zDHHC5 and zDHHC8 operate in a completely functionally redundant manner in the context of ankyrin-G palmitoylation in polarized epithelial cells [39], they also exhibit distinct specificity for substrates such as δ-catenin, which is predominantly palmitoylated by zDHHC5 [65, 89]. It is possible that distinct substrate profiles (or lack thereof, i.e. functional redundance) for zDHHC5 and zDHHC8 is cell-type dependent process, depending

on cell excitability or polarization. We must keep in mind that PAT identification for a substrate like phospholemman involved co-immunoprecipitation of the substrate with each individual PAT, which precluded identification of zDHHC8 as a potential binding partner due to the difficulties associated with its solubilization. However, PAT-substrate interactions are often transient; thus, failure to co-immunoprecipitate a substrate with its PAT does not rule out the possibility of the PAT-substrate pair. In cases where only zDHHC5 was identified as substrate-specific PAT, there may have been experimental limitations or transient PAT-substrate interactions that precluded the identification of zDHHC8 as capable of palmitoylating that substrate. Nevertheless, whether zDHHC8 can respond to activity needs to be further investigated.

Plasma-membrane PATs contain localization motifs that contribute to their PM subcellular localization.

Given that zDHHC2 cycles between the PM and endosomes **(Figure 1.3)**, Salaun *et al* looked for an existing endocytic sorting signal within the C-terminus of zDHHC2 that could account for zDHHC2's ability to cycle between PM and REs. The authors identified two atypical, but distinct sequences within the C-terminus of zDHHC2, $N^{357}P^{358}$ and $SxxxL^{334}L^{335}$, both of which deviate from the canonical endocytic (Fx)NPxY/F and D/ExxxLL signals, respectively. Both of these play a significant role in zDHHC2 localization as mutation of these individual endocytic sequences to alanine residues resulted in increased retention of mutant zDHHC2 at the PM [90]. A few phosphorylation sites were also identified in zDHHC2, of which serine-330 is located four amino acids upstream of the dileucine sorting motif. Mutation of this residue in zDHHC2 to an aspartate, to mimic constitutive phosphorylation, results in zDHHC2

internalization and reduces its presence at the PM, whereas mutation to render it phosphorylation-deficient (S330A) results in enhancement of zDHHC2 PM-association. Thus, phosphorylation is able to modulate the effects of the endocytic dileucine motif, which appears to be zDHHC2-specific. Additionally, Ser330 is part of an SQ motif, whose phosphorylation appears to be regulated by synaptic activity [91]. That is, synaptic activity would increase phosphorylation of SQ-containing proteins, thereby "activating" the endocytic motif and remove zDHHC2 from the plasma membrane for internalization to recycling endosomes. Thus, it is possible that phosphorylation dynamics at Ser-330, along with other serine residues in proximity to the dileucine endocytic motif at the C-terminus of zDHHC2 could act to regulate the activity of the sorting motif and thereby the localization of zDHHC2, in an activity-dependent manner [90]. In fact, it has been more broadly shown that synaptic strength itself can be controlled by phosphorylation dynamics [87]. Depending on whether neuronal activity-dependent phosphorylation dynamics do in fact regulate the endocytic capacities of the sorting signals within zDHHC2, or whether phosphorylation on its own is sufficient to rapidly trigger the trafficking of zDHHC2 from one compartment to the other, these mechanisms could account for zDHHC2's mobility between the PM and endosomes. It is worth mentioning that other zDHHCs contain phosphorylation sites; as mentioned previously, zDHHC5 phosphorylation regulates its PM-localization [65]. Phosphopeptides were identified in zDHHC8 in response to β adrenergic receptor stimulation by mass spectrometry [92]. Phosphorylation of Golgi-localized zDHHC3 regulates its enzymatic activity and plays a role in neuronal morphogenesis, although it remains unclear whether zDHHC3 phosphorylation regulates zDHHC3 localization [93].

Given that clathrin adaptor proteins bind NPxY motifs [94], Salaun *et al* hypothesized the possibility that clathrin adaptor proteins could recognize the atypical NP sorting motif present in

zDHHC2 to trigger zDHHC endocytosis, which may or may not be regulated by phosphorylation of proximal serines [90]. The mechanisms underlying the exact role of phosphorylation for zDHHC2 trafficking between PM and endosomes warrant further investigation.

Further studies demonstrated that zDHHC2 enzymatic activity does not drive zDHHC2 localization at the PM of PC12 cells, suggesting that enzyme activity is not responsible for determining how zDHHC2 is targeted to the PM [75, 87]. Instead, the C-terminal domain of zDHHC2 has been shown to regulate its PM association, given that truncation of the entire C-terminal domain leads to the enzyme redistributing to the ER. Truncating the C-terminus of Golgi-localized zDHHC3, however, did not lead to ER retention, suggesting that not all zDHHCs depend on an intact C-terminal domain to exit the ER [75]. Rather, this appears to be a zDHHC2-specific phenomenon. Furthermore, zDHHC15, which is homologous to zDHHC2, but is localized to the Golgi, differs in the final half of its C-terminal tail, compared to zDHHC2. The divergent C-terminal sequence between zDHHC2 and zDHHC15 appears to govern the localization, since swapping C-termini reverses the subcellular localization pattern [75]. Thus, for certain PATs like zDHHC2 and zDHHC15, the C-terminus is a critical trafficking signal.

Polarized epithelial cells provide a feasible cell model system to more thoroughly study the polarized targeting of proteins, as they contain distinctly organized membrane domains with unique protein distributions. Interestingly, overexpressed HA-tagged zDHHC2 in polarized epithelial cells was not found to be PM-associated, but rather localized to intracellular compartments [39], highlighting the cell-type-specific targeting of PAT enzymes. In polarized epithelial cells, zDHHC5 and zDHHC8 predominantly localize to the lateral membrane, compared to zDHHC14, which localizes non-specifically throughout the plasma membrane. Unlike zDHHC2

which relies on its intact C-terminus to drive its PM association in nonpolarized cells, the C-termini of zDHHC5 and zDHHC8 do not drive their lateral membrane-targeting in polarized epithelial cells; replacing the C-terminal domain of zDHHC5 with that of zDHHC14 did not abolish lateral membrane localization of zDHHC5 in epithelial cells [39]. zDHHC5 and zDHHC8 have a conserved AP2μ-binding site or YDNL motif close to a poly-proline SH3-motif as well as dileucine endocytic motifs that can bind endocytosis machinery, such as the clathrin adaptor proteins AP2 [65, 94]. As Brigidi *et al* demonstrated, the ability for zDHHC5 to interact with endocytosis machinery highly influences its ability to cycle between subcellular compartments to regulate synaptic plasticity, and likely affects its ability to locally palmitoylate the substrates it gains access to as it cycles through different subcellular compartments.

Interaction motifs may not be the sole contributor to substrate-enzyme specificity.

How non-Golgi PATs like zDHHC2, zDHHC5, or zDHHC8 achieve specificity for their substrates remains incompletely understood. zDHHC2 does not possess any obvious substrate interaction motifs such as a PDZ-binding motif that contribute to substrate recognition [87]. zDHHC5 and zDHHC8 are closely related and distinct from other zDHHC PAT family members as they exhibit greatly extended and disordered C-terminal tails, which in some cases has proven important for substrate recognition [34, 55]. Howie *et al* demonstrated that the zDHHC5 disordered C-terminal tail is critical for zDHHC5 to bind to and mediate the palmitoylation of PLM [67]. This extended C-terminal tail contains a PDZ-binding motif predicted to bind other PDZ-containing domains, present in many proteins largely involved in neuronal regulation, and synapse formation and maintenance [95-97]. Most of the mentioned zDHHC5 and zDHHC8

substrates contain PDZ domains [66, 67, 98], which in some instances explain the ability for zDHHC5 and zDHHC8 to recognize and palmitoylate substrates, like GRIP1b. However, if the presence of PDZ-binding motifs or PDZ-containing domains were the sole contributor to enzyme-substrate specificity, then all zDHHC PATs containing PDZ-binding motifs would likely be capable of palmitoylating all PDZ-containing substrates. However, two other PATs with PDZ-binding motifs, zDHHC3 and zDHHC7, are not capable of palmitoylating any of the aforementioned PDZ-containing, zDHHC5- or zDHHC8-specific substrates like GRIP1b, δ-catenin, and PLM. Interestingly, zDHHC3 and zDHHC7 localize to the Golgi [55], compared to plasma membrane targeted zDHHC5 and zDHHC8, which palmitoylate substrates whose predominant final destination is the PM. Thus, subcellular localization of non-Golgi PATs likely contributes to substrate recognition to drive specific substrate localization for proper formation of PM microdomains.

ER-localized PAT zDHHC6 is also involved in local palmitoylation of ER substrates

Although it is most commonly thought that palmitoylation enhances protein affinity for specific microdomains at the plasma membrane, palmitoylome profiling has shown that ER membranes also contain active PATs to palmitoylate proteins directly at the ER. The major ER glycoprotein chaperone calnexin is palmitoylated by ER-localized zDHHC6 in HeLa cells, which targets calnexin to the perinuclear rough ER to stabilize it for substrate capture [99]. The proper ER localization of calnexin is highly dependent on its palmitoylation, concordant with the necessity for calnexin's palmitoyl transferase zDHHC6 to be localized to the ER to locally palmitoylate and sort calnexin to its specific ER compartments. ER-localized zDHHC6 was also

shown to drive the palmitoylation and subsequent peripheral-ER localization of the E3 ubiquitin ligase, gp78, critically involved in ER-associated degradation pathways [100]. Lastly, Fredericks *et al* showed that palmitoylation of the inositol 1,4,5-triphosphate receptor (IP_3R) by zDHHC6 is critical for IP_3R expression and localization at the ER membrane of immune cells, important for calcium release from the ER. IP_3R is palmitoylated in a manner dependent on zDHHC6 interacting with another ER-localized selenium-containing protein, selenoprotein K. Both zDHHC6 and selenoprotein K associate through Src-homology 3 (SH3) binding domains [101].

Interestingly, overexpression of zDHHC6 in immune cells did not affect the palmitoylation of other palmitoylated ER substrates, such as the Wnt co-receptor lipoprotein Receptor-related Protein 6 (LRP6) [99]. This suggests that zDHHC6 does not mediate the palmitoylation of all ER palmitoylated substrates, and that there must be other active zDHHCs in the ER, such as zDHHC4, as suggested by Gorleku *et al* [47]. LRP6 must exit the ER, a process mediated by palmitoylation, and travel through the Golgi before reaching the plasma membrane, where it is able to mediate Wnt signaling [102, 103]. Given that the functional importance of LRP6 palmitoylation is to drive its sorting *away* from the ER *towards* the plasma membrane for further signaling, one could rationalize the recruitment of a different PAT than zDHHC6 to mediate LRP6 palmitoylation, as zDHHC6 has shown to specifically palmitoylate ER substrates that *remain* in the ER. Additionally, whether palmitoylation of LRP6 actually occurs in the ER, and whether the zDHHC that palmitoylates it is localized to the ER, remain unknown. Abrami *et al* reported that palmitoylation of LRP6 may induce a tilt of the transmembrane domain, in order to allow the protein to conform to the thin lipid membrane of the ER [102]; whether this differential conformation changes PAT specificity remains unknown given that no LRP6-specific PAT has yet been identified.

ER PATs contain localization motifs that contribute to their ER targeting and substrate specificity.

Similar to PM PATs, how ER PATs reach the ER is not completely established. ER-localized zDHHC6 contains a dilysine-based ER localization motif located in its C- terminus, conforming to the KKXX ER sorting motif [47]. The addition of this dilysine based signal onto the C-terminus of zDHHC3, a Golgi-localized PAT, was sufficient to re-localize zDHHC3 to ER membranes. Interestingly, ER-localized zDHHC3 mutants retained their capacity to palmitoylate known substrates of zDHHC3, SNAP25, and cysteine string protein (CSP). However, a mutant CSP that mislocalizes to the ER is only palmitoylated by an ER-localized zDHHC3 mutant, and cannot be palmitoylated by wild-type, Golgi-localized zDHHC3 [47]. Because the CSP mutant is no longer able to localize to the Golgi and instead is re-localized to the ER, Golgi-localized zDHHC3 is also not able to mediate CSP mutant palmitoylation [47]. However, it is only when zDHHC3 is forced to an ER membrane that it is able to enhance ER-localized CSP mutant palmitoylation [47], consistent with local palmitoylation.

PAT localization in health and disease.

Alterations in protein palmitoylation and aberrant PAT activity have been associated with a wide range of human diseases, including neurological, cardiovascular, and infectious diseases. Loss-of-function variants in the golgi-localized *ZDHHC9* are linked to X-linked intellectual disability (XLID) [18, 19, 104-106], sometimes with an increased incidence of epilepsy [107]. zDHHC9 regulates of dendritic growth and inhibitory synapse formation through the palmitoylation of the two GTPases, Ras and TC10, with significant implications for maintaining

excitatory/inhibitory (E/I) balance in the brain [108]. *Zdhhc9*-knockout mice have altered E/I balance and exhibit seizure-like activity, which could contribute to XLID etiology [108]. Genome-wide association studies have found deletions in the region of chromosome 11 that encodes *ZDHHC5* in patients with bipolar disorder and schizophrenia [109, 110]. A *de novo* missense mutation in *ZDHHC5* has also been reported in schizophrenic patients [111]. However, which schizophrenic- and bipolar disorder-associated substrates and pathways are altered as a result of alterations in zDHHC5 currently remains unexplored. A number of polymorphisms within the *ZDHHC8* gene, specifically those associated with the 22q11.2 chromosomal microdeletion, are also highly linked to schizophrenia [15, 17], but its substrate dependence remains incompletely understood. In a 22q11.2 microdeletion mouse model, which lacks functional *Zdhhc8*, Mukai *et al* observed decreased postsynaptic PSD95 puncta, as well as decreased presynaptic VGLUT1 puncta, leading to lower spine density and glutamatergic synapses, which could be rescued by re-introduction of enzymatically active zDHHC8 protein [17]. As expected by the decreased PSD95 puncta in this mouse model, PSD95, as well as other substrates such as Cdc42, Rho GTPases, and Rac1, were found to be substrates for zDHHC8 [17, 112]. Another proteomic study also observed reduced palmitoylation of the vesicular glutamate transporter 1 (VGLUT1), the small GTPase Ras, and myelin basic protein (MBP) in post-mortem dorsolateral prefrontal cortices of schizophrenic patients, suggesting that the loss of zDHHC8-mediated palmitoylation of these substrates may contribute to the underlying mechanisms of schizophrenia [113]. Given the data highlighted in this review, one could predict that human-variant-driven loss of zDHHC8 expression or mistargeting of zDHHC8 at spines would result in loss of proper targeting of PSD95, Cdc42, and PICK1 at dendritic spine membranes, with severe consequences for the formation of synaptic connections and neuronal connectivity, potentially contributing to schizophrenia etiology. Given the critical

role of zDHHC5 and zDHHC8 in mediating the palmitoylation of synaptic substrates involved in important processes like synaptic trafficking, transmission, and plasticity, it will be important to further investigate how broad dysfunction of these synaptic PATs alter substrates' capacities to localize to and function at synaptic membranes, and how these enzyme-substrate defects contribute to underlying mechanisms of neuropsychiatric diseases. In light of the role of zDHHC5-mediated palmitoylation of the cardiac phosphoprotein PLM [67], it would be unsurprising that mutations in *ZDHHC5* may also alter cardiac function through PLM's ability to modulate the cardiac sodium pump or through currently unidentified zDHHC5 cardiac substrates whose plasma-membrane localization is indispensable for function. In the future, investigating disease etiology from the perspective of alterations in PAT expression, localization, and function may provide insights into a much wider set of dysregulated substrates that may converge on one pathophysiological pathway.

Conclusions, current knowledge, and outstanding questions.

Excluding Golgi-mediated palmitoylation in which a substrate is palmitoylated at the Golgi by Golgi-localized PATs before being trafficked to the plasma membrane, many substrates are locally palmitoylated and targeted to non-Golgi membranes by active PATs residing at PM and ER membranes (non-Golgi PATs). Thus, the precise regulation of substrate localization and function at these PM and ER domains is often highly dependent on the proper PM and ER localization of their respective PATs. Despite improvements in our understanding of PAT enzyme-substrate specificity in recent years, consensus sequences that distinguish which PATs palmitoylate which substrates remain elusive. In this review, we highlight evidence showing that non-Golgi-PAT-substrate specificity is not always contingent on interaction motifs; interaction

motifs contribute to a PAT being able to bind and recognize its substrate, but a previously unappreciated factors such as local palmitoylation also appears to be an important determinant of specificity. In fact, we rationalize that for the PAT and its substrate to be able to bind (through an interaction motif), they would need to be in the same subcellular compartment to engage in palmitoylation. In some cases, it may be that both local palmitoylation and an interaction motif are involved in ensuring proper palmitoylation of a substrate by a non-Golgi PAT. Although interaction motifs like PDZ domains clearly play an important role for PAT-substrate recognition, such as zDHHC5 for GRIP1b, we also reviewed examples where non-PDZ-containing substrates were specifically palmitoylated by PATs containing PDZ-binding motifs, such as zDHHC5 and ankyrin-G, suggesting that interaction motifs may not always drive PAT-substrate specificity. Instead, it is worth considering the role of local palmitoylation for substrates like ankyrin-G, where palmitoylation by lateral-membrane-localized zDHHC5 and zDHHC8 are indispensable for ankyrin-G targeting to lateral membranes of epithelial cells. No other PATs are able to mediate the palmitoylation and localization of ankyrin-G in epithelial cells, highlighting that proximity between PATs and substrates within membrane domains may be an important driver of specificity. A better understanding of the role of local palmitoylation for substrate specificity, targeting, and function, as well as its contributions alongside with or independent of interaction motifs, may provide molecular determinants to more effectively map PAT-substrate profiles. An outstanding question that stems from the local palmitoylation hypothesis is how soluble substrates, like ankyrin-G, which do not go through the Golgi for palmitoylation and only rely on PM palmitoylation to reach the membrane, achieve proximity near their respective non-Golgi, PM-associated PATs prior to palmitoylation. Whether these substrates are locally translated or somehow transported near their PAT post-translationally is a question that remains to be answered.

Overall goals, aims, and significance of this thesis work:

The overall goal of the work described in this thesis is to explore how the posttranslational modification, *S*-palmitoylation, regulates the localization and functions of neuronal substrates, such as the voltage-gated sodium channel (VGSC) β1 subunit and ankyrin-B, both of which are critical substrates involved in the initiation and propagation of neuronal excitability. A striking 10% of neuronal proteins are modified by *S*-palmitoylation, including presynaptic proteins, cytosolic proteins, scaffolding proteins, integral membrane proteins, and ion channels [13, 14]. By directing the proper localization, microdomain organization, stability, and subsequent function at the neuronal substrate level, palmitoylation plays broad roles in promoting, facilitating, and fine-tuning neuronal processes such as development, polarization, synaptic plasticity, axonal growth, dendritogenesis, spinogenesis, and neuronal transmission [2, 3, 114]. Despite the abundance of palmitoylated proteins within the neuronal proteome, many neuronal proteins still remain to be identified as substrates of *S*-palmitoylation. Additionally, understanding the role of palmitoylation for neuronal substrate function provides insight into how normal neuronal processes may be regulated and in turn how pathophysiological processes may arise when palmitoylation and other regulatory processes go awry. *S*-palmitoylation is a reversible process, involving tunable enzymes that promote palmitoylation and depalmitoylation, which makes for a potentially targetable and "druggable" regulatory mechanism. Thus, understanding palmitoylation's role in disease pathogenesis could lead to potentially impactful ways of targeting dysfunctional processes without targeting the substrate itself.

The goal of this thesis was to explore the role of *S*-palmitoylation for proper localization, stability, and respective functions of two neuronal proteins, VGSC β1 subunits and ankyrin-B,

both previously unknown to be palmitoylated and both highly disease-associated. This work highlights that both β1 and ankyrin-B rely on palmitoylation for their respective localization and functions, which may provide insights into β1 subunit- and ankyrin-B-associated pathophysiologies, such as epilepsy and autism spectrum disorders, respectively.

Though β1 and ankyrin-B are not inherently related substrates, this work has been made especially relevant in light of the recently discovered convergent mechanisms between voltage gated sodium channels and ankyrin-B. β1 subunits mediate neuronal excitability by modulating VGSC α subunit biophysical properties and cell surface expression [115]. Recent work in our laboratory in collaboration with Kevin Bender's laboratory at UCSF has implicated ankyrin-B as an important modulator of dendritic excitability [116]. Dendritic excitability is in part mediated by the presence of VGSC $Na_v1.2$ at dendrites in mature cortical pyramidal neurons [117]. Ankyrin-B is also present at dendritic membranes, and is thereby conveniently located to scaffold $Na_v1.2$ at dendritic membranes. Indeed, recent work by our laboratory has shown ankyrin-B in mature cortical pyramidal neurons scaffolds VGSC $Na_v1.2$ at dendritic membranes to regulate dendritic excitability and synaptic plasticity, thereby directly implicating ankyrin-B in mediating dendritic excitability for the first time [116]. Given that VGSCs, β subunits, and ankyrins form macromolecular complexes essential for proper neuronal activity, and that disruption of any of these members in complex can lead to neurodevelopmental and neuropsychiatric diseases, it has become ever more important to mechanistically understand the regulatory mechanisms underlying proper localization and function of these substrates as they mediate neuronal excitability individually and in concert with each other.

Chapter 2: Investigate the role of palmitoylation in VGSC β1 subunit plasma membrane localization and for β1 Regulated Intramembrane Proteolysis (RIP).

VGSC β1 subunits are multifunctional proteins that canonically modulate VGSC α subunit biophysical properties and cell surface localization, while also participating in cell-cell and cell-matrix adhesion, necessary for intracellular signal transduction, cell migration, and differentiation. Recently, work showed VGSC β1 subunits undergo RIP to generate a β1 intracellular C-terminal domain that translocates to the nucleus and participates in transcriptional regulation, a potentially important mechanism underlying *SCN1B*-linked pathophysiology. However, the mechanisms that regulate proteolysis of β1 were unknown. Chapter 2 investigates the role of *S*-palmitoylation for β1 plasma membrane localization, β1 RIP (cleavage), and β1 modulation of $Na_v1.5$ sodium current (I_{Na}). We find for the time first time that β1 subunits are *S*-palmitoylated in whole mouse brains at one single cysteine, Cys162. Mutating Cys162 to an alanine (β1-p.C162A) abolishes β1 palmitoylation, which reduces β1 plasma membrane localization and subsequently reduces the surface fraction of β1 available for RIP. Furthermore, we determine that increased endocytosis may be a potential mechanism to explain the reduction of PM localization of the β1-p.C162A mutant, compared to WT β1. Interestingly, β1 modulation of I_{Na} is not dependent on *S*-palmitoylation. These findings reveal for the first time that a β subunit is modified by *S*-palmitoylation, and that *S*-palmitoylation localizes β1 at the plasma membrane to facilitate proteolytic cleavage of β1, which may have important implications for the downstream transcriptional output of β1.

Chapter 3: Investigate the role of palmitoylation for ankyrin-B-mediated scaffolding of VGSC $Na_v1.2$ at dendritic membranes of neurons.

Ankyrins act as general adaptor proteins that localize membrane, cytoskeletal, and cytoplasmic proteins at specialized membrane domains, and promote cell polarity and function in many vertebrate tissues. One of these ankyrin family members, ankyrin-B, plays a multitude of roles at the axon of neurons, including mediating axonal cargo transport, scaffolding of cell adhesion molecules at the axon, and promoting the proper positioning of ankyrin-G at the axon initial segment. Recently, ankyrin-B was discovered to play a novel role at the dendritic membranes of neurons, where it scaffolds voltage-gated sodium channels $Na_v1.2$ to promote dendritic excitability and synaptic plasticity. However, how ankyrin-B itself properly localizes to dendritic membranes to subsequently scaffold $Na_v1.2$ there is unknown. Chapter 3 investigates the role of *S*-palmitoylation for ankyrin-B localization and function at dendritic membranes. Our studies highlight that ankyrin-B is lipid-modified by *S*-palmitoylation in both whole mouse brains and in neurons, at multiple cysteines harbored within the N-terminal ankyrin-repeat domain of ankyrin-B. Mutating five cysteines in ankyrin-B's ankyrin-repeat domain abolishes ankyrin-B palmitoylation, and prevents ankyrin-B from scaffolding $Na_v1.2$ at dendritic membranes due to loss of proper dendritic localization of ankyrin-B in cortical neurons. Interestingly, palmitoylation does not regulate the ability of ankyrin-B to mediate axonal cargo transport, suggesting that palmitoylation is a mechanism specific for ankyrin-B's functions at dendrites. Furthermore, we determine that ankyrin-B palmitoylation is mediated by the palmitoyl acyl transferase zDHHC17 both in heterologous cells and in cultured neurons. Interestingly, we found zDHHC17 regulates ankyrin-B protein levels independently of its palmitoylation function, through a conserved binding

mechanism between the ANK repeat domain of zDHHC17 and the zDHHC ankyrin-repeat binding motif of ankyrin-B. These findings reveal an important regulatory mechanism underlying the localization and function of dendritic ankyrin-B in neurons, and may have important implications in the etiology of ankyrin-B-associated autism spectrum disorder.

Chapter 4: Discussion and Future Directions

Chapter 2: Sodium Channels β1 Subunits are Post-Translationally Modified by Tyrosine Phosphorylation, *S*-Palmitoylation, and Regulated Intramembrane Proteolysis

(This chapter has been published in *Journal of Biological Chemistry*. 2020;295(30):10380-10393. doi: 10.1074/jbc.RA120.013978)

Alexandra A. Bouza[&], Julie M. Philippe[&], Nnamdi Edokobi, Alexa M. Pinsky, James Offord, PhD, Jeffrey D. Calhoun, PhD, Mariana Lopez-Florán, Luis F. Lopez-Santiago, Paul M. Jenkins, PhD, and Lori L. Isom, PhD

[&] Co-first authors

Summary

Voltage-gated sodium channel (VGSC) β1 subunits are multifunctional proteins that modulate VGSC α subunit biophysical properties and cell surface localization, as well as participate in cell-cell and cell-matrix adhesion, all with important implications for intracellular signal transduction, cell migration, and differentiation. Human loss-of-function variants in *SCN1B*, encoding the VGSC β1 subunits, are linked to severe diseases with high risk of sudden death, including epileptic encephalopathy and cardiac arrhythmia. We showed previously that β1

subunits are post-translationally modified by tyrosine phosphorylation. We also showed that β1 subunits undergo regulated intramembrane proteolysis (RIP) via the activity of BACE1 and γ-secretase, resulting in the generation of a soluble intracellular domain, β1-ICD, which modulates transcription. Here, we show that β1 subunits are phosphorylated by FYN kinase. In addition, we show that β1 subunits are *S*-palmitoylated. Mutation of a single residue in β1, cysteine (C) 162 to alanine (A), prevents palmitoylation, reduces the level of β1 polypeptides at the plasma membrane, and results in a reduction in the extent of β1 RIP, suggesting that the plasma membrane is the site of β1 proteolytic processing. Treatment with the clathrin-mediated endocytosis inhibitor, Dyngo- 4a, restores plasma membrane association of β1-p.C162A to WT levels. Despite these observations, palmitoylation-null β1-p.C162A modulates sodium current and sorts to detergent-resistant membrane fractions normally. This is the first demonstration of *S*-palmitoylation of a VGSC β subunit, establishing precedence for this post-translational modification as a regulatory mechanism in this protein family.

Introduction

Voltage gated sodium channels (VGSCs) are heterotrimeric protein complexes composed of one pore-forming α subunit and two non-pore forming subunits [118]. VGSC β1 through β4 subunits contain a single, extracellular V-type immunoglobulin (Ig) domain and are thus members of the Ig superfamily of cell adhesion molecules (Ig-CAMs) [115, 118]. β1 subunits are expressed in multiple tissues, including brain and heart, where they modulate the gating, kinetics, and plasma membrane localization of VGSC α subunits through non-covalent association [115, 119-121]. β1 subunits are multi-functional and play both conducting and non-conducting roles. In addition to modulating VGSCs, they contribute to voltage-gated potassium channel function, cell-cell and cell-matrix adhesion and cell migration, intracellular calcium signaling, neuronal pathfinding and fasciculation, neurite outgrowth, and cardiac intercalated disk formation [115, 122-128]. Concordant with their CAM function, β1-β1 *trans* homophilic cell adhesion *in vitro* results in outside-in signaling that includes ankyrin recruitment to points of cell-cell contact, which is terminated by β1 tyrosine phosphorylation [125, 129]. In cultured cerebellar granule neurons, β1-β1 *trans* homophilic cell adhesion drives neurite extension through a mechanism that includes *fyn* kinase [124]. β1 subunits form heterophilic partnerships with other CAMs, including contactin, N-cadherin, NrCAM, neurofascin, and VGSC β2 subunits, and associate with the extracellular matrix protein, tenascin-R, to modulate cell migration [130-132]. Thus, β1 CAM activity is critical for brain and heart development.

Human variants in VGSC genes are linked to the developmental and epileptic encephalopathies (DEEs) and to cardiac arrhythmia. Loss-of- function (LOF) variants in *SCN1B*,

encoding β1, result in early infantile developmental and epileptic encephalopathy (EI-DEE) and Generalized Epilepsy with Febrile Seizures plus [115, 133]. *Scn1b*-null mice model EI-DEE, with severe spontaneous seizures of multiple etiologies, ataxia, and sudden death in the third week of life [134]. Consistent with loss of β1-mediated cell-cell and cell-matrix adhesion, *Scn1b*-null mice have neuronal pathfinding and fasciculation defects in brain [122, 124]. *SCN1B* is expressed in heart in addition to brain. *Scn1b*-null mice have prolonged QT and RR intervals. *Scn1b*-null ventricular cardiomyocytes have increased sodium current (I_{Na}), altered calcium handling, altered intercalated disc structure, and prolonged action potential duration [128, 135, 136]. *SCN1B* variants are associated with human cardiac disease, including Brugada syndrome and atrial fibrillation [137-141]. Taken together, these data show that *SCN1B* is critical for the regulation of excitability in multiple organ systems.

β1 subunits undergo regulated intramembrane proteolysis (RIP) through the sequential activity of β-site Amyloid Precursor Protein (APP) cleaving enzyme-1 (BACE1) and γ-secretase [142, 143]. BACE1 cleavage, the rate-limiting step in this process, releases the extracellular β1 Ig domain, which functions as a CAM ligand to stimulate neurite outgrowth [144, 145]. The remaining membrane-bound C-terminal fragment (β1-CTF) is cleaved by γ-secretase in the lumen of the membrane, generating a soluble, intracellular domain, β1-ICD, that translocates to the nucleus to regulate transcription [142, 146]. Thus, β1 RIP plays important roles in neurite outgrowth, cell migration, cell adhesion, and transcription [147, 148].

BACE1- and γ-secretase-mediated processing of the well-studied RIP substrate, amyloid-β precursor protein (APP), is regulated by *S*- palmitoylation, the covalent addition of a 16- carbon

fatty acid to cysteine residues via thioester bond formation [149]. Palmitoylation targets APP to its proper membrane domains, bringing it in close proximity to proteolytic enzymes for subsequent cleavage [149]. Here, we asked whether post-translational modification of β1 subunits by tyrosine phosphorylation or *S*-palmitoylation could regulate its plasma membrane localization and subsequent RIP. In contrast to β1-ankyrin association, for which β1 tyrosine phosphorylation is critical [129], we found that the tyrosine phosphorylation state of β1 has no effect on its plasma membrane localization, intramembrane cleavage, or ability to modulate I_{Na}. We report for the first time that β1 subunits are *S*-palmitoylated in mouse brain. Using heterologous cells, we found that substitution of cysteine (C) residue 162 with alanine (A) abolishes β1 palmitoylation, decreases the fraction of β1 in the plasma membrane as assessed by surface biotinylation, and thus reduces the level of β1 that is available for RIP. Treatment of cells with the clathrin-mediated endocytosis inhibitor, Dyngo-4a, restores β1-p.C162A to wild-type (WT) levels at the plasma membrane, suggesting that *S*-palmitoylation confers plasma membrane stability to β1. Finally, we show that β1-mediated modulation of I_{Na} as well as β1 sorting to detergent-resistant membrane fractions do not depend on β1 palmitoylation. Taken together, our work suggests that multiple post-translational modification events regulate β1 function. Tyrosine phosphorylation regulates the association of β1 subunits with ankyrin but does not affect their plasma membrane localization. In contrast, *S*-palmitoylation regulates the cell-surface localization of β1 and consequently its extent of RIP, indicating that β1 cleavage occurs at the plasma membrane. This work provides novel insights into β1 subunit function that may aid in understanding the mechanism of *SCN1B*- associated pathophysiologies.

Results

β1 RIP occurs independently of β1 tyrosine phosphorylation.

β1 tyrosine residue (Y) 181, located in the intracellular domain, is important for β1-mediated downstream signaling (**Fig. 2.1A**) [129]. In previous work, we used phosphorylation-null and phosphomimetic mutant constructs to show that phosphorylation of residue Y181 is a key regulatory mechanism for ankyrin binding [129]. Our work in cerebellar granule neurons demonstrated that β1-β1 *trans* homophilic adhesion-mediated neurite outgrowth is inhibited by the administration of γ-secretase inhibitors and in neurons isolated from *fyn* null mice [124, 147]. Taken together, these data suggested that β1-mediated neurite outgrowth requires association of the β1 intracellular domain with ankyrin, via residue Y181, which then triggers β1 RIP. Here, we tested the hypothesis that β1 tyrosine phosphorylation regulates cleavage using a multi-disciplinary approach.

We used a cell-free fyn kinase assay (Promega), in which ADP was measured via luciferase activity and positively correlated to kinase activity, to determine whether fyn directly phosphorylates a β1 peptide, QENASEYLAITC, at position Y7, which is equivalent to position Y181 in the full-length polypeptide. Poly E_4Y_1 peptide was used as a positive control for fyn kinase activity (**Fig. 2.1B**). Inclusion of WT β1 peptide in the assay increased luciferase activity by approximately 3-fold over the no-substrate control. In contrast, luciferase activity levels in the presence of Y181E β1 peptide (pYβ1) were not different from the no-substrate control. These data indicate that fyn kinase can directly phosphorylate β1 at the Y181 position (**Fig. 2.1B**).

To understand whether β1 phosphorylation at Y181 affects β1 RIP, we generated phosphorylation-null, β1-p.Y181A-V5-2AeGFP, and phosphomimetic, β1-p.Y181E-V5-2AeGFP mutant constructs, based on our previous work [129]. Chinese Hamster Lung (CHL) cell lines stably overexpressing each construct were generated, and plasma membrane localization of each mutant polypeptide was investigated using cell-surface biotinylation assays [145, 146]. Similar to WT β1, both β1 mutants were detected in the plasma membrane fraction (**Fig. 2.1C**). Quantification of these results showed no differences in the plasma membrane association of any of the mutants compared to WT β1 (**Fig. 2.1D**). To determine if β1 phosphorylation at residue Y181 regulates BACE1- and γ-secretase-mediated cleavage of β1, each cell line was treated with vehicle (0.1% DMSO) or 1 μM of the γ-secretase inhibitor, DAPT, and analyzed by western blot. Treatment with DAPT leads to an accumulation of the intermediary cleavage product, β1-CTF, generated by BACE1 cleavage [143]. We found that levels of β1-CTF were generated similarly to WT in both mutant lines and accumulated similarly to WT following treatment with DAPT, suggesting that neither BACE1 nor γ-secretase cleavage of β1 depends on its phosphorylation state (**Fig. 2.1E, F**). β1-CTF fragments generated from DAPT-treatment of β1 phosphorylation mutants had variable molecular weights, compared to WT β1-CTF. This effect may be similar to previously observed shifting of the cleavage site resulting from the introduction of mutations into other BACE1 substrates [150], and warrants future investigation. These results also suggest that our previous work, demonstrating that γ-secretase inhibitors block β1-mediated neurite outgrowth [147], may have implicated γ-secretase substrates other than β1.

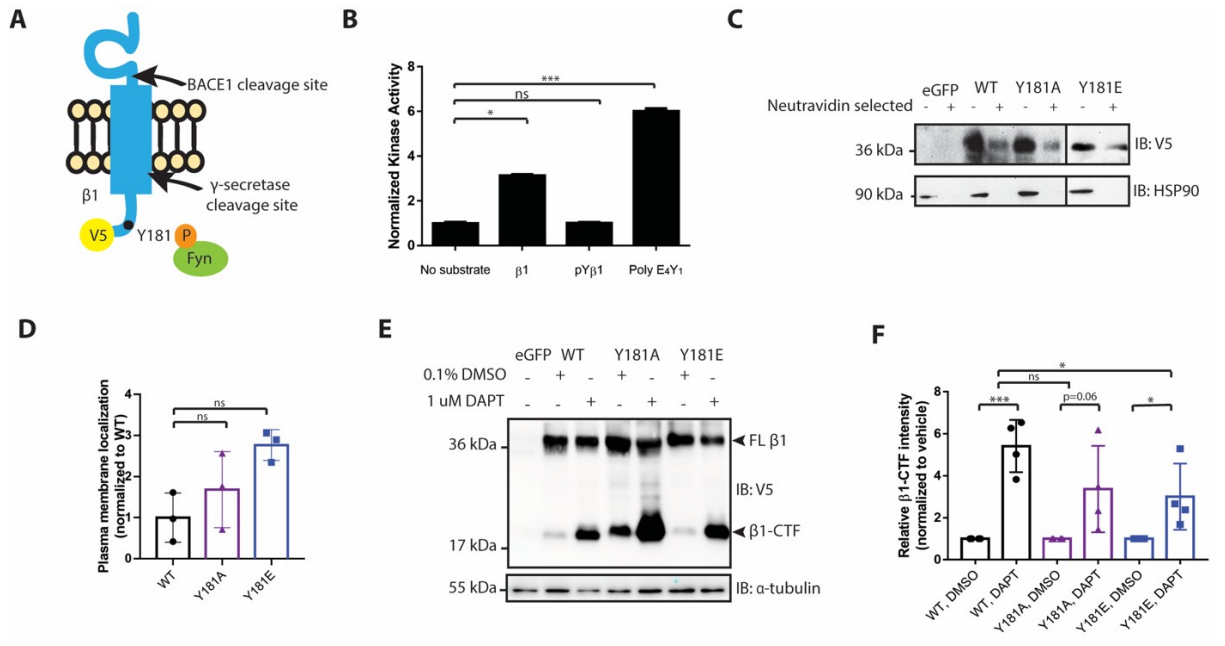

Figure 2.1. β1 phosphorylation at residue Y181 does not affect its RIP.

A. Schematic of β1 identifying the location of the phosphorylation site, Y181, as well as BACE1 and *γ*-secretase cleavage sites. **B.** A β1 peptide (QENASEYLAITC) is directly phosphorylated at Y181 by fyn kinase in a cell-free assay. N=3. **C.** Cell surface biotinylation indicates that similar to WT β1-V5, β1- p.Y181A-V5 and β1-p.Y181E-V5 are localized to the plasma membrane. N=3. **D.** Quantification of C. Plasma membrane fraction was normalized to total protein for that construct (% plasma membrane/total) and normalized again to WT β1-V5 plasma membrane levels. Significance ($p < 0.05$) was determined using a one-way ANOVA. **E.** WT β1-V5, β1-p.Y181A-V5, and β1-p.Y181E-V5 are cleaved by BACE1 and γ- secretase. N=4. **F.** Quantification of E. Protein levels were normalized to the loading control and reported as fold change respective to the vehicle treated group. Significance ($p < 0.05$) was determined using student's t-test between DMSO and DAPT treated constructs. One-way ANOVA was utilized to compare between constructs.

β1 modulation of I_{Na} occurs independently of β1 tyrosine phosphorylation.

We next asked whether the phosphorylation state of residue Y181 affects the ability of β1 to modulate I_{Na}. Human Embryonic Kidney (HEK) cells stably expressing human $Na_v1.5$ (HEK-hNav1.5) were transiently transfected with soluble enhanced Green Fluorescent Protein (eGFP), WT β1-V5-2AeGFP, β1-p.Y181A-V5-2AeGFP, or β1-p.Y181E-V5-2AeGFP. Inclusion of eGFP facilitated the identification of transfected cells for whole cell voltage patch clamp recordings. Co-expression of WT β1-V5-2AeGFP, β1-p.Y181A-V5-2AeGFP, or β1-p.Y181E-V5-2AeGFP with $hNa_v1.5$ increased I_{Na} density compared to eGFP alone, suggesting that the phosphorylation state of residue Y181 does not affect the ability of β1 to modulate I_{Na} density (**Fig. 2.2A, B**). In agreement with the observed increase in peak I_{Na} density, peak conductance was increased by co-expression of WTβ1-V5-2AeGFP, β1-p.Y181A-V5-2AeGFP, or β1-p.Y181E-V5-2AeGFP (**Fig. 2.2C**). No changes in capacitance were observed (**Fig. 2.2D**). We observed no effects of any of the β1 constructs on the voltage-dependence of I_{Na} activation or inactivation compared to the eGFP control (**Table 2.1**).

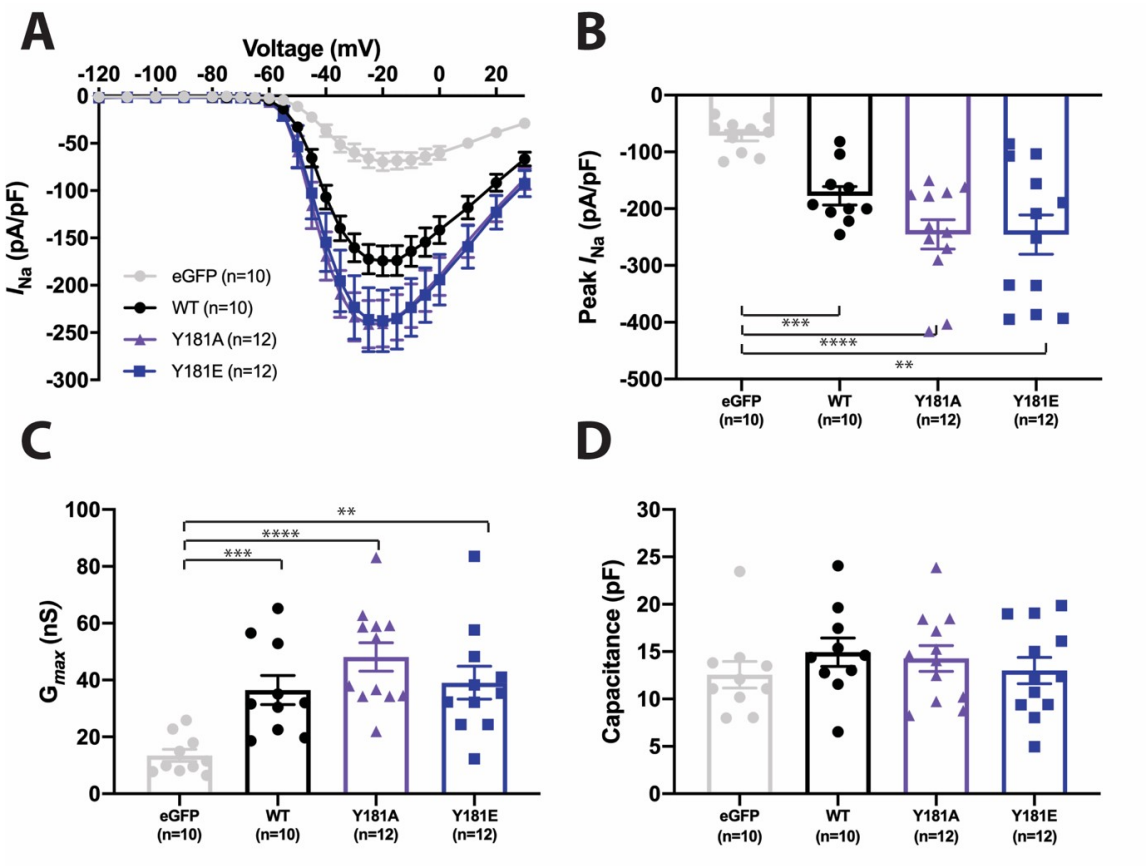

Figure 2.2. β1-mediated modulation of I_{Na} is not dependent on phosphorylation of residue Y181.

HEK- hNa$_v$1.5 cells were transiently co-transfected with WTβ1 (black circles), β1-p.Y181E (blue squares), or β1- p.Y181A (purple triangles). HEKhNa$_v$1.5 cells transfected with eGFP (light grey circles) were used as negative controls. I_{Na} was recorded in response to a series of voltage steps between -120 and +30mV in 5 mV increments, from a holding potential of -120 mV for 200 msec. **A.** I_{Na} current-voltage (I-V) relationship. **B.** Peak I_{Na} is significantly increased with co-expression of WTβ1, β1-p.Y181E, or β1-p.Y181A over eGFP. **C.** Peak conductance (G_{max}) is significantly increased with co-expression of WTβ1, β1-p.Y181E, or β1- p.Y181A over eGFP. Data were obtained by fitting individual activation or inactivation curves to a Boltzmann equation. G_{Na} was calculated from $G_{Na} = I_{Na}/(V - V_{rev})$, where I_{Na} is the peak I_{Na} during the test depolarization (V), and V_{rev} is the reversal potential. **D.** There were no significant differences in capacitance (in pF) measured from each cell. Data were acquired using pClamp 11 (Molecular Devices) software. Data presented in (A), (B) and (C) result from at least 3 separate transfections and are presented as means ± SEM. **p < 0.01 versus eGFP; ***p < 0.001 versus eGFP; ****p < 0.0001 versus eGFP.

HEK 293	Activation			Inactivation		
	$V_{½}$ (mV)	*k* (mV)	n	$V_{½}$ (mV)	*h* (mV)	n
$Na_v1.5$ + eGFP	-36.42 ± 0.27	6.70 ± 0.24	20	-81.42 ± 0.52	-9.21 ± 0.47	20
$Na_v1.5$ + WTβ1	-41.80 ± 0.28	5.83 ± 0.25	22	-78.42 ± 0.36	-7.65 ± 0.31	22
$Na_v1.5$ + Y181Eβ1	-37.96 ± 0.42	7.05 ± 0.36	12	-80.43 ± 0.52	-7.69 ± 0.42	12
$Na_v1.5$ + Y181Aβ1	-39.81 ± 0.30	6.59 ± 0.26	12	-79.77 ± 0.57	-7.80 ± 0.47	12
$Na_v1.5$ + Y181Fβ1	-35.08 ± 0.40	7.38 ± 0.35	8	-75.58 ± 0.40	-7.29 ± 0.35	8
$Na_v1.5$ + C162Aβ1	-41.05 ± 0.33	6.70 ± 0.29	10	-85.60 ± 0.34	-7.54 ± 0.25	10

Table 2.1. Voltage-dependent properties of HEK-h$Na_v1.5$ cells in the absence or presence of WT or mutant β1 subunits.

β1 is S-palmitoylated in vitro and in vivo.

APP is a type I transmembrane topology BACE1 substrate that results in the generation of Aβ peptides to form protein aggregates that can contribute to Alzheimer's disease pathogenesis [151]. BACE1-mediated cleavage of APP is highly dependent on its proper localization in lipid raft microdomains [149]. The post-translational lipid modification, *S*-palmitoylation, is required for proper targeting of APP to lipid rafts [149]. In lipid rafts, palmitoylated APP interacts with BACE1 for subsequent cleavage [149]. Given its similarity to APP, we asked whether β1 is also *S*- palmitoylated and, if so, whether *S*-palmitoylation regulates β1 subcellular localization and RIP. To assess steady-state palmitoylation of β1, we used the Acyl Resin Assisted Capture (Acyl-RAC) assay, in which free cysteines are first blocked with the alkylating reagent methyl methanethiosulfonate (MMTS). Then, thioester bonds between the cysteine residue of the protein and the palmitate are cleaved using the reducing agent hydroxylamine (HA/NH_2OH), to liberate the previously palmitoylated cysteine residues. The liberated cysteines are selectively captured on activated thiol sepharose beads and eluted, allowing for specific immunoblotting of palmitoylated proteins of interest [152]. We used endogenous flotillin-1, a known constitutively palmitoylated protein [153], as a positive control for the Acyl-RAC assay. In cells stably expressing WT β1-V5- 2AeGFP, we observed that β1 is *S*-palmitoylated, as evidenced by hydroxylamine-dependent binding of β1-V5 to thiopropyl sepharose beads (**Fig. 2.3A, Fig. 2.4A**).

We next asked whether β1 palmitoylation occurs *in vivo*. Using C57Bl/6J adult mouse whole brain lysates subjected to Acyl-RAC, we observed β1 palmitoylation, as evidenced by

hydroxylamine- dependent binding of endogenous β1 to thiopropyl sepharose beads (**Fig. 2.3B**). These data demonstrate that β1 is *S*-palmitoylated *in vitro* as well as in mouse brain, providing feasibility for investigating the role of *S*-palmitoylation in β1 localization and proteolytic processing.

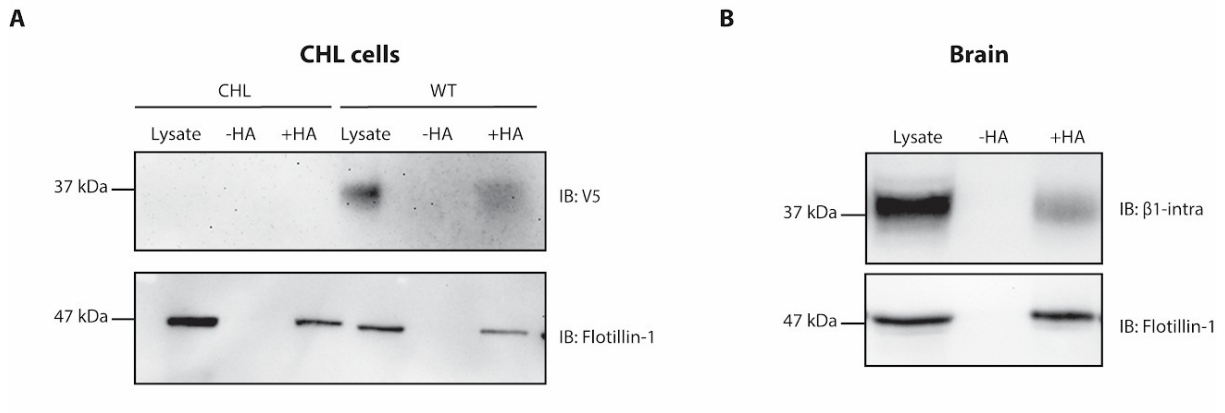

Figure 2.3. β1 is *S*-palmitoylated in CHL cells and in mouse brain.

A. CHL cells stably expressing β1-V5-2AeGFP were processed for the Acyl-RAC assay to detect *S*- palmitoylation. *S*-palmitoylation of β1-V5 is detected in CHL cells using an antibody against V5, as shown by the anti-V5 signal in the +HA lane, compared to the expected absence of signal in the -HA lane. Flotillin- 1 is used as a positive control for the Acyl-RAC assay. N=3. **B.** Whole mouse brain lysates were subjected to the Acyl-RAC assay to detect *S*-palmitoylation. *S*-palmitoylation of endogenous β1 is detected in whole mouse brains, using an antibody against the C-terminus of β1, as shown by the anti-β1 signal in the +HA lane, compared to the expected absence of signal in the -HA lane. N=3.

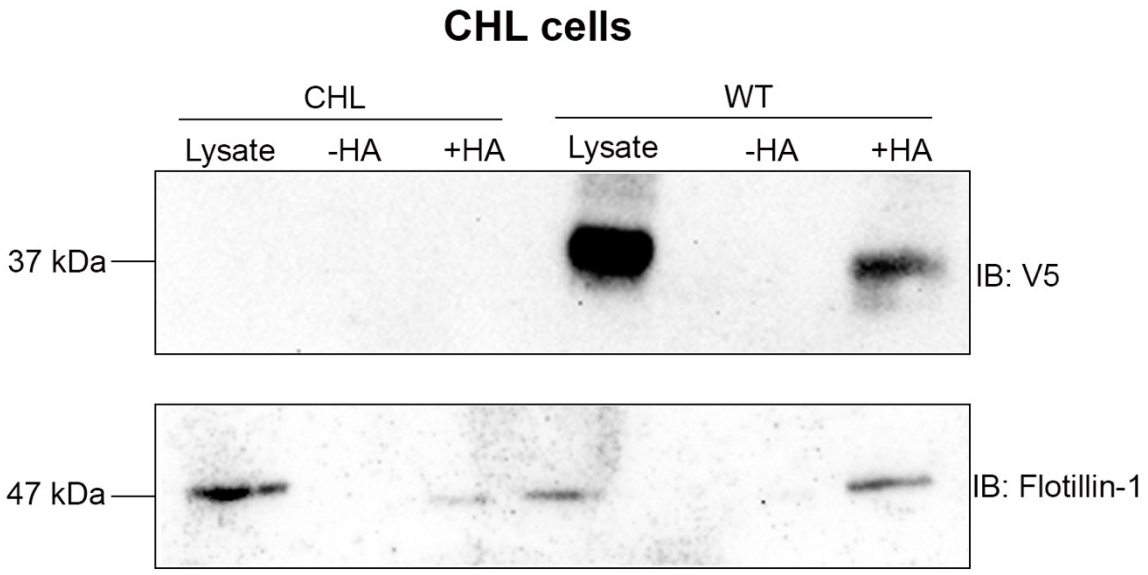

Figure 2.4. β1 is *S*-palmitoylated in CHL cells stably expressing β1-V5-2AeGFP.

Additional representative experiment of CHL cells stably expressing β1-V5-2AeGFP processed for the Acyl-RAC assay. *S*-palmitoylation of β1-V5 is detected in CHL cells using an antibody against V5, as shown by the hydroxylamine-dependent V5 signal, compared to the expected absence of V5 signal in the -HA lane. Flotillin-1 is used as a positive control for the Acyl-RAC assay.

β1 is S-palmitoylated at cysteine residue 162.

To identify the palmitoylated cysteine residue(s) in β1, we first determined the number of palmitoylated sites on β1 using a mass-tag labeling technique, Acyl PolyEthylene Glycol exchange (Acyl PEG). In this assay, free cysteine residues are blocked with the alkylating reagent, N-ethyl maleimide. Palmitate groups linked to cysteine residues are subsequently cleaved with hydroxylamine and replaced with a 10 kDa PEG- maleimide group, resulting in a 10 kDa shift in the apparent molecular weight of the polypeptide for each palmitoylated cysteine residue, as detected by western blot [154]. CHL cells stably expressing WT β1-V5-2AeGFP were subjected to Acyl PEG. We observed a single 10 kDa shift in the apparent molecular weight of β1-V5, which occurred in a hydroxylamine specific manner, suggesting that β1 is singly palmitoylated (**Fig. 2.5A, Fig. 2.6A**). Based on homology models with the CAM myelin P0, which is *S*-palmitoylated at cysteine 153, we predicted that β1 would be palmitoylated at the homologous residue, cysteine 162 [155]. Using site-directed mutagenesis, we engineered a cDNA construct in which β1 cysteine (C) residue 162 was converted to an alanine (A) and generated a stable β1-p.C162A-V5-2AeGFP CHL cell line. To test the effects of the C162A mutation on β1 palmitoylation, we subjected β1-p.C162A-V5-2AeGFP CHL cell lysates to both Acyl PEG and Acyl-RAC. Using Acyl PEG, showed a hydroxylamine-dependent PEGylation-induced mass shift in WT β1-V5 but not in β1-p.C162A-V5, suggesting that β1-p.C162A-V5 cannot be palmitoylated (**Fig. 2.5A, Fig. 2.6A**). Fig. 2.5A demonstrates a faint, yet present "apo" β1-p.C162A-V5 signal in the -HA lane, which represents unmodified polypeptide. The control lane is included to show that any PEGylation-induced mass shift observed in the +HA lane is hydroxylamine dependent. In this instance, despite the faint "apo" β1-p.C162A-V5 signal in the -HA lane, the β1-p.C162A-V5

signal in the lysate lane is comparable to the WT β1-V5 signal in the lysate lane, suggesting that the lack of mass shift observed in the +HA lane for β1-p.C162A-V5 mutant is not due to the lack of starting material, but rather due to the loss of the only palmitoylated cysteine residue in β1. We confirmed these results by subjecting β1-p.C162A-V5-2AeGFP CHL cell lysates to Acyl-RAC, where we observed a 92% reduction in the hydroxylamine-dependent signal for β1-p.C162A-V5, compared to WT β1-V5 (**Fig. 2.5B, C**). These results demonstrate that β1 is singly palmitoylated at cysteine 162 and that mutating this site to alanine completely abolishes β1 palmitoylation (**Fig. 2.5D**).

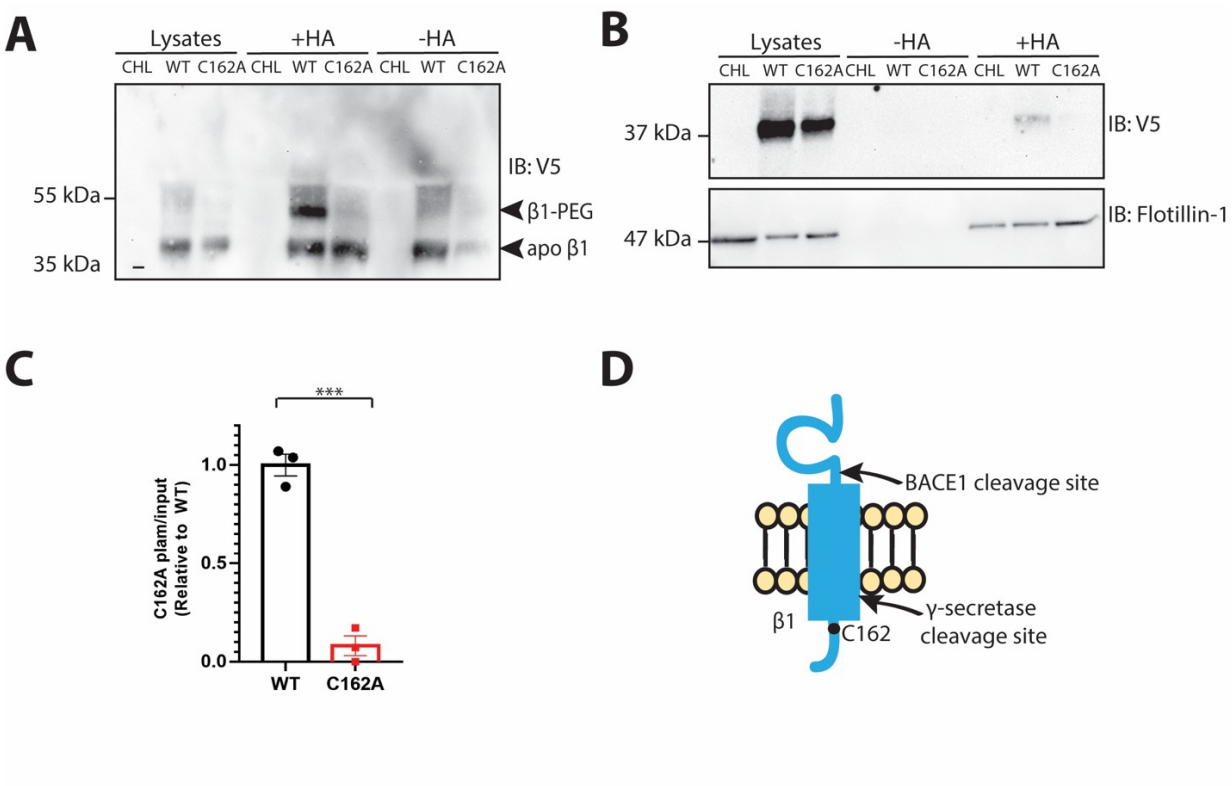

Figure 2.5. β1 is *S*-palmitoylated at cysteine 162.

A. CHL cells stably expressing β1-V5-2AeGFP or β1-p.C162A-V5-2AeGFP were processed for the Acyl PEG assay to determine the number of palmitoylated cysteines on β1. A single 10 kDa shift in the apparent molecular weight of β1 was observed in a hydroxylamine-specific manner, using an antibody against V5. Compared to WT β1-V5, β1-p.C162A-V5 showed no hydroxylamine-dependent PEGylation-induced mass shift, suggesting loss of the palmitoylation site upon mutation of cysteine to alanine at β1 residue 162 of β1. N=3. **B.** CHL cells stably expressing β1-p.C162A-V5-2AeGFP were subjected to the Acyl-RAC assay to detect the effect of the mutation of β1 *S*-palmitoylation. *S*-palmitoylation of β1-p.C162A-V5 is not detected in CHL cells using an antibody against V5, as shown by the absence of anti-V5 signal in the +HA lane, compared to WT β1-V5. N=3. **C.** Quantification of B. Signal from +HA lane was normalized to total protein for that construct and normalized again to WT β1-V5 palmitoylation levels. Significance ($p = 0.0003$) was determined using a student's *t-test*. **D.** Cartoon diagram of β1 and its identified palmitoylation site.

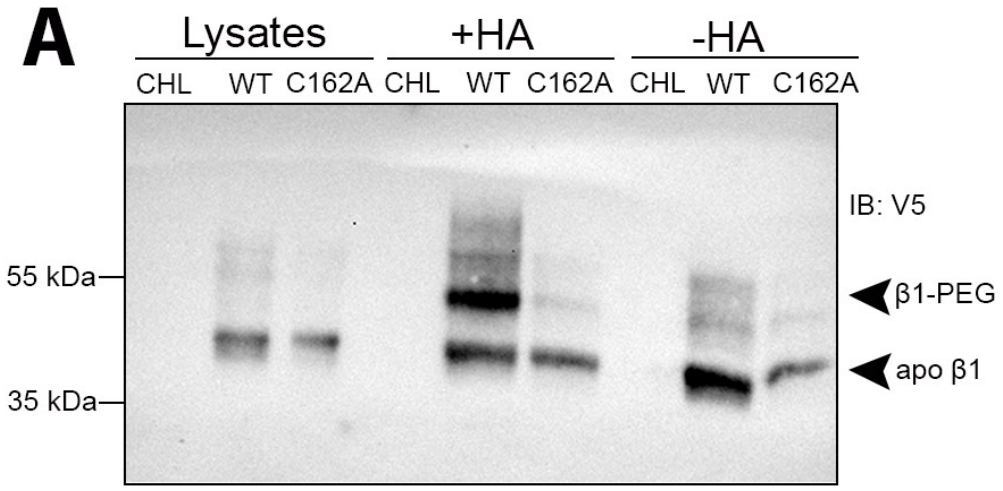

Figure 2.6. β1 is singly *S*-palmitoylated at cysteine 162 by the acyl PEG assay.

A. Additional representative experiment of β1-V5-2AeGFP-stably expressing CHL cell lysates subjected to acyl PEG revealed a single 10 kDa shift in the apparent molecular weight of β1 in a hydroxylamine-specific manner, using an antibody against V5. In contrast, β1-p.C162A-V5-2AeGFP-stably expressing CHL cell lysates subjected to acyl PEG did not reveal a 10 kDa shift in the apparent molecular weight of β1 in a hydroxylamine-dependent manner, using an antibody against V5, suggesting loss of β1 palmitoylation when cysteine 162 is mutated to an alanine.

β1 S-palmitoylation regulates its plasma membrane localization.

We asked whether palmitoylation regulates β1 association with the plasma membrane by comparing β1-p.C162A-V5 to WT β1-V5 in cell surface biotinylation assays. We found the level of β1-p.C162A-V5 polypeptide associated with the plasma membrane to be 78% less than WT (1.00±0.1621 for WT versus 0.2271±0.0142 for β1-p.C162A), as indicated by the reduced β1-p.C162A-V5 signal in the neutravidin-selected lane (normalized to total protein expression), compared to WT β1-V5 (**Fig. 2.7A, B, Fig. 2.8A**). HSP90 was used as a negative control, as in previous work, to ensure that no intracellular biotinylation is occurring [156, 157]. These results suggest that *S*-palmitoylation promotes plasma membrane association of β1.

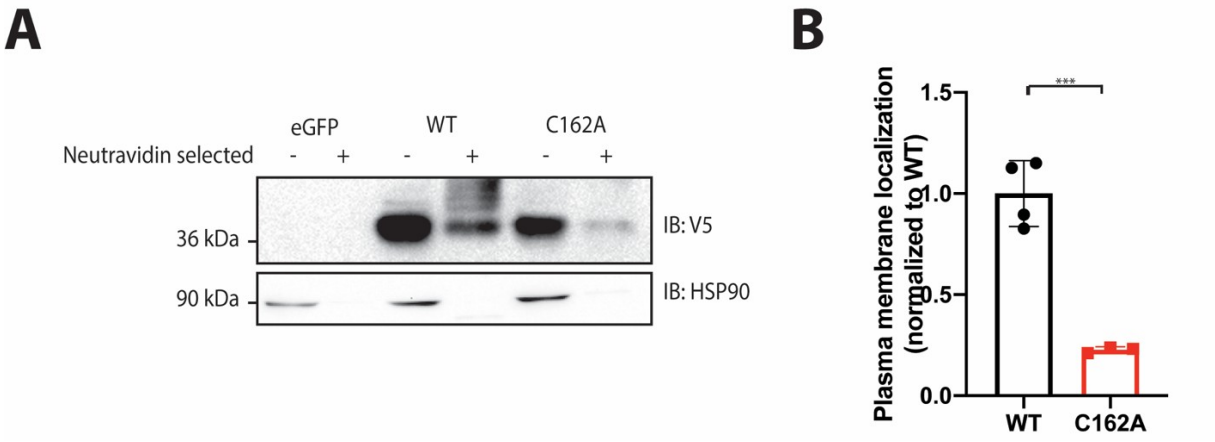

Figure 2.7. *S*-palmitoylation regulates plasma membrane localization of β1.

A. CHL cells stably expressing β1-V5-2AeGFP or β1-p.C162A-V5-2AeGFP were processed for cell surface biotinylation assay. The level of β1-p.C162A-V5 protein in the biotinylated plasma membrane fraction was reduced compared to WT β1-V5, as evidenced by the lower anti-V5 signal in the neutravidin- selected lane. Soluble HSP90 was used as a negative control. N=3-4. **B.** Quantification of A. Quantification represents the amount of β1 at the membrane/total β1 protein expression, normalized to WT plasma membrane levels, to obtain a percent reduction in plasma membrane localization in the mutant relative to WT β1 (N=3-4 for each construct).

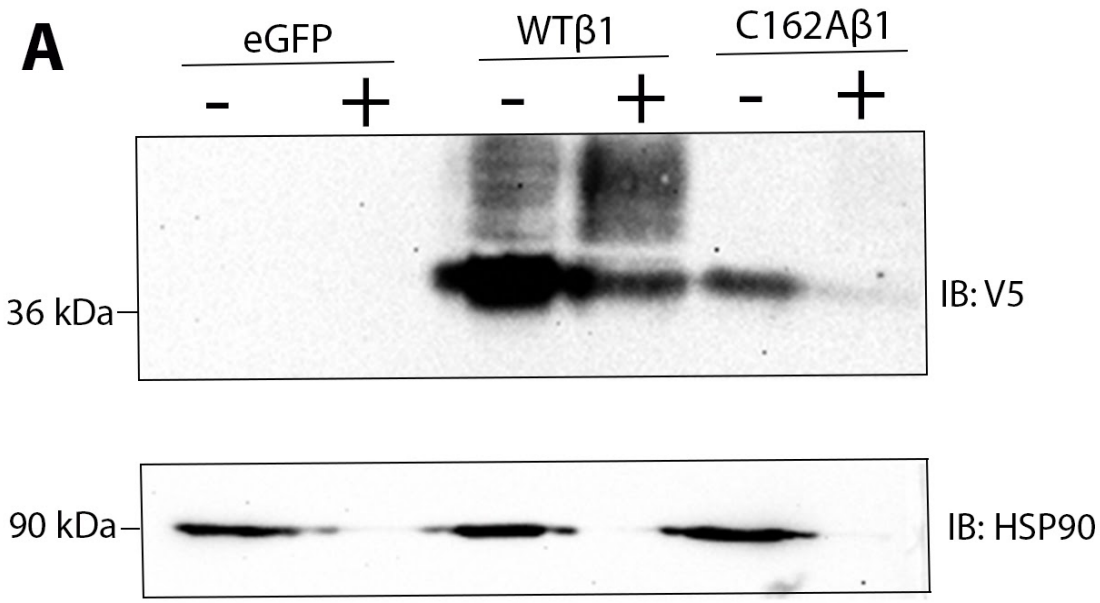

Figure 2.8. Localization of palmitoylation-null β1-pC162A is reduced at the plasma membrane, compared to WTβ1.

A. Additional representative experiment demonstrating that the level of β1-p.C162A-V5 protein in the biotinylated plasma membrane fraction was reduced compared to WT β1-V5, as evidenced by the lower anti-V5 signal in the neutravidin-selected lane. This biotinylation experiment was performed from lysates from CHL cells stably expressing β1-V5-2AeGFP or β1-p.C162A-V5-2AeGFP. Soluble HSP90 was used as a negative control. Quantification of this experiment was included in *Fig 2.7B.*

S-palmitoylation regulates β1 endocytosis, but not sorting into detergent-resistant membranes.

Palmitoylation has been shown to regulate the partitioning of certain proteins to cholesterol-rich lipid raft microdomains [158]. We asked whether palmitoylation governed the localization of β1 to lipid rafts, similarly to what has been shown previously for APP [149]. β1 is known to localize to detergent-resistant membrane (DRM) fractions of mouse brain and primary neuronal cultures [124, 142]. To verify the presence of β1 in DRM fractions in CHL cells stably expressing WT β1- V5, we prepared DRMs using density gradient centrifugation and analyzed them by western blot using anti-V5 antibody. We found that WT β1- V5 was present in both detergent-insoluble fractions, marked with flotillin-1, and in detergent-soluble fractions, marked with transferrin receptor, similar to previous results (**Fig. 2.9A**) [145]. We observed no differences in this distribution for the palmitoylation-null mutant, β1-p.C162A-V5, as evidenced by the presence of anti-V5 signal in both flotillin-1-marked DRMs and transferrin receptor-marked non-lipid raft domains (**Fig. 2.9A**). These data suggest that, while palmitoylation of β1 is necessary for its proper association with the plasma membrane, it does not regulate the partitioning of β1 into lipid-raft domains.

Due to the observed reduction of β1-p.C162A at the plasma membrane, we compared the extent of WT β1 vs. β1-p.C162A internalization through endocytosis. We treated CHL cells stably expressing β1-V5-2A-eGFP or β1-p.C162A-V5-2A-eGFP with vehicle (0.1% DMSO) or 1 μM of the dynamin inhibitor, Dyngo-4a, and assessed the amount of β1-V5 vs. β1-p.C162A-V5 accumulation at the cell surface by biotinylation. Anti-HSP90 antibody was used as a negative control for the plasma membrane fraction and anti-transferrin receptor (TfR) antibody

was used as a positive control for endocytosis inhibition with Dyngo-4a. We found that Dyngo-4a administration normalized the level of β1-p.C162A-V5 in the plasma membrane fraction to that of WT β1, implicating clathrin-dependent endocytosis in this process (**Fig. 2.9B**). Immunoprecipitation experiments are inherently variable. This variability accounts for the apparent presence of higher levels of plasma membrane association of β1-p.C162A in the DMSO-treated control samples compared to WT β1 DMSO-treated control samples. It is important to note that, in this particular instance, pull-down was more efficient in the mutant DMSO-treated samples compared to WT, as evident by the higher TfR signal. This work adds new information to the VGSC field, showing that WT β1 subunits undergo endocytosis via a clathrin-dependent mechanism and suggest the palmitoylation may confer plasma membrane stability to β1 polypeptides.

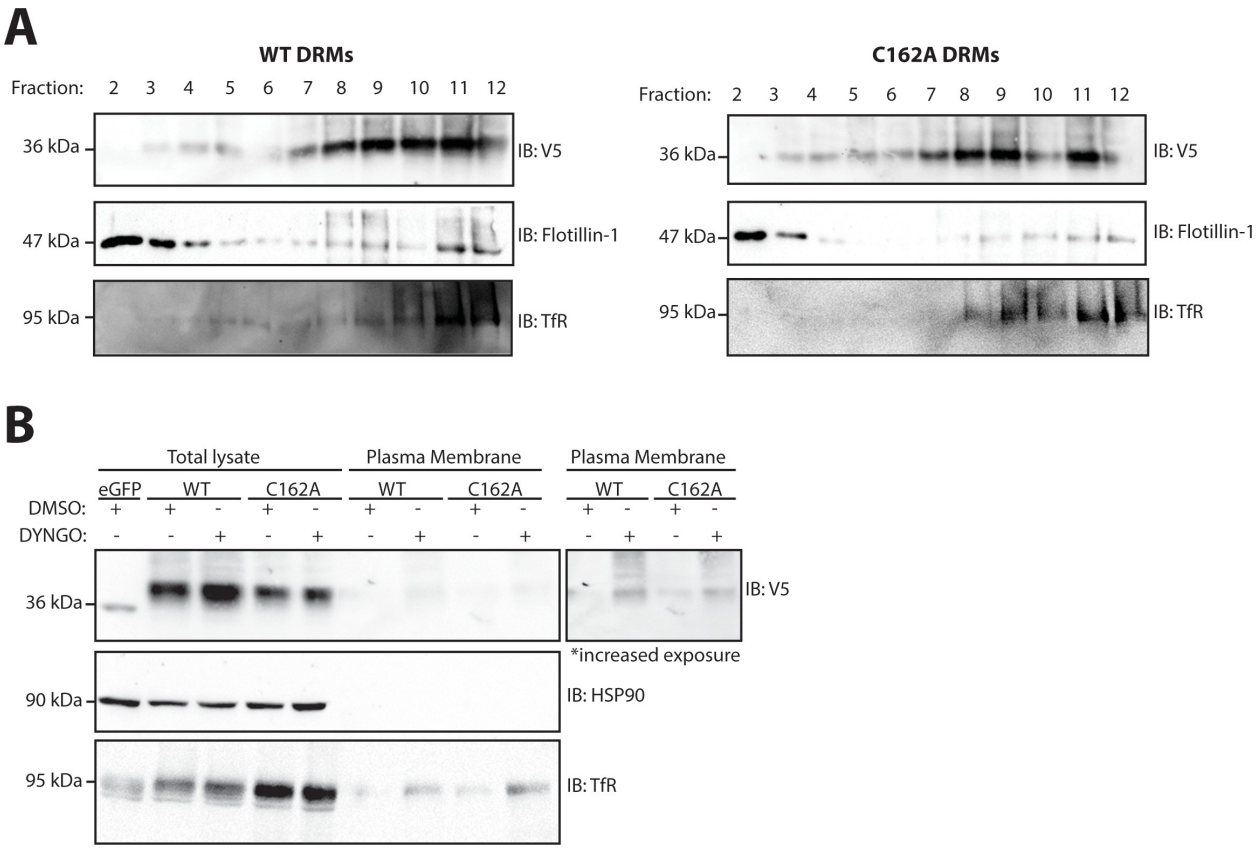

Figure 2.9. *S*-palmitoylation regulates β1 endocytosis, but not sorting into detergent-resistant membranes.

A. CHL cells stably expressing β1-V5-2A-eGFP or β1-p.C162A-V5-2A-eGFP were processed for discontinuous flotation density gradients to investigate the role of palmitoylation in detergent-resistant membrane partitioning of β1. β1-p.C162A-V5 did not partition differently than WT β1-V5. Flotillin-1 was used as a marker for lipid rafts, whereas Transferrin Receptor (TfR) was used as a marker for non-raft domains. N=3. **B.** CHL cells stably expressing β1-V5-2A-eGFP or β1-p.C162A-V5-2A-eGFP were treated with vehicle (0.1% DMSO) or 1 μM Dyngo-4a and assessed by cell surface biotinylation. Dyngo-4a treatment restores the plasma membrane level of β1-p.C162A-V5 to that of WT β1. N=3.

The level of β1-p.C162A RIP is reduced compared to WT.

We hypothesized that reduction in plasma membrane localization of β1-p.C162A-V5 would reduce its level of RIP. To test this hypothesis, we treated stable β1-V5-2AeGFP or β1-p.C162A-V5-2AeGFP CHL cells with vehicle (0.1% DMSO) or 1 μM DAPT, and assessed formation of the ~20 kDa β1 intramembrane CTF by western blot analysis. As shown previously, inhibition of γ-secretase by DAPT results in β1-CTF accumulation in the presence of normally occurring BACE1 cleavage [143]. If BACE1-mediated β1 cleavage were altered or reduced, DAPT administration would result in reduced levels of β1-CTF accumulation due to a reduction in available substrate for γ-secretase-mediated RIP. As expected, DAPT treatment of CHL cells stably expressing WT β1-V5 resulted in β1-CTF accumulation (**Fig. 2.10A, B**). In contrast, using the β1-p.C162A-V5 mutant construct as substrate resulted in an 80% loss in the level of cleavage product compared to WT (**Fig. 2.10A, B**). This result suggests that BACE1 cleaves the small fraction of β1-p.C162A-V5 that is localized to the plasma membrane, generating a reduced level of β1-CTF in response to DAPT treatment, compared to WT β1. These data demonstrate that β1 palmitoylation promotes β1 plasma membrane localization, which allows RIP to occur.

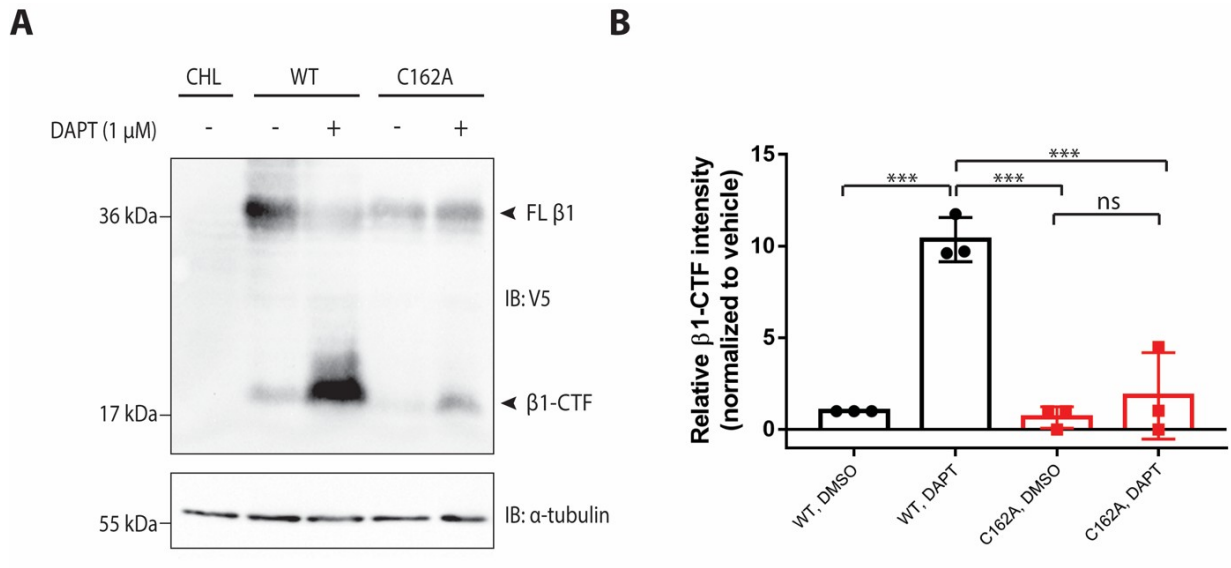

Figure 2.10. The absence of β1 *S*-palmitoylation at cysteine 162 reduces its level of RIP.

A. CHL cells stably expressing β1-V5-2AeGFP or β1-p.C162A-V5-2AeGFP were treated with vehicle (0.1% DMSO) or 1 µM DAPT. Lysates were subjected to western blotting analysis to investigate the level of β1 cleavage. Compared to WT β1-V5, β1-p.C162A-V5, shows little to no cleavage product. N=3. **B.** Quantification of A. Protein levels were normalized to the loading control and reported as fold change respective to the vehicle treated group. Significance (p-value<0.05) was determined using one-way ANOVA. Plotted as the mean ∓SD.

β1 mediated modulation of I_{Na} is not affected by palmitoylation.

We next asked whether palmitoylation-deficient β1-p.C162A-V5 could modulate I_{Na}. WT β1-V5-2AeGFP, β1-p.C162A-V5-2AeGFP, or eGFP were transiently expressed in HEK-hNa$_v$1.5 cells. We found that WT β1-V5 and β1-p.C162A-V5 increased I_{Na} density to a similar extent, compared to the soluble eGFP control (**Fig. 2.11A, B**). In agreement with the observed increase in peak I_{Na} density, peak conductance was increased by co-expression of WT β1-V5-2AeGFP or β1- p.C162A-V5-2AeGFP (**Fig. 2.11C**). No changes in capacitance were observed (**Fig. 2.11D**). We observed no effect of either β1 construct on the voltage-dependence of I_{Na} activation or inactivation (**Table 2.1**). These data suggest that the small fraction of β1-p.C162A-V5 that remains properly localized to the plasma membrane (**Fig. 2.7A, B**) is sufficient to modulate I_{Na}.

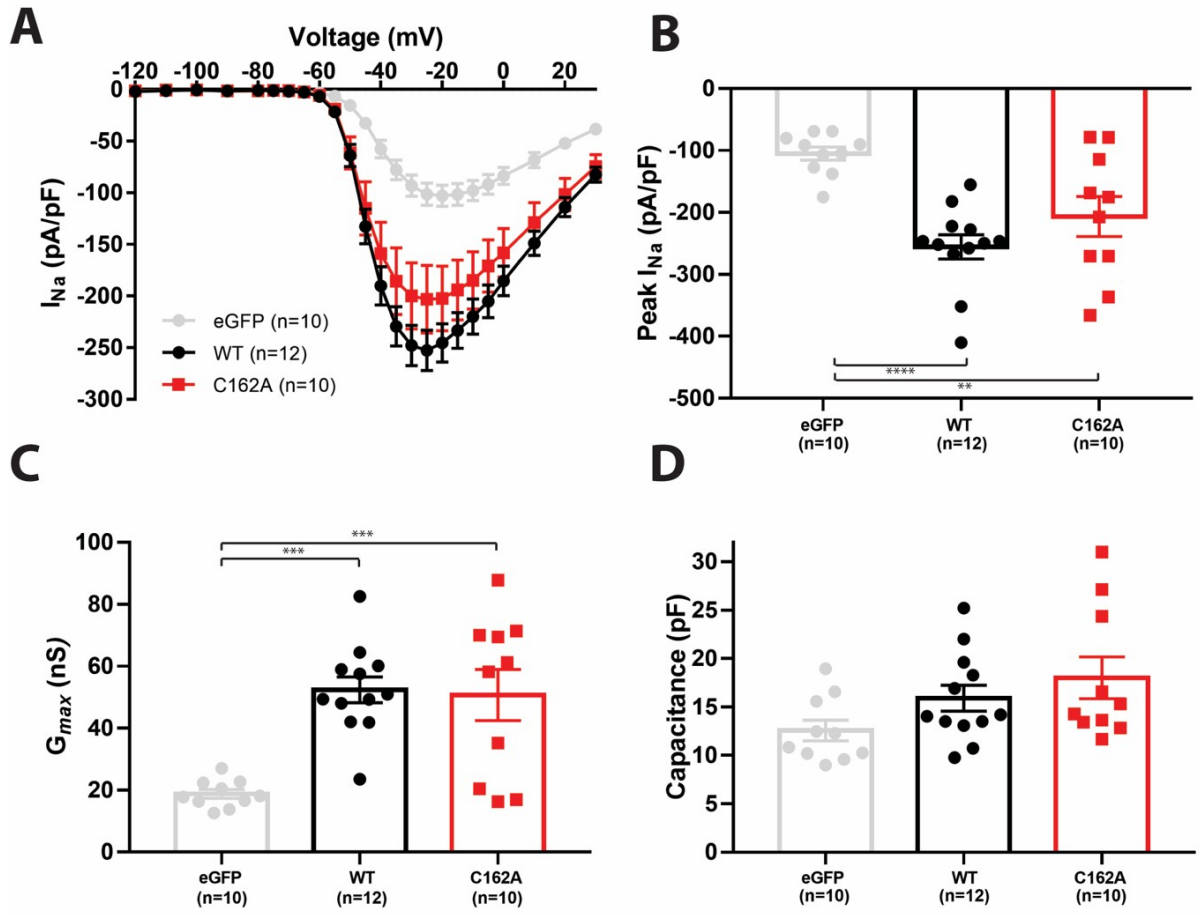

Figure 2.11. β1-mediated modulation of I_{Na} density is not dependent on *S*-palmitoylation of β1 at residue C162.

HEK-hNa$_v$1.5 cells were transiently co-transfected with eGFP (light grey; black circles), WTβ1 (black circles), or β1-p.C162A (red squares). **A.** I_{Na} current-voltage (I-V) relationship. **B.** Peak I_{Na} is significantly increased with co-expression of WTβ1 or β1-p.C162A over eGFP. **C.** Peak conductance (G_{max}) is significantly increased with co-expression of WTβ1 or β1-p.C162A over eGFP. **D.** No significant difference in the capacitance (in pF) measured from each cell. Data presented in (A), (B) and (C) result from at least 3 separate transfections and are presented as mean ± SEM. *$p < 0.05$ versus eGFP; ***$p < 0.001$ versus eGFP; ****$p < 0.0001$ versus eGFP.

Discussion

VGSC β1 subunits are multi-functional signaling molecules. In addition to modulating the gating, kinetics, and localization of VGSC α subunits, β1 subunits function in cell-cell and cell-matrix adhesion, cell migration, calcium handling, modulation of potassium currents, neuronal pathfinding, fasciculation, and neurite outgrowth [115]. Human *SCN1B* LOF variants are linked to EI-DEE and cardiac arrhythmia, often resulting in sudden death [115].

It is important to understand how β1 subunits are post-translationally processed and whether this differential processing affects their functionality. We showed previously that β1 is tyrosine phosphorylated [129]. Here, we extend those findings to show that fyn kinase directly phosphorylates a β1 peptide, supporting our previous, indirect, hypothesis using neurons from *fyn* null mice [124]. β1 subunits undergo RIP through the activity of BACE1 and γ-secretase [142, 143]. Initial cleavage of β1 by BACE1 sheds the β1 Ig ectodomain and leaves behind the β1 C- terminal fragment in the membrane, which undergoes subsequent cleavage by γ-secretase to generate a soluble intracellular domain, the β1-ICD [142]. Recent work by our laboratory demonstrated that the β1-ICD can translocate to the nucleus, where it participates in transcriptional regulation to ultimately modulate sodium, potassium, and calcium currents in mouse ventricular myocytes [143]. Overexpression of the β1-ICD resulted in the downregulation of genes related to proliferation, immune response, and sodium and potassium channels. In contrast, loss of β1-ICD in *Scn1b*-null mouse cardiac ventricular tissue resulted in the upregulation of these gene groups, suggesting that the β1-ICD may act as part of a transcriptional repressor complex under normal physiological conditions. Here, we asked whether β1 tyrosine

phosphorylation or β1 *S*- palmitoylation can regulate β1 RIP. Using β1 phosphorylation-null and phosphomimetic mutant constructs, we found that β1 tyrosine phosphorylation at Y181 does not regulate β1 RIP.

Here, we demonstrate that β1 is lipid-modified by *S*-palmitoylation in the brain, that *S*-palmitoylation, but not tyrosine phosphorylation, regulates β1 RIP by facilitating β1 localization to the plasma membrane, and that β1 subunits undergo clathrin-mediated endocytosis, at least in the absence of VGSC β subunits. Our results suggest that β1 must be associated with the plasma membrane for RIP to occur and that *S*-palmitoylation at residue C162 stabilizes β1 plasma membrane association and reduces its level of endocytosis. Given that *S*-palmitoylation has been shown to contribute to protein stability in other work [150], it is possible that reduction of palmitoylation-null β1-C162A protein expression compared to WT β1 is due to decreased β1 protein stability. It will be important to test this hypothesis in follow-up studies. Residue C162, at which β1 is palmitoylated, is conserved in VGSC β3 subunits, and thus may implicate palmitoylation as a similar regulatory mechanism in these proteins. The absence of this conserved residue in VGSC β2 and β4 suggests alternative regulatory mechanisms (**Fig. 2.12**). Previous work has shown that palmitoylation of APP promotes its RIP through regulating its subcellular localization [149]. Although other RIP substrates, e.g. LRP1 and N-cadherin, have been shown to be palmitoylated, whether palmitoylation also regulates their RIP is not known [146, 157].

The biochemical experiments described here were performed in the absence of VGSC α subunits. It will be interesting in future work to consider the effects of α subunit co-expression on

β1 subunit post-translational processing. While a large body of work has shown that β1 subunits function as molecular chaperones for VGSC α subunits to the plasma membrane [159], there is no evidence to support the promotion of β1 subunit cell surface expression by α subunits. We do not know whether the reduction in β1-C162A cell surface expression compared to WT β1 shown here could be due to the absence of a co-expressed α subunit. One possible interpretation of our electrophysiological data showing that β1-C162A increases I_{Na} density similar to WT is that the presence of an α subunit changes the behavior of this mutant, resulting in inter-subunit, synergistic effects. Biochemical assessment of whether α subunits can promote β1 cell surface expression would be complicated by the non-covalent association of these subunits. Non-covalent α–β1 association precludes separation of the pool of β1 subunits associated with α from those that are not, using standard immunoprecipitation techniques. Furthermore, because VGSC α and β1 subunits are each ankyrin-binding proteins [125, 129, 160, 161], they may associate in a complex, as assessed by co-immunoprecipitation, but not physically interact. Nevertheless, examining the effects of β1 palmitoylation and phosphorylation in the presence of VGSC α subunits, both in heterologous systems and within the channelome complex in brain and heart *in vivo*, will be interesting future directions of this work.

The effects of β1 co-expression on I_{Na} voltage-dependent properties in heterologous systems are inconsistent throughout the literature [159]. Here, we show that co-expression of $hNa_v1.5$ with β1 or the mutant β1 subunits did not statistically change the voltage dependence of activation or steady-state inactivation compared to α (eGFP) alone. In contrast, we observed increased peak I_{Na} density and peak conductance, in agreement with the well-established role of WT β1 subunits in increasing VGSC function by increasing their plasma membrane expression

[159]. Interestingly, co-expression of the Y181 or C162 β1 mutants resulted in increased peak I_{Na} density and maximal conductance. Finally, while $Na_v1.5$ is the major cardiac VGSC, a sizable body of work in recent years has also identified $Na_v1.5$ in the brain [162-164], suggesting that our results may be applicable to other VGSCs.

Importantly, *Scn1b* deletion in mice and heterologous β1 expression in cell culture are not comparable. *Scn1b* null mouse cardiac myocytes have increased I_{Na} density due to developmentally regulated increases in the expression of *Scn3a* and *Scn5a* mRNA and protein [135, 136]. As described above, our group has recently shown that β1 is a substrate for RIP by BACE1 and gamma-secretase *in vivo* [143]. The cleaved C-terminal fragment of β1 can translocate to the nucleus, resulting in reduced expression of a number of genes, including ion channels. We have proposed that the absence of β1 subunits in *Scn1b* null animals results in the absence of gene repression and subsequent increased ion channel expression. This situation is very different than acute, heterologous overexpression of VGSC β1 and α subunit cDNAs, in which β1 subunits function to chaperone α subunits to the plasma membrane, as demonstrated here. The required genetic regulatory elements are not present in the cDNA plasmids. Moreover, while β1-chaperone function is lost in *Scn1b* null mouse myocytes, I_{Na} reductions are not observed. It is likely that the presence of a host of other protein components of the channel proteome that retain VGSCs in the cardiac myocyte plasma membrane [165].

In conclusion, *S*-palmitoylation is a reversible post-translational modification, making it a highly dynamic and tunable process [36, 65, 77, 89]. Multiple palmitoyl acyltransferase enzymes, which mediate substrate palmitoylation, as well as protein thioesterases, which depalmitoylate

substrates, are implicated in this process. The molecular identities of the enzymes that palmitoylate and depalmitoylate β1 subunits are not known, but may be identified in the future to discover novel targets for *SCN1B*-linked pathophysiology. In addition, we do not yet know whether the level of β1 palmitoylation can be dynamically regulated by extracellular stimuli or by altered excitability, but this information will be important to elucidate as attempts to implicate this post-translational processing in disease mechanisms move forward. It is possible that β1-mediated transcriptional regulation via RIP can be manipulated by altering the level of β1 palmitoylation. Additionally, the effects of *SCN1B* disease-linked variants on β1 subunit palmitoylation, RIP, and transcriptional regulation should be considered.

A

```
sp|Q07699|SCN1B_HUMAN      MYVLIVV-----LTIWLVAEMIYCYKKIAAATETAAQENASEYLAITSESKENCTGVQVA 217
sp|Q9NY72|SCN3B_HUMAN      MYILLVF-----LTLWLLIEMIYCYRKVSKAE-EAAQENASDYLAIPSENKENSAVP-VE 214
sp|O60939|SCN2B_HUMAN      GASVGGFLAVVILVLMVVKCV-------RRKK---------EQKL-STDDLKTEEEGKTDG 206
sp|Q8IWT1|SCN4B_HUMAN      LAVVGGVIGLLILILLIKKLIIFILKKTREKK---------KECLVSSSGNDN------TE 212
                              :  .     * : :   :                  .: *   .  .
```

Figure 2.12. Protein sequence alignment of β1-β4 in region surrounding the palmitoylation site.

Alignment was completed using standard settings on Clustal Omega. Asterisk (*) indicates completely conserved residue; Colon (:) indicates conservation of residues with strongly similar properties; Period (.) indicates conservation of residues with weakly similar properties.

Materials and Methods

Cell culture

CHL cell lines stably expressing β1 or β1 mutants and stable HEK-hNa$_v$1.5 cells were grown in Dulbecco's Modified Eagle Medium with 5% heat inactivated fetal bovine serum, penicillin/streptomycin, and 600 μg/mL at 37°C, 5% CO_2. Stable cell lines were generated by transfecting parental CHL cells with 1 μg of cDNA with 5 μL of Lipofectamine 2000. 48 hours following transfection, cells were split into media containing 600 μg /mL G418 (Gibco). The cells were grown for approximately one week or until eGFP positive colonies were large enough to isolate. Individual colonies were selected and grown until confluent and characterized by western blot analysis. Patch clamp experiments used transient transfection of β1 cDNAs into stable HEK-hNav1.5 cells. 1 μg of cDNA was transfected with 5 μL of Lipofectamine 2000 (Invitrogen). Approximately 12 hours post-transfection cells were plated for electrophysiological recordings. Patch clamp was completed approximately 12 hours post final plating.

Antibodies

Primary antibodies used were: anti-β1$_{intra}$ (1:1000 dilution, Cell Signaling Technology), anti-V5 (1:1000 dilution, Invitrogen), anti-α-tubulin (1:10,000 dilution, Cedar Lane), anti-BACE1 (1:1000, Invitrogen), anti-HSP90 (1:1000 dilution, EnzoScientific), anti-TfR (1:1000 dilution, Thermo), and anti-flotillin-1 (1:1000, Cell Signaling Technologies). The specificity of anti-β1$_{intra}$ has been shown previously by western blot [156]. HRP-conjugated secondary antibodies were used in this study. Goat anti-rabbit or goat anti-mouse HRP-conjugated antibodies were diluted 1:1000 (anti-β1$_{intra}$, anti-α-tubulin, anti- presenilin-1, anti-BACE1, anti-TfR) or 1:10,000

(anti-V5, anti-flotillin-1 or anti-HSP90). Alexa Fluor 568 anti-mouse was used as a secondary (1:500 dilution) as a secondary antibody for anti-V5 in immunocytochemistry experiments.

Expression Vectors

A synthesis-optimized human WT β1-V5-2A- eGFP cDNA was generated by gBLOCK from Integrated DNA technologies based on NP_001028.1. The bicistronic cDNA construct included an in-frame β1 C-terminal V5 epitope tag followed by a self-cleaving 2A peptide and enhanced Green Fluorescent Protein (eGFP) to facilitate immune-detection of β1 as well as transfected cells by eGFP. β1-p.C162A-V5-2A- eGFP, β1-p.Y181A-V5-2A-eGFP, and β1-p.Y181E-V5-2A-eGFP were generated by site-directed mutagenesis using the WT β1-V5-2A-eGFP cDNA construct in pENTR-SD/D TOPO as the template. The eGFP alone control was generated by PCR from their respective full-length template cDNAs containing WT β1-V5-2A-eGFP. Using the Gateway cloning system, all constructs were moved from pENTR-SD/D- TOPO to pcDNAdest40 via LR Clonase reaction according to the manufacturers' protocol.

The amino acid numbering scheme for the β1 polypeptides used throughout the paper excludes the N-terminal, 19 amino acid signal peptide, as described in the original report of the β1 cDNA sequence [120].

Animals

Animals were housed in the Unit for Laboratory Animal Medicine at the University of Michigan. All procedures were performed in accordance with the NIH and the University of Michigan Institutional Animal Care and Use Committee (IACUC).

Measurement of I_{Na} by whole-cell voltage clamp

Voltage-clamp recordings were performed at room temperature (RT) in the whole-cell configuration using an Axopatch 700B amplifier and pClamp (versions 11, Axon Instruments, Foster City, CA) with 1.5–2.5 MΩ patch pipettes. I_{Na} was recorded in the presence of a bath solution containing (in mM): 120 NaCl, 1 $BaCl_2$, 2 $MgCl_2$, 0.2 $CdCl_2$, 1 $CaCl_2$, 10 HEPES, 20 TEA-Cl and 10 glucose (pH 7.35 with CsOH, Osmolarity: 300–305 mOsm). Fire-polished patch pipettes were filled with an internal solution containing (in mM): 1 NaCl, 150 N-methyl-D-glucamine, 10 EGTA, 2 $MgCl_2$, 40 HEPES, and 25 phosphocreatine-tris, 2 MgATP, 0.02 Na2GTP, 0.1 Leupectin (pH 7.2 with H2SO4). Sodium current was recorded in response to a series of voltage steps between -100 and +30 mV in 5 mV increments, from a holding potential of -90 mV for 200 msec. A step back to -20 mV for 200 msec was used to determine the voltage-dependence of inactivation. Series resistance was compensated 40–65% and leak subtraction performed by application of a standard P/4 protocol. Normalized conductance and inactivation curves were generated as described previously [166]. Current densities were determined by dividing current amplitude by the cell capacitance (Cm), as determined by application of +10 mV depolarizing test pulses.

Cleavage assays

Stably transfected CHL cells were grown to approximately 70% confluence in 100 mm tissue culture plates. Cells were treated with vehicle (0.1% DMSO) or 1 μM DAPT (Cayman Chemical), as indicated in the figure legends. After a 24-hour treatment, cells were harvested, and membranes were prepared. Briefly, cells pellets were harvested and resuspended in 50 mM

Tris, pH 8.0 with Complete protease inhibitors, EDTA-Free (Roche). On ice, cells were homogenized 10 times with a dounce followed by sonication. To remove nuclei and insoluble material, lysates were spun at 2,537xg for 10 at 4°C. The supernatant was removed and spun at 80,000 x g for 15 min at 4°C. The supernatant was removed, and the membrane-containing pellets were resuspended in 133 µL of 50 mM Tris, pH 8.0 with Complete protease inhibitors, EDTA-Free (Roche) and sonicated on ice to resuspend the membrane-containing pellets. Samples were heated at 85°C for 10 minutes and separated using 12% SDS-PAGE gels and western blots were performed as described below.

Surface biotinylation assays

Stably transfected cells were grown to 90%-100% confluence in 100 mm tissue culture plates. Cell surface proteins were biotinylated using the Cell Surface Protein Isolation Kit (Pierce) following the manufacturer's instructions and as previously described [166]. All samples were heated at 85°C for 10 minutes and separated on 10% SDS-PAGE gels. Western blots were performed as described above. For endocytosis experiments, prior to cell surface biotinylation, cells were treated with vehicle (0.1% DMSO) or 1 □M Dyngo-4a for two hours in a 37□C incubator with 5% CO_2. HSP90 was used as a negative control to detect intracellular biotinylation. Any experiments in which intracellular contamination in the plasma membrane fraction was detected (e.g. HSP90 signal in the neutravidin-selected lane) were excluded.

DRM preparations

10 - 100mm dishes of CHL cells stably transfected with WT □1-V5-2AeGFP or p.C162A □1-V5-2AeGFP were grown to 90-100% confluence. As described previously [167], cells were

washed and resuspended in 2.5 mL of HES buffer (20 mM HEPES, 1 mM EDTA, 250 mM sucrose, pH 7.4) supplemented with 1 mM Na_3VO_4 and Complete Protease Inhibitors (Roche). Cells were homogenized by 10 passages through a 22-gauge needle and centrifuged at 245,000 x g for 90 minutes at 4°C. Membranes were resuspended with 10 passages through a 22 gauge needle in 2.5 mL of MBS buffer (25 mM MES, 15 mM NaCl, pH 6.5) with 1% Triton X- 100 and Complete Protease Inhibitors (Roche) and incubated for 20 minutes at 4°C. Homogenate was mixed with 2.5 mL of 90% sucrose. 5 mL of 35% sucrose and 2.5 mL of 5% sucrose were overlaid and samples were centrifuged at 200,000 x g in a swinging bucket rotor for 17 hours. 1 mL fractions were collected from top to bottom, heated at 85°C for 10 minutes with sample buffer, and subsequently analyzed by western blot.

Western blot analysis of cell lysates

Cell lysates were prepared either as described above for cleavage assays, surface biotinylation assays or DRMs, as appropriate. Loading buffer containing SDS, 5 mM β-mercaptoethanol, and 1% dithiothreitol was added to samples and heated for 10 min at 85°C. Protein lysates were separated by SDS-PAGE on 10 or 12% Tris-Glycine polyacrylamide gels as indicated in the figure legends, transferred to nitrocellulose membrane overnight (16 h, 55 mA, 4°C), and probed with antibodies, as indicated in the figure legends. Incubations with anti-V5 or anti-$\beta1_{intra}$ and their respective secondary antibodies were performed using a SnapID with 10-20 min incubations. Anti-α-tubulin, anti-TfR, anti- flotillin-1, and anti-HSP90 antibodies were incubated overnight at 4°C. Secondary antibodies were incubated for 1 h at RT. Immunoreactive bands were detected using West Femto chemiluminescent substrate (GE Health Sciences) and imaged using

an iBrightFL1000 (Invitrogen). Blots for each antibody were individually detected within the linear range using the smart exposure feature included in the software package for the Invitrogen iBright imager. Immunoreactive signals from cleavage assays were quantified using ImageJ and normalized to the level of α-tubulin and subsequently to vehicle treated samples.

Acyl Resin Assisted Capture (Acyl RAC)

Stably transfected cells were grown to approximately 90% confluence in 100 mm tissue culture plates. Cells were lysed in buffer containing 100 mM HEPES, 1 mM EDTA, 2.5% SDS, and 2% methyl methanethiosulfonate (MMTS) (Sigma), adjusted to pH 7.5, sonicated, and left to rotate at 40°C overnight. Acetone precipitation was performed to remove MMTS: 3x volume of cold acetone were used to precipitate the protein for 20 minutes at -20°C, before spinning down in standard bench-top ultracentrifuge at 5000 x g for 1 min. The supernatant was discarded and the pellet was washed 3x with 70% acetone, each time discarding the supernatant. Protein pellet was left to dry in air and stored overnight at -20°C. Twelve hours later, protein was resuspended in 500 µL of "binding" buffer containing 100 mM HEPES, 1 mM EDTA, and 1% SDS, adjusted to pH 7.5, sonicated, and vigorously shook for 1 h, before splitting the protein sample into 3 1.5 mL tubes, 1 with 40 µL for "unmanipulated" starting material, and 2 with 220 µL for the palmitoylation assay (one for +HA and one for -HA condition). A 1:1 slurry of pre-activated thiopropyl sepharose beads (GE) was prepared using binding buffer (50 mg beads = 250 µL of binding buffer). 50 µL of the activated bead slurry was added to each 220□L lysate. 50 µL of freshly prepared 2 M hydroxylamine (HA) (Sigma), adjusted to pH 7.5, were then added to the lysate designated "+HA", while 50 µL of 2M NaCl were added to the sample designated "-HA". Hydroxylamine/bead/lysate mixtures were left to incubate at RT for 2.5 h, rotating. To wash out

the hydroxylamine and NaCl, the beads were spun at 5000 x g for 1 minute, and the supernatant was removed and discarded. Bead resin was washed 5x with 1 mL of binding buffer, each time spinning at 5000 x g for 1 minute and discarding the supernatant to recover the beads. Palmitoylated proteins were eluted using 50 µL of 5x sample buffer supplemented with 100 mM DTT. Samples were heated at 65°C for 10 minutes, separated on a 10% SDS-PAGE gel, transferred to nitrocellulose, and probed with anti-V5, using anti-flotillin-1 as a positive control.

Acyl PolyEthylene Glycol (Acyl PEG)

Stably transfected cells were grown to approximately 90% confluence in 100 mm tissue culture plates. Cells were lysed with blocking buffer consisting of 100 mM HEPES, 150 mM NaCl, 5 mM EDTA, 2.5% SDS, and 200 mM tris(2-carboxyethyl)phosphine (TCEP) (Sigma), adjusted to pH 7.5, sonicated, and rotated at RT for 1 h. After 1 h, 12.5 µL of freshly prepared 1 M N-ethyl maleimide (NEM) (dissolved in ethanol) (Sigma) for 25 mM final NEM concentration were added to each lysate, with rotation overnight at RT. To scavenge the NEM, 12.5 µL of 2,3-dimethyl 1,3-butadiene (Sigma) were added to each sample and rotated vigorously for one hour at RT. 100 µL of chloroform were added to each sample, vortexed vigorously for 1 minute, and centrifuged at max speed for 3 minutes to achieve phase separation. The supernatant on top of the resulting 'protein pancake' was split into 3 1.5 mL tubes: 1 containing 40 µL for "unmanipulated" starting material, 1 containing 100 µL designed for "+HA" condition, and 1 containing 100 µL designated for "-HA" condition. 20 µL of 2 M freshly prepared hydroxylamine (HA) (Sigma), adjusted to pH 7.5, were added to the lysate designated "+HA", while 20 µL of 2 M NaCl were added to the lysate designated "-HA". The HA/lysate mixture was incubated for 2 h at 40°C, rotating. The HA and NaCl were desalted using a pre-

equilibrated 40K MWCO Zebaspin desalting column (Thermofisher). 10 µL of a freshly prepared 20 mM stock of 5 kDa mPEG- maleimide (Sigma) (dissolved in water) were added to each desalted lysate and incubated for 2 h at 40°C, rotating. 100 µL of 5x sample buffer supplemented with 100 mM DTT were added to stop the mPEG-maleimide alkylation reaction and heated for 10 min at 65°C. The samples were separated on a 10% SDS-PAGE gel, blotted to nitrocellulose, and probed with anti-V5.

Fyn kinase assay

Fyn kinase assays were performed according to manufacturer's recommendations (Fyn kinase assay kit, Promega). Reactions were performed in triplicate and each reaction contained 200 ng of active GST-tagged Fyn kinase, 50 uM Ultrapure ATP, 0.2 mg/mL peptide substrate, 50 µM DTT diluted in a standard kinase reaction buffer (contents of 5X buffer: 40 mM Tris pH 7.5, 20 mM MgCl2, 0.1 mg/mL BSA). β1 peptides corresponded to intracellular domain of β1 surrounding Y181 (amino acids 175 to 185; β1 peptide, QENASEYLAITC; pYβ1 peptide, QENASE[pY]LAITC). The Poly E 4 Y 1 peptide is a well-characterized substrate of fyn kinase. Kinase reactions lacking substrate were used to normalize the kinase activity in substrate containing reactions. Three independent experiments were performed. Statistical significance was determined with Student's t-test.

Statistics

Statistical analysis for cleavage assay experiments were completed with n=3-4 for each experiment. Data are represented as the mean ± SEM. β1 mutant cleavage experiments were completed as one-way ANOVA with multiple comparisons to WT β1 treated with DAPT. For

the fyn kinase assay, three independent experiments were performed. Statistical significance was determined with Student's t-test. Data are represented as the mean ± SEM. Electrophysiology experiments had an n of 10-15 cells per condition for each experiment. The voltage-dependence of activation and inactivation were compared using nonlinear fit, maximum current was analyzed using one-way ANOVA with multiple comparisons, and current density was compared to the control, eGFP, with an unpaired t-test at each voltage-step.

Chapter 3: Ankyrin-B is Lipid-Modified by *S*-Palmitoylation to Promote Dendritic Membrane Scaffolding of Voltage-Gated Sodium Channel $Na_V1.2$ in Neurons

Julie M. Philippe and Paul M. Jenkins, PhD

Summary

Neuronal ankyrin-B is an intracellular scaffolding protein that plays multiple roles in the axon. By contrast, relatively little is known about the function of ankyrin-B in dendrites, where ankyrin-B is also localized in mature neurons. Recently, we showed that ankyrin-B acts as a scaffold for the voltage-gated sodium channel, $Na_V1.2$, in dendrites of neocortical pyramidal neurons. How ankyrin-B is itself targeted to the dendritic membrane is not well understood. Here, we report that ankyrin-B is lipid-modified by *S*-palmitoylation to promote dendritic localization of $Na_V1.2$. We identify the palmitoyl acyl transferase zDHHC17 as a key mediator of ankyrin-B palmitoylation in heterologous cells and in neurons. Additionally, we find zDHHC17 regulates ankyrin-B protein levels independently of its *S*-acylation function, through a conserved binding mechanism between the ANK repeat domain of zDHHC17 and the zDHHC ankyrin-repeat binding motif of ankyrin-B. We subsequently identify five cysteines in the N-terminal ankyrin repeat domain of ankyrin-B that are necessary for ankyrin-B palmitoylation. Mutation of these five cysteines to alanines not only abolishes ankyrin-B palmitoylation, but also prevents ankyrin-B

from scaffolding $Na_v1.2$ at dendritic membranes of neurons, suggesting palmitoylation is important for function of ankyrin-B at dendrites. Strikingly, loss of ankyrin-B palmitoylation does not affect ankyrin-B-mediated axonal cargo transport of synaptic vesicle synaptotagmin-1 in neurons. These data imply there may be two pools of ankyrin-B in neurons, one palmitoylation-dependent plasma-membrane pool at the dendrites, and one palmitoylation-independent vesicular pool at the distal axon.

Introduction

The ankyrin family of scaffolding proteins target and anchor membrane, cytoskeletal, and cytoplasmic proteins at specialized membrane domains to establish and maintain cell polarity and function in many vertebrate tissues [168]. One member of the ankyrin family, ankyrin-B, encoded by the *ANK2* gene, localizes ion channels, transporters, structural proteins, as well as signaling molecules to specialized membranes in the heart, skeletal muscle, adipocytes, and brain [169-174]. In neurons, multiple axonal roles have been shown for ankyrin-B, including axonal cargo transport, scaffolding of cell adhesion molecules to repress axonal branching, and proper positioning of ankyrin-G at the axon initial segment (AIS) [172, 175, 176]. By contrast, the role of ankyrin-B at dendritic membranes had been relatively understudied until recently, when ankyrin-B was shown to serve as an essential scaffold for voltage-gated sodium channels, $Na_v1.2$, at dendrites to promote dendritic excitability and synaptic plasticity in neocortical pyramidal neurons [116]. Heterozygous loss of *Ank2* causes dramatic impairments in dendritic excitability and synaptic plasticity, and phenocopies effects of heterozygous loss of *Scn2a*, which encodes $Na_v1.2$, suggesting ankyrin-B is critical for $Na_v1.2$-mediated dendritic function [116, 117].

ANK2 is amongst the top genes linked to autism spectrum disorder (ASD) [177, 178]. R2608fs, an ASD-associated variant in exon 37 of *ANK2*, which encodes the 440-kDa isoform of ankyrin-B, induces a frameshift that disrupts axonal scaffolding of the cell adhesion molecule L1CAM, causing alterations in axonal connectivity and behavior reminiscent of the deficits in communicative and social behaviors observed in human ASD patients [175]. *SCN2A*, which encodes $Na_v1.2$, is also a high-risk gene for ASD [179-181]. $Na_v1.2$ and ankyrin-B interacting to

promote dendritic excitability provides strong rationale that deficits in dendritic excitability may be a common point of convergence in ASD etiology. Although it is clear that $Na_v1.2$ relies on ankyrin-B to properly target to dendritic membranes in neurons, how ankyrin-B itself reaches the dendritic membrane is unknown. Understanding how ankyrin-B targets to the dendritic membrane to mediate the localization and function of $Na_v1.2$ may shed light onto ASD pathophysiology.

Another member of the ankyrin family, ankyrin-G, relies on the posttranslational modification, *S*-palmitoylation, to localize specifically to the lateral membrane of epithelial cells and to the axon initial segment (AIS) of neurons [71]. *S*-palmitoylation is the covalent addition of a 16-carbon fatty acid to cysteine residues of proteins through the formation of a labile thioester bond, and is catalyzed by a family of 23 enzymes known as palmitoyl acyl transferases (zDHHC PATs) [2]. Ankyrin-G is *S*-palmitoylated at a single cysteine in its N-terminal ankyrin repeat domain, Cys70 [71]. Mutation of Cys70 to alanine (C70A) renders ankyrin-G palmitoylation-dead and subsequently incapable of associating with the lateral membrane of epithelial cells. Under normal circumstances, ankyrin-G assembles and maintains the localization of necessary components of the epithelial lateral membrane, such as βII-spectrin, to ensure membrane biogenesis and cell polarity. However, palmitoylation-dead C70A ankyrin-G is incapable of clustering itself as well as βII-spectrin to the epithelial lateral membrane, resulting in loss of membrane biogenesis and loss of membrane height [39, 71]. In cultured hippocampal neurons, rescue of Cre-dependent deletion of ankyrin-G at the AIS with C70A ankyrin-G prevents ankyrin-G from specifically clustering at the AIS and instead distributes ankyrin-G in a non-polarized manner throughout neuronal compartments [71, 182]. Ankyrin-G is palmitoylated by two zDHHC PATs, zDHHC5 and zDHHC8 [39]. Knockdown of zDHHC5 and zDHHC8 abolishes ankyrin-G

palmitoylation and phenocopies the loss of membrane height and biogenesis observed with C70A ankyrin-G [39]. Taken together, these data demonstrate that ankyrin-G *S*-palmitoylation is required for ankyrin-G localization and function at the lateral membrane of epithelial cells as well as at the neuronal AIS. Another ankyrin family member, ankyrin-R, is also *S*-palmitoylated in erythrocytes, though no function has been described for this modification [183]. Whether ankyrin-B is also palmitoylated as a mechanism to regulate its plasma membrane localization and scaffolding of $Na_v1.2$ at dendrites remains unclear.

Here, we asked if ankyrin-B was *S*-palmitoylated and whether palmitoylation could regulate ankyrin-B localization and function at dendrites of neocortical neurons. We also investigate whether palmitoylation is important for ankyrin-B's cargo transport function at the axon. We report for the first time that ankyrin-B is indeed palmitoylated in whole mouse brain and in neurons. Our study identified zDHHC17 as a key mediator of ankyrin-B palmitoylation in heterologous cells and in hippocampal neurons. We also demonstrate zDHHC17 regulates ankyrin-B protein levels in a palmitoylation-independent manner, through a conserved binding mechanism between the ANK repeat of zDHHC17 and the zDHHC ankyrin-repeat binding motif (zDABM) of ankyrin-B. We identify five cysteines as possible ankyrin-B palmitoylation sites. Mutation of these five cysteines in the N-terminal ANK repeat domain of ankyrin-B renders ankyrin-B palmitoylation-dead. While ankyrin-B palmitoylation does not regulate its ability to mediate axonal cargo function, ankyrin-B palmitoylation is required to target $Na_v1.2$ to dendrites in neocortical pyramidal neurons. These data provide evidence for two pools of ankyrin-B in neurons, one palmitoylation-dependent pool at dendrites, and one palmitoylation-independent pool

in vesicles at the axon. This work highlights novel mechanisms regulating ankyrin-B localization and function in neurons that may provide insights into *ANK2*-associated ASD.

Results

Ankyrin-B is S-palmitoylated in whole mouse brain and in neurons.

The homologous family member of ankyrin-B, ankyrin-G, is *S*-palmitoylated to drive ankyrin-G localization and function in epithelial cells and in neurons [71]. Ankyrin-G and ankyrin-B share significant homology across their shared domains, with 74% homology shared in their N-terminal ankyrin repeat domain, where ankyrin-G's palmitoylated cysteine resides [184]. Given such high homology, we asked whether ankyrin-B is also *S*-palmitoylated and if so, whether *S*-palmitoylation regulates ankyrin-B's diverse functions in neurons. We used the Acyl Resin Assisted Capture (Acyl-RAC) assay to assess steady-state palmitoylation of ankyrin-B (previously described [185]). To validate this assay in our laboratory, we confirmed previous results demonstrating ankyrin-G is *S*-palmitoylated [71, 182]. Using C57Bl/6J adult mouse whole-brain lysates subjected to Acyl-RAC, we observed that all three neuronal isoforms of ankyrin-G, 190-, 270-, and 480-kDa ankyrin-G, are *S*-palmitoylated, as demonstrated by hydroxylamine-dependent binding of endogenous ankyrin-G to thiopropyl sepharose beads ("+HA" lane) (**Figure 3.1A,B**). We also observed that the 220-kDa and 440-kDa isoforms of ankyrin-B are *S*-palmitoylated in whole mouse brain, as evidenced by the presence of hydroxylamine-dependent ankyrin-B signal (**Figure 3.1A,C**). Given our interest in understanding whether palmitoylation regulates the diverse functions of ankyrin-B in neurons, we asked whether ankyrin-B is also palmitoylated in cultured hippocampal neurons from C57Bl/6J mice. Cultured hippocampal neurons represent a rational model from which to test ankyrin-B palmitoylation given that the axonal cargo transport function of ankyrin-B was previously established in hippocampal neurons [172]. Indeed, we observed

palmitoylation of both 220- and 440-kDa isoforms of ankyrin-B in cultured hippocampal neurons by Acyl-RAC, as shown by the hydroxylamine-dependent ankyrin-B signal (**Figure 3.1D**). Taken together, these data provide the first evidence that ankyrin-B is *S*-palmitoylated in whole mouse brain and in cultured neurons, implicating palmitoylation as a potential mechanism underlying ankyrin-B localization and function in neurons.

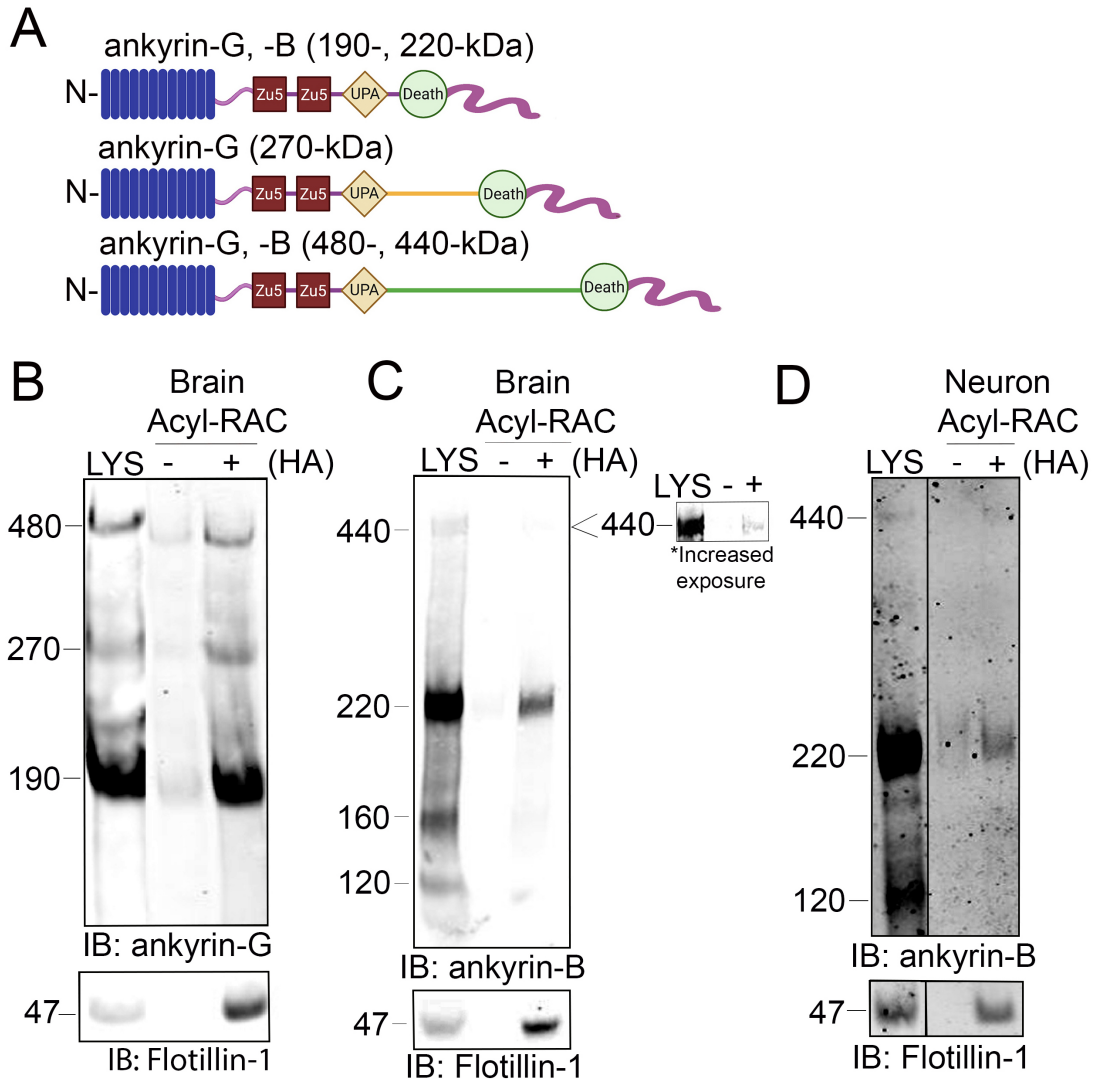

Figure 3.1. Ankyrin-B is *S*-palmitoylated in whole mouse brain and in cultured neurons.

A. Schematic of neuronal ankyrin-G and ankyrin-B, which share highly homologous domains: the N-terminal ankyrin repeat domain (blue), two ZU5 spectrin binding domains (red), a UPA domain (yellow), a death domain (light green), and a highly divergent unstructured C-terminal regulatory domain (pink). The giant isoforms (480-kDa ankyrin-G and 440-kDa ankyrin-B) have a large single exon (orange and dark green) inserted between their respective UPA and death domains. **B.** Whole brains from C57Bl/6J mice were processed for the Acyl-RAC assay to detect *S*-palmitoylation. *S*-palmitoylation of all neuronal isoforms of ankyrin-G (190-, 270-, and 480-kDa) is detected in whole brain from C57Bl/6J mice using an antibody against endogenous ankyrin-G, as demonstrated by the anti-ankyrin-G signal in the '+HA' lane, compared to the minimal background signal in the negative control '-HA' lane. Flotillin-1 is used as a positive control for the acyl-RAC assay (n=3). **C**. *S*-palmitoylation of the known neuronal isoforms of ankyrin-B (220- and 440-kDa) is detected by Acyl-RAC in whole brain from C57Bl/6J mice using an antibody against endogenous ankyrin-B, as demonstrated by the hydroxylamine-dependent ankyrin-B signal

('+HA' lane) (n=3). **D**. DIV17 cultured hippocampal neurons from C57Bl/6J mice were subjected to the Acyl-RAC assay. *S*-palmitoylation of the 220-kDa and 440-kDa isoforms of ankyrin-B is detected in cultured hippocampal neurons using an antibody against endogenous ankyrin-B, as evidenced by the hydroxylamine-dependent ankyrin-B signal (n=3). All conditions shown are run on the same blot; black line delineates spliced portion of the gel containing a condition not relevant to this figure. IB, immunoblotting.

Ankyrin-B expression and S-palmitoylation are increased by the palmitoyl acyltransferase zDHHC17 in heterologous cells.

Multiple studies have shown that the palmitoyl acyltransferase (PAT) zDHHC17 binds tightly to its substrates in order to palmitoylate them [50, 186]. The N-terminal ANK repeat (AR) domain of zDHHC17 recognizes a conserved zDHHC AR-binding motif (zDABM), (VIAP)(VIT)XXQP (where X is any amino acid) in its substrates [46, 50, 186]. Interestingly, a previous study identified the zDABM domain in the ankyrin family, including in ankyrin-B, using a peptide array screening approach (**Figure 3.2A**) [187]. This finding provided rationale for investigating the role of zDHHC17 in ankyrin-B palmitoylation. We subjected lysates from HEK293T cells transiently transfected with HA-tagged zDHHC17 and ankyrin-B-GFP to Acyl-RAC and found that zDHHC17 significantly enhanced both the palmitoylation and protein levels of ankyrin-B-GFP, compared to ankyrin-B-GFP in the absence of any exogenous PATs (**Figure 3.2B-E**). The presence of GFP signal in the negative control "-HA" lane is likely due to incomplete blocking of all free cysteines in ankyrin-B-GFP, presumably due to the GFP tag, which has numerous cysteines embedded in stable secondary structure that our lysis conditions may not disrupt completely. However, our quantification accounts for this background signal by subtracting any signal in the "-HA" lane from the "+HA" signal. To ensure that the increase in palmitoylation and expression levels of ankyrin-B-GFP seen with zDHHC17 were PAT-specific and not a function of overexpression, we screened the zDHHC library consisting of all 23 PATs (**Supplemental Figure 3.1A-D**). Using Acyl-RAC, we observed most zDHHC PATs did not enhance the palmitoylation nor the expression levels of ankyrin-B-GFP, compared to ankyrin-B-GFP alone, suggesting that the assay is able to detect PAT-dependent differences in palmitoylation

and protein expression. Consistent with our results from Figure 3.2, our PAT screen revealed zDHHC17 was the only exogenous PAT able to significantly enhance the palmitoylation of ankyrin-B, compared to ankyrin-B alone (**Supplemental figure 3.1A,B**). zDHHC17 was also the only PAT that significantly increased ankyrin-B protein expression, compared to ankyrin-B alone (**Supplemental figure 3.1C,D**). To test whether the increase in ankyrin-B-GFP protein levels seen in the presence of zDHHC17 was dependent on palmitoylation, we transiently transfected ankyrin-B-GFP with a catalytically-dead version of HA-tagged zDHHC17 (zDHHA17) in HEK293T cells and subjected the lysates to Acyl-RAC. zDHHA17 retains its recognition site for substrates (ANK repeat domain) but loses its enzymatic activity as the cysteine of the catalytic DHHC motif (C467) is mutated to alanine [188]. We observed that palmitoylation of ankyrin-B-GFP was completely abolished in the presence of enzymatically-dead zDHHA17, as compared to that with WT zDHHC17 (**Figure 3.2B-D**). In fact, there was no significant difference in ankyrin-B-GFP palmitoylation between ankyrin-B-GFP alone and ankyrin-B-GFP co-expressed with zDHHA17 (**Figure 3.2B-D**). Thus, increase in ankyrin-B-GFP palmitoylation observed upon co-expression of WT zDHHC17 is indeed driven by the catalytic activity of zDHHC17. Notably, however, ankyrin-B-GFP levels were still increased by zDHHA17, similar to what we observed with WT zDHHC17 (**Figure 3.2B, E**). These results suggest that the observed increase in ankyrin-B-GFP protein levels in the presence of zDHHC17 is not palmitoylation-dependent and may instead be due to recognition of ankyrin-B-GFP by zDHHC17. To test whether the enhancement in ankyrin-B protein levels are dependent on zDHHC17 recognition, we co-expressed a version of zDHHC17 whose substrate binding site is abolished, the HA-tagged N100A zDHHC17. N100A zDHHC17 is a well-characterized ANK repeat mutant that fails to recognize zDABM-containing substrates [186, 189]. Notably, ankyrin-B-GFP protein levels were reduced approximately three fold in the

presence of N100A zDHHC17 compared to that with WT or zDHHA17 (**Figure 3.2B, E**), suggesting that zDHHC17 recognition of ankyrin-B regulates ankyrin-B protein expression in heterologous cells. Surprisingly, ankyrin-B protein stability was unchanged in the presence of WT or N100A zDHHC17, compared to ankyrin-B alone by cycloheximide chase assay, suggesting that zDHHC17 is not regulating ankyrin-B expression by conferring stability in heterologous cells, at least in the context of our experimental time points and experimental conditions (**Supplementary figure 3.2A,B)**. Future studies will need to investigate the mechanisms underlying zDHHC17-dependent increases in ankyrin-B protein expression in heterologous cells. Given that zDHHC17 often requires direct interaction with its substrates to palmitoylate them [187], we hypothesized that the N100A mutation in zDHHC17 would also prevent palmitoylation. As predicted, loss of zDHHC17-ankyrin-B recognition induced by the N100A mutation in zDHHC17 or zDHHA17 results in drastically reduced palmitoylation levels compared to that with WT zDHHC17 (**Figure 3.2B-D**). These results are consistent with the canonical zDHHC17 AR-substrate zDABM binding paradigm necessary for palmitoylation, and confirms the findings of the peptide array screen that showed ankyrin-B has a zDABM domain [187].

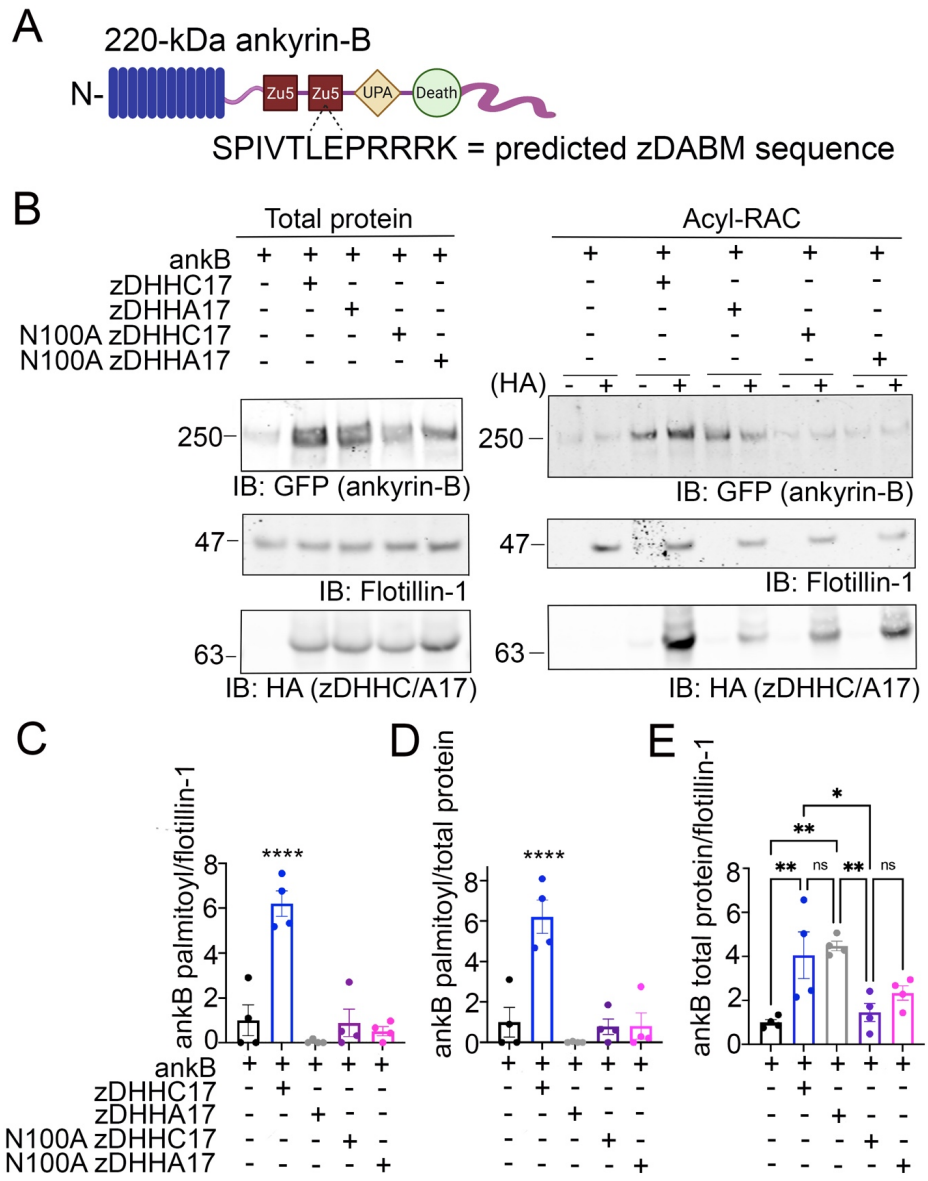

Figure 3.2. zDHHC17 recognizes the zDABM domain of ankyrin-B to regulate ankyrin-B protein expression and palmitoylation in HEK293T cells.

A. Schematic of ankyrin-B with the predicted zDHHC ANK repeat binding motif sequence (zDHHC17 recognition site, predicted from [187]) located in the second ZU5 domain. **B.** Representative western blot showing total protein levels of ankyrin-B-GFP (*left*) and palmitoylation levels of ankyrin-B-GFP (*right*) from lysates of HEK293T cells transiently transfected with WT ankyrin-B-GFP alone or together with WT zDHHC17, enzymatically-dead zDHHA17, N100A zDHHC17, or N100A zDHHA17 subjected to the Acyl-RAC assay. Ankyrin-B-GFP protein and palmitoylation levels are detected with an antibody against GFP. Palmitoylation of ankyrin-B-GFP is strongly detected in a hydroxylamine-dependent manner ('+HA' lane), compared to the background signal in the negative control '-HA' lane. Co-expression of zDHHC17 increases both the protein levels (*left*) and palmitoylation levels (*right*)

of ankyrin-B-GFP, compared to ankyrin-B expressed alone. WT ankyrin-B-GFP with zDHHA17, N100A zDHH17, or N100A zDHHA17 is not palmitoylated, compared to when ankyrin-B-GFP is co-expressed with zDHHC17. Ankyrin-B-GFP protein levels are unaffected by co-expression of zDHHA17, but are drastically reduced with co-expression of N100A zDHHC17 or N100A zDHHA17. **C.** Quantified *S*-palmitoylation levels of ankyrin-B-GFP from n=4 independent replicates per condition from *A*. ****P<0.0001 relative to ankB alone; one way ANOVA with Tukey's *post-hoc* test. For each condition, the palmitoylation signal was calculated by subtracting the *-HA* lane signal from that of the *+HA* lane and normalized to the flotillin signal from the *+HA* lane, and normalized (norm.) again to the average of ankyrin-B alone signal to get the relative fold change in ankyrin-B-GFP palmitoylation. **D.** Quantified ankyrin-B-GFP *S*-palmitoylation levels normalized to total ankyrin-B protein levels for each condition, relative to ankyrin-B alone palmitoylation levels (norm.). Data from n=4 independent replicates per condition from *A*. ****P<0.0001 relative to ankB alone; one way ANOVA with Tukey's *post-hoc* test. **E.** Quantified ankyrin-B-GFP protein levels normalized to total flotillin levels, relative to ankyrin-B alone protein levels. Data from n=4 independent replicates per condition from *A*. **P<0.01, *P<0.05; one way ANOVA with Tukey's *post-hoc* test.

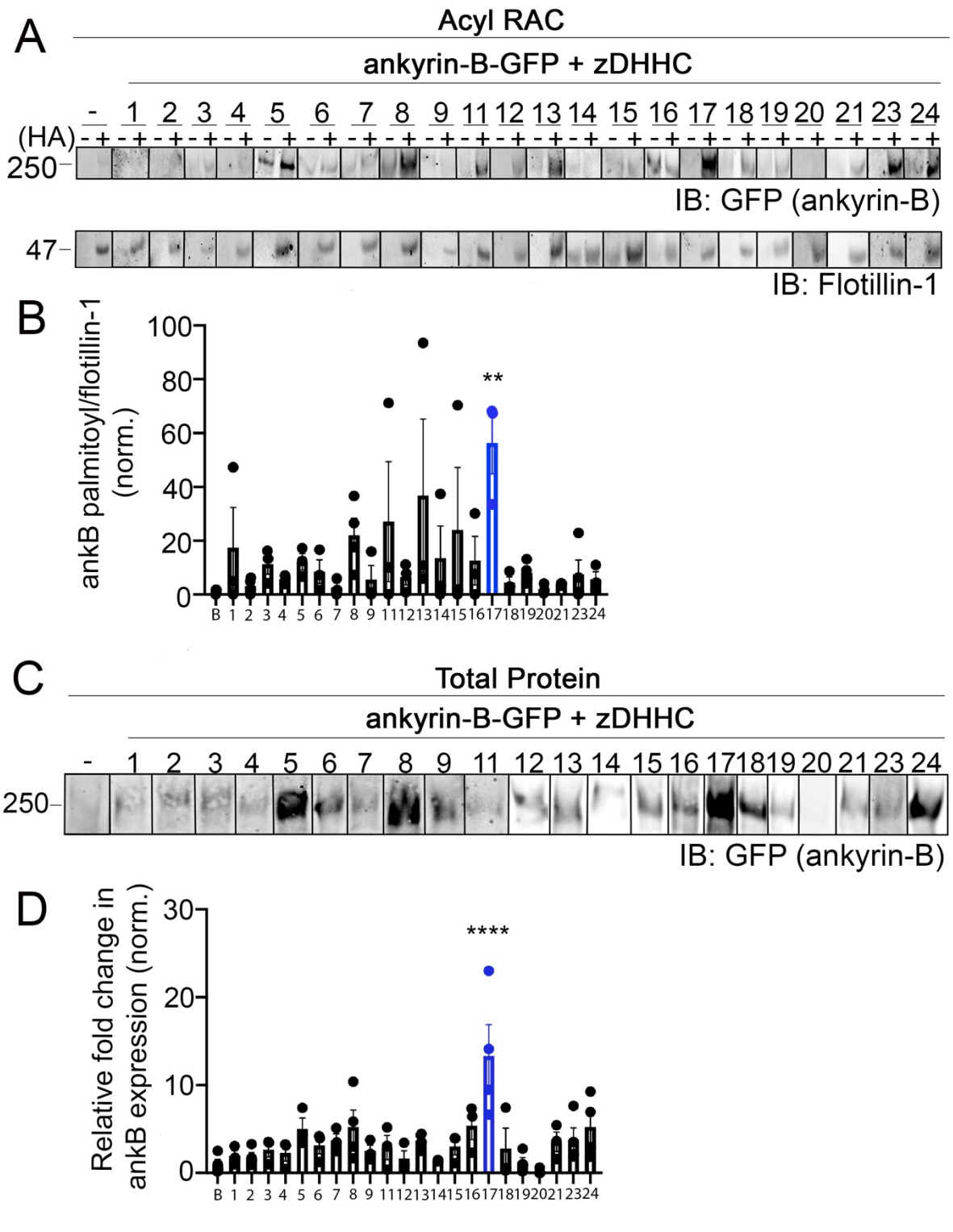
A
Acyl RAC
ankyrin-B-GFP + zDHHC
- 1 2 3 4 5 6 7 8 9 11 12 13 14 15 16 17 18 19 20 21 23 24
(HA) - + - + - + - + - + - + - + - + - + - + - + - + - + - + - + - + - + - + - +
250
IB: GFP (ankyrin-B)
47
IB: Flotillin-1
B
ankB palmitoyl/flotillin-1 (norm.)
100
80
60
40
20
0
**
B 1 2 3 4 5 6 7 8 9 11 12 13 14 15 16 17 18 19 20 21 23 24
C
Total Protein
ankyrin-B-GFP + zDHHC
- 1 2 3 4 5 6 7 8 9 11 12 13 14 15 16 17 18 19 20 21 23 24
250
IB: GFP (ankyrin-B)
D
Relative fold change in ankB expression (norm.)
30
20
10
0
****
B 1 2 3 4 5 6 7 8 9 11 12 13 14 15 16 17 18 19 20 21 23 24

Supplementary Figure 3.1. zDHHC17 increases ankyrin-B palmitoylation and protein expression in HEK293T cells.

A. Representative western blot showing ankyrin-B-GFP palmitoylation in the absence or presence of each individual zDHHC enzyme. Lysates from HEK cells transiently transfected with 220-kDa ankyrin-B-GFP alone (indicated as "-" in figure) or with each individual zDHHC enzyme were subjected to the Acyl-RAC assay to detect which zDHHC enzymes selectively enhance the palmitoylation of ankyrin-B-GFP compared to ankyrin-B alone. *S*-palmitoylation of ankyrin-B-GFP is detected using an antibody against GFP, as shown by the anti-GFP signal in '*+HA'* lane, compared to the expected low amount of signal in the negative control *-HA* lane. Flotillin-1 is used as a positive control for the Acyl-RAC assay as it is constitutively palmitoylated. **B**. Quantification of *A*. zDHHC17 significantly enhances the *S*-palmitoylation of ankyrin-B-GFP by approximately 91 fold compared to ankyrin-B-GFP alone (n=3). For each condition, the palmitoylation signal is calculated by subtracting the '*-HA'* lane signal from that of the '*+HA'* lane and normalizing to the flotillin signal from the '*+HA'* lane, and further normalizing to the average of ankyrin-B alone signal to get the relative fold change in ankyrin-B-GFP palmitoylation. Significance ($p = 0.0012$) was determined using an ordinary one-way ANOVA and Tukey's post-hoc multiple comparisons test. **C.** Representative western blot showing ankyrin-B-GFP total protein expression in the absence or presence of each individual zDHHC enzyme. **D**. Quantification of *C*. zDHHC17 significantly increases the protein expression of ankyrin-B-GFP by approximately 13 fold compared to ankyrin-B alone, while none of the other zDHHC enzymes significantly increase ankyrin-B-GFP expression (n=3), ****$p<0.0001$ (one-way ANOVA, Tukey's post-hoc).

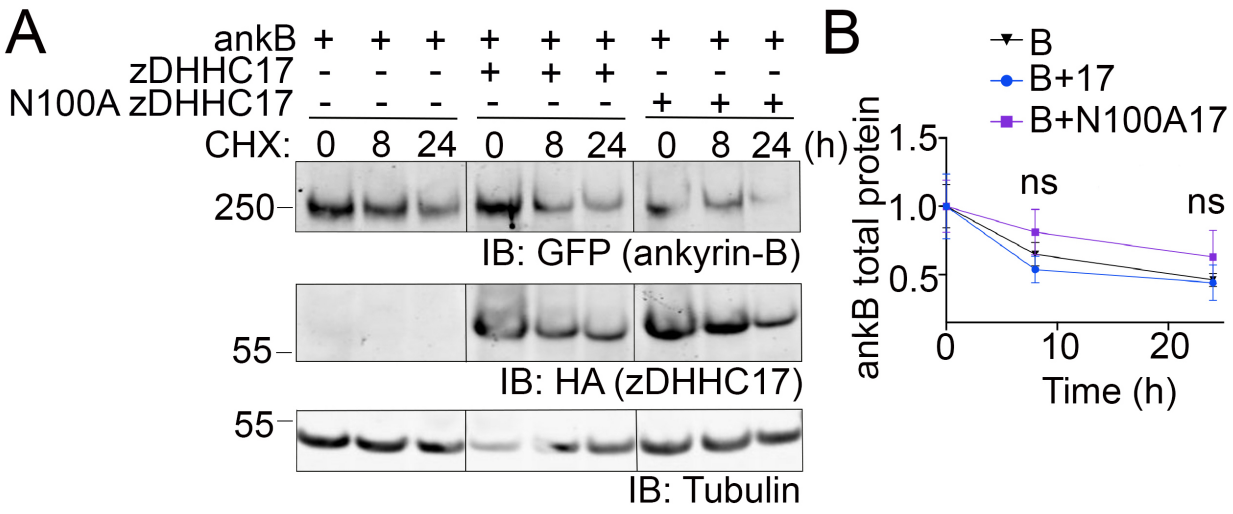

Supplementary Figure 3.2. zDHHC17 does not alter protein stability of ankyrin-B in heterologous cells by the cycloheximide (CHX) chase assay.

A. Representative western blot showing ankyrin-B protein expression alone or in the presence of WT zDHHC17 or N100A zDHHC17 after 8 and 24 hours of cycloheximide treatment. HEK293T cells transiently transfected with 220-kDa ankyrin-B-GFP alone or with WT zDHHC17 or N100A zDHHC17 were treated with 100 μg/mL CHX and lysates were collected after 8 hours and 24 hours of CHX treatment before western blotting. Ankyrin-B expression is detected using an antibody against GFP. Absence or presence of zDHHC17 is detected using an antibody against HA. Tubulin is used as a loading control. **B.** Quantification of *A*. Co-expression of zDHHC17 or N100A zDHHC17 does not alter the stability of ankyrin-B, compared to ankyrin-B in the absence of zDHHC17. For each condition, each time point is normalized to tubulin, and further normalized to Time 0h. Results are from n=6 for each condition; not significant (ns) by multiple unpaired *t-test*.

zDHHC17 is required to palmitoylate endogenous ankyrin-B in cultured hippocampal neurons.

Our findings using overexpression in heterologous cells suggest that zDHHC17 is a strong candidate for ankyrin-B palmitoylation. To address whether zDHHC17 palmitoylates endogenous ankyrin-B, we used cultured hippocampal neurons from floxed *Zdhhc17* mice [190] that were transduced with either a β-galactosidase control adenovirus or a Cre-recombinase adenovirus before lysates were either subjected to RT-PCR analysis to probe for extent of *Zdhhc17* deletion or the Acyl-RAC assay to probe for effects on ankyrin-B palmitoylation. RT-PCR analysis revealed a 95% reduction of *Zdhhc17* mRNA levels ten days post-transduction of Cre adenovirus in floxed *Zdhhc17* hippocampal neurons, compared to neurons treated with β-galactosidase control adenovirus (**Figure 3.3A**). Acyl-RAC revealed an 80% loss of ankyrin-B palmitoylation in Cre-treated floxed *Zdhhc17* hippocampal neurons, compared to that with the control virus (**Figure 3.3B-D**). Results from Figure 3.2 demonstrating that zDHHC17 recognizing ankyrin-B is sufficient to increase protein levels lead us to hypothesize that loss of endogenous zDHHC17 would reduce endogenous ankyrin-B protein levels. However, there was no significant difference in ankyrin-B protein levels between the Cre virus-treated and the control virus-treated neurons (**Figure 3.3E**), suggesting that neurons may utilize mechanisms independent of zDHHC17 to regulate ankyrin-B protein levels, unlike in heterologous cells. Taken together, these data demonstrate zDHHC17 is a major regulator of ankyrin-B palmitoylation in neurons.

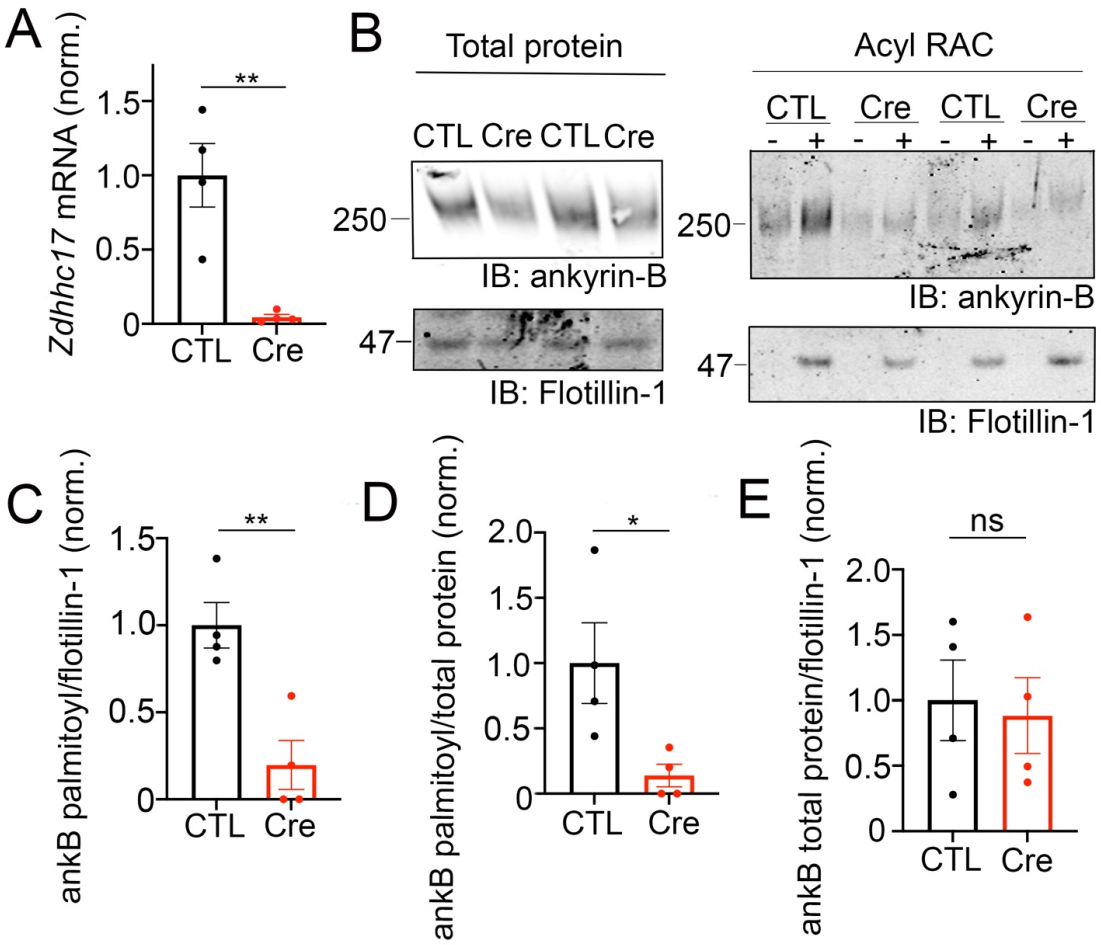

Figure 3.3. zDHHC17 is a critical regulator of endogenous ankyrin-B palmitoylation in cultured hippocampal neurons.

A. *Zdhhc17* mRNA levels in cultured hippocampal *Zdhhc17* floxed neurons transduced with either a β-galactosidase control adenovirus or Cre-recombinase adenovirus for 10 days prior to sample collection for RT-PCR analysis (n=4). *Zdhhc17* mRNA was decreased by ~95% in the Cre-recombinase condition compared to control. **P<0.01; Student's *t-test* (unpaired). **B.** Representative western blot showing total protein levels of endogenous ankyrin-B (*left*) and palmitoylation levels of endogenous ankyrin-B (*right*) from lysates of floxed *Zdhhc17* hippocampal neurons transduced with either a β-galactosidase control adenovirus or Cre-recombinase adenovirus for 10 days before Acyl-RAC processing (n=4). Both protein (*left*) and palmitoylation (*right*) levels of endogenous ankyrin-B are immunoblotted with an antibody against ankyrin-B for all conditions. Palmitoylation of ankyrin-B is strongly detected in a hydroxylamine dependent manner ('+HA' lane) from cultures infected with the control virus, but is greatly reduced in cultures infected with the Cre virus, as demonstrated by the lower ankyrin-B signal intensity in the '+HA' lane. **C.** Quantified endogenous ankyrin-B *S*-palmitoylation normalized to flotillin levels from the Acyl-RAC fractions and further normalized to control virus. Data from n=4 independent replicates per condition from *A*. **P<0.01; Student's *t-test* (unpaired). **D.** Quantified endogenous ankyrin-B *S*-palmitoylation normalized to total ankyrin-B protein levels

for each condition, and further normalized to control virus. Data from n=4 independent replicates per condition from *A*. **P<0.05; Student's *t-test* (unpaired). **E**. Quantified endogenous ankyrin-B levels normalized to total flotillin levels for each condition, and further normalized to control virus. Data from n=4 independent replicates per condition from *A*. not significant (ns); Student's *t-test* (unpaired).

Ankyrin-B is S-palmitoylated at multiple cysteines in its N-terminal ankyrin repeat domain.

The palmitoylation sites within ankyrin-B are unknown. Ankyrin-B's homologous family member, ankyrin-G, is *S*-palmitoylated at a single cysteine in its N-terminal ankyrin repeat domain, Cys70 [71]. Cys70 is conserved among all three human ankyrin members and vertebrate ankyrins [71], with ankyrin-B possessing a homologous cysteine at Cys60 (**Figure 3.4A**). Given the conservation of this amino acid, we hypothesized that Cys60 in ankyrin-B is the principal palmitoylated cysteine. Using site-directed mutagenesis, we engineered a cDNA construct in which Cys60 in ankyrin-B was converted to an alanine (C60A ankyrin-B-GFP). The C60A ankyrin-B-GFP mutant construct was transiently transfected with HA-tagged zDHHC17 into HEK293T cells, and lysates were subjected to Acyl-RAC to test the mutant's effects on ankyrin-B palmitoylation. The C60A ankyrin-B mutant lead to a 60% reduction in ankyrin-B palmitoylation, compared to WT ankyrin-B (**Figure 3.4B,C**). These data suggest that there are additional palmitoylated cysteine sites in ankyrin-B beyond Cys60.

Ankyrin-B has 26 cysteines, seven of which are harbored in the N-terminal ankyrin repeat domain, a domain necessary for ankyrins to interact with their membrane-associated partners (**Figure 3.4A**) [168]. To narrow down on additional palmitoylation sites in ankyrin-B, we asked whether palmitoylation sites were restricted to the N-terminal ankyrin repeat domain of ankyrin-B. Acyl-RAC on lysates from HEK293T cells transiently transfected with a truncated version of ankyrin-B which completely lacks the ankyrin repeat domain (120-kDa ankyrin-B-GFP) as well as zDHHC17 demonstrated an almost complete reduction of ankyrin-B-GFP palmitoylation, compared to WT ankyrin-B-GFP (**Figure 3.4D, E**). These data suggest that additional palmitoylation sites of ankyrin-B are located within the ankyrin repeat domain.

To determine which cysteines may be additional palmitoylation sites within the ankyrin-B ankyrin repeat domain, we employed mass spectrometry to identify peptides with *S*-palmitoylated cysteine sites in ankyrin-B. Lysates from HEK293T cells transfected with ankyrin-B-GFP and zDHHC17-HA were processed for the Acyl-RAC assay, digested, and analyzed by nano Liquid Chromatography tandem Mass Spectrometry (LC-MS/MS). With this approach, we identified five ankyrin-B peptides containing Cys60, Cys305, Cys347, Cys375, and Cys406 (**Figure 3.4A (bolded)**, **Supplementary figure 3.3A**). We did not detect peptides containing Cys482 and Cys736, likely indicating that these cysteines were not palmitoylated (**Supplementary figure 3.3A**). To confirm that Cys482 and Cys736 were not palmitoylation sites in ankyrin-B, we engineered cDNA constructs containing a cysteine-to-alanine mutation at C482A and another at C736A in ankyrin-B-GFP. C482A ankyrin-B-GFP and C736A ankyrin-B-GFP were individually expressed with zDHHC17-HA in HEK293T cells and processed for the Acyl-RAC assay to test their individual effects on ankyrin-B palmitoylation. Indeed, co-expression of zDHHC17-HA and either C482A ankyrin-B-GFP or C736A ankyrin-B-GFP did not affect ankyrin-B palmitoylation, compared to WT ankyrin-B (**Supplementary figure 3.3B, C**).

To further investigate the functional role of the remaining four candidate palmitoylation sites in ankyrin-B identified in the mass spectrometry study (C305, C347, C375, C406) (**Figure 3.4A**), we constructed a mutant version of ankyrin-B with the five cysteine residues, Cys60 included, substituted to alanine residues using site-directed mutagenesis. This mutant GFP-tagged ankyrin-B construct is referred to as AAAAA-ankyrin-B-GFP (or A5B), and when co-expressed with zDHHC17, demonstrated virtually no ability to be palmitoylated compared to WT ankyrin-B-GFP (**Figure 3.4F, G**). This is shown by the loss of hydroxylamine-dependent GFP signal in the presence of AAAAA-ankyrin-B-GFP, compared to WT and C60A ankyrin-B-GFP. These data

suggest that ankyrin-B is palmitoylated at multiple cysteine sites harbored in its N-terminal ankyrin-repeat domain. Furthermore, the palmitoylation-dead ankyrin-B mutant, AAAAA-ankyrin-B-GFP, represents a novel tool for investigating the functional consequences of ankyrin-B palmitoylation on downstream ankyrin-B localization and function.

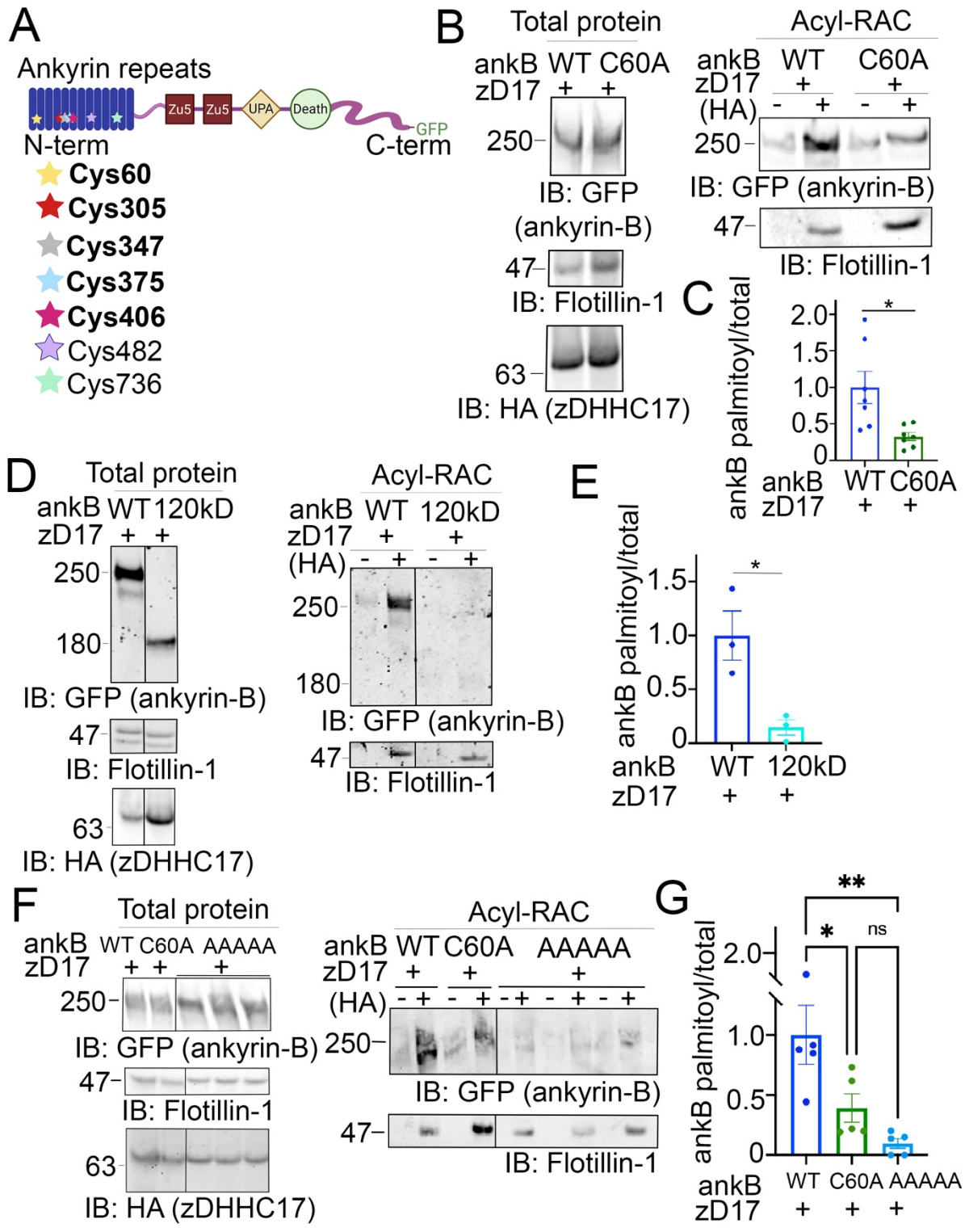

Figure 3.4. Identification of ankyrin-B *S*-palmitoylated cysteine sites.

A. Schematic of the domains in ankyrin-B and the cysteine residues harbored in the N-terminal ankyrin repeat domain, which are candidates palmitoylation sites. Bolded cysteine residues are the

cysteine residues that were substituted to alanine to generate the palmitoylation-dead ankyrin-B mutant. **B.** Representative western blot showing total protein levels of ankyrin-B-GFP (*left*) and palmitoylation levels of ankyrin-B-GFP (*right*) from lysates of HEK293T cells transiently co-transfected with WT ankyrin-B-GFP or C60A ankyrin-B-GFP and zDHHC17 processed for the Acyl-RAC assay (n=7). *S*-palmitoylation of C60A ankyrin-B-GFP is greatly reduced, as evidenced by the lower GFP signal in the '+HA' lane compared to that of the WT ankyrin-B-GFP. **C.** Quantified ankyrin-B-GFP *S*-palmitoylation levels normalized to total ankyrin-B protein levels for each condition, relative to palmitoylation levels of WT ankyrin-B-GFP co-expressed with zDHHC17. Data from n=7 independent replicates per condition from *A*. *P=0.0119; Student's *t-test* (unpaired). **D.** Representative western blot showing total protein levels of ankyrin-B-GFP (*left*) and palmitoylation levels of ankyrin-B-GFP (*right*) from lysates of HEK293T cells transiently co-transfected with WT ankyrin-B-GFP or 120-kDa ankyrin-B-GFP and zDHHC17 processed for the Acyl-RAC assay (n=3). All conditions shown are run on the same blot; black line delineates spliced portion of the gel containing a condition not relevant to this figure. *S*-palmitoylation of 120-kDa ankyrin-B-GFP is not detected using an antibody against GFP, as shown by the absence of anti-GFP signal in the '+HA' lane, compared to that when WT ankyrin-B-GFP is co-expressed with zDHHC17. **E.** Quantified ankyrin-B-GFP *S*-palmitoylation levels normalized to total ankyrin-B protein levels for each condition, relative to palmitoylation levels of WT ankyrin-B-GFP co-expressed with zDHHC17. Data from n=3 independent replicates per condition from *D*. *P=0.0241; Student's *t-test* (unpaired). **F.** Representative western blot showing total protein levels of ankyrin-B-GFP (*left*) and palmitoylation levels of ankyrin-B-GFP (*right*) from lysates of HEK293T cells transiently co-transfected with WT ankyrin-B-GFP, C60A ankyrin-B-GFP, or AAAAA-ankyrin-B-GFP and zDHHC17 processed for the Acyl-RAC assay (n=5). All conditions shown are run on the same blot; black line delineates spliced portion of the gel containing a condition not relevant to this figure. Compared to WT ankyrin-B-GFP and C60A ankyrin-B-GFP, *S*-palmitoylation of AAAAA-ankyrin-B-GFP is almost completely abolished, as shown by the absence of GFP signal in the '+HA' lanes. **G.** Quantified ankyrin-B-GFP *S*-palmitoylation levels normalized to total ankyrin-B protein levels for each condition, relative to palmitoylation levels of WT ankyrin-B-GFP co-expressed with zDHHC17. Data from n=5 independent replicates per condition from *F*. **P<0.01, *P<0.05; one way ANOVA with Tukey's *post-hoc* test.

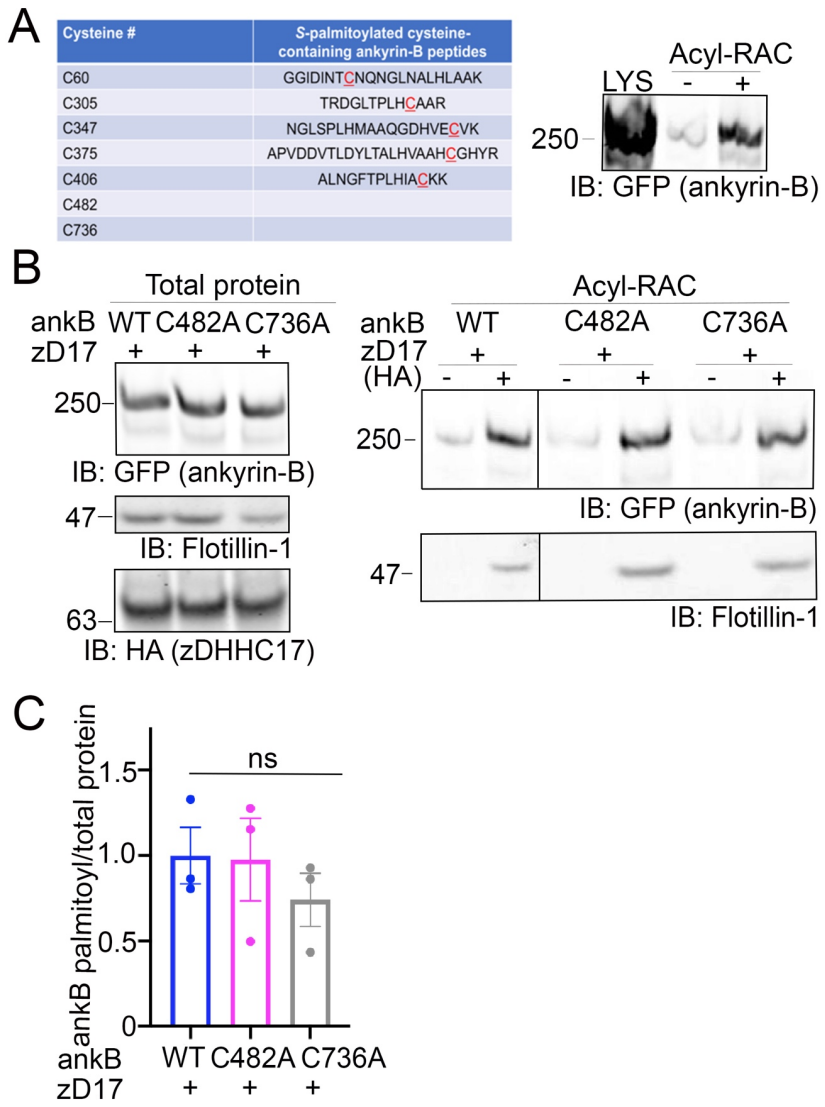

Supplementary Figure 3.3. Cys482 and Cys736 in ankyrin-B are not *S*-palmitoylated.

A. Five cysteine-containing peptides were identified by mass spectrometry from HEK293T cells co-transfected with ankyrin-B-GFP and zDHHC17 processed for the Acyl-RAC assay. These cysteine-containing peptides corresponded to Cys60, Cys305, Cys347, Cys375, and Cys406 in ankyrin-B. Western blot demonstrates efficiency of the Acyl-RAC assay for sample containing overexpressed ankyrin-B-GFP and zDHHC17-HA submitted for mass spectrometry analysis. **B.** Validation that the two cysteines, Cys482 and Cys736 not identified as palmitoylated in the mass spectrometry analysis were indeed not palmitoylated by Acyl-RAC. Western blot shows total protein levels of ankyrin-B-GFP (*left*) and palmitoylation levels of ankyrin-B-GFP (*right*) from lysates of HEK293T cells transiently co-transfected with WT ankyrin-B-GFP, C482A ankyrin-B-GFP, or C736A ankyrin-B-GFP and zDHHC17 processed for the Acyl-RAC assay. No change in the palmitoylation levels of C482A or C736A ankyrin-B-GFP were observed compared to WT ankyrin-B-GFP, as evidenced by the unchanged level of GFP signal in the '+HA' lane for these two mutants compared to WT ankyrin-B-GFP. All conditions shown are run on the same blot; black line delineates spliced portion of the gel containing a condition not relevant to this figure.

C. Quantified ankyrin-B-GFP *S*-palmitoylation levels normalized to total ankyrin-B protein levels for each condition, relative to palmitoylation levels of WT ankyrin-B-GFP co-expressed with zDHHC17. Data from n=3 independent replicates per condition from *B*. ns; one-way ANOVA, Tukey's post-hoc test.

S-palmitoylation does not regulate ankyrin-B-mediated axonal cargo transport in hippocampal neurons.

Deletion of *Ank2*, which encodes ankyrin-B, leads to impaired organelle transport in axons of cultured hippocampal neurons [172]. Here, we asked whether palmitoylation could regulate the axonal transport function of ankyrin-B. To study the effects of the palmitoylation-dead form of ankyrin-B on an ankyrin-B-null background, we used cultured hippocampal neurons from floxed *Ank2* mice to knock out ankyrin-B with transfection of Cre recombinase and simultaneously rescued with either wild-type (WT) 220-kDa ankyrin-B-GFP or palmitoylation-dead AAAAA-ankyrin-B-GFP (A5B) cDNA. Transfection of Cre-recombinase and rescue cDNA at 2 days in vitro (DIV) and imaging by time-lapse video microscopy 48 hours later allowed for observation of optimal motility of synaptic vesicle protein TdTomato-tagged synaptotagmin-1 (Syt1-TdTomato) along the axon in real time. Syt1-TdTomato moved bidirectionally along the axon with high processivity in control neurons only transfected with Syt1-TdTomato (**Figure 3.5A, B**), as observed previously [172]. In neurons transfected with Syt1-TdTomato and Cre recombinase-2A-BFP to knock out ankyrin-B, we observed an increased percentage of stationary or trapped synaptic vesicles in axonal swellings along the axons (**Figure 3.5B**). Additionally, the Syt1-TdTomato vesicles that still retained motility in the Cre-knockout condition exhibited slower velocities and traveled shorter distances bidirectionally along the axons, compared to controls (**Figure 3.5A, B**), which recapitulated the organelle transport deficits observed in the *AnkB*$^{-/-}$ mice [172]. The retrograde velocity deficits of Syt1-TdTomato particles observed upon deletion of ankyrin-B (Cre-2A-BFP) were partially rescued with addition of WT 220-kDa ankyrin-B-GFP or palmitoylation-dead AAAAA-ankyrin-B-GFP, whereas neither WT or AAAAA-ankyrin-B-GFP rescued the

anterograde velocity deficits of Syt1 particles induced by deletion of ankyrin-B (**Figure 3.5A, B**). The retrograde run length deficits of Syt1-TdTomato particles in the absence of ankyrin-B (Cre-2A-BFP) were fully rescued with addition of WT ankyrin-B-GFP or palmitoylation-dead AAAAA-ankyrin-B-GFP, whereas neither WT or AAAAA-ankyrin-B-GFP rescued anterograde run length deficits of Syt1 particles induced by deletion of ankyrin-B (**Figure 3.5A, B**). Longer expression times may be necessary to observe rescue of anterograde velocity or run length deficits with WT ankyrin-B-GFP. Addition of WT or AAAAA-ankyrin-B-GFP also rescued the increase in Syt1-Tdtomato stationary particles induced by deletion of ankyrin-B (Cre-2A-BFP) (**Figure 3.5B**). Furthermore, we did not observe any significant differences in the speed, distance, or relative mobility of WT or palmitoylation-dead AAAAA-ankyrin-B-GFP particles (**Figure 3.5C, D**). Taken together, these results suggest palmitoylation-dead ankyrin-B is capable of mediating axonal cargo transport of Syt1 similar to WT ankyrin-B. Thus, ankyrin-B-mediated cargo transport of synaptic vesicles like Syt1 is not dependent on ankyrin-B palmitoylation.

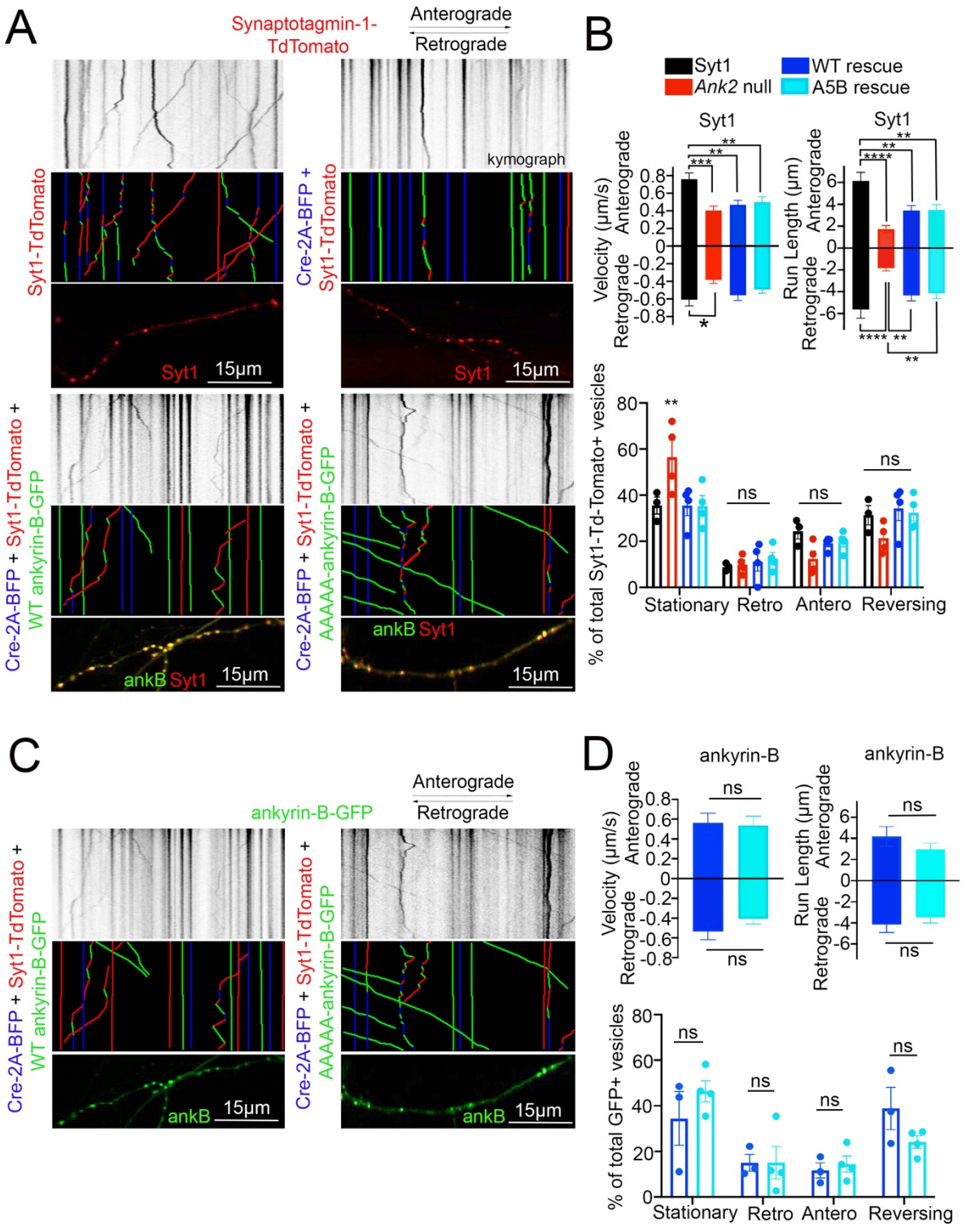

Figure 3.5. Loss of ankyrin-B palmitoylation does not affect axonal cargo transport of synaptic vesicle protein Synaptotagmin-1 (Syt1).

A. (Top) Representative kymographs of Td-tomato-tagged Syt1 particle movement along DIV4

axons of floxed *Ank2* hippocampal neurons in the absence or presence of Cre-2A-BFP to knock-out ankyrin-B and WT or palmitoylation-dead AAAAA-ankyrin-B-GFP as rescue plasmids. (Middle) Corresponding color-coded trajectories for Td-Tomato-positive particles demonstrating static vesicles (blue), anterograde-moving particles (green), and retrograde-moving particles (red). (Bottom) Puncta distribution of Syt1-TdTomato vesicles along axons (region of axon used to generate kymographs). **B.** Axonal velocity and run length for Syt1 particles. Data shown is from one representative experiment out of 4 independent repeats. n=4-8 axons per condition (n=88-154 particles per condition). Data represent means ± SEM. **P<0.01, ***P<0.001, ****P<0.0001. For velocity and run lengths analyses, one way ANOVA with Tukey's *post-hoc* test were performed. For % motility analysis, two-way ANOVA with multiple comparisons and Tukey's *post-hoc* was performed. **C**. (Top) Representative kymographs of GFP-tagged ankyrin-B particle movement along DIV4 axons of floxed *Ank2* hippocampal neurons in the absence or presence of Cre-2A-BFP to knock-out ankyrin-B and WT or palmitoylation-dead AAAAA-ankyrin-B-GFP as rescue plasmids. (Middle) Corresponding color-coded trajectories for GFP-positive particles demonstrating static vesicles (blue), anterograde-moving particles (green), and retrograde-moving particles (red). (Bottom) Puncta distribution of WT or AAAAA-ankyrin-B-GFP vesicles along axons (region of axon used to generate kymographs). **D.** Axonal velocity and run length for ankyrin-B particles. Data shown is from one representative experiment out of 4 independent repeats. n=3-7 axons per condition (n=38-76 particles per condition). Data represent means ± SEM. non-significant (ns). For velocity and run lengths analyses, Student's *t-test*s were performed. For % motility analysis, two-way ANOVA with multiple comparisons and Tukey's *post-hoc* was performed.

S-palmitoylation is required for ankyrin-B-mediated scaffolding of $Na_v1.2$ at the dendritic membranes of neocortical pyramidal neurons.

Our groups recently showed that ankyrin-B scaffolds the voltage-gated sodium channel $Na_v1.2$ at the dendritic membrane to promote dendritic excitability and synaptic function [116]. Here, we asked whether palmitoylation was required for ankyrin-B to scaffold $Na_v1.2$ at the dendritic membrane. Given that the dendritic deficits observed upon heterozygous loss of ankyrin-B *in vivo* were observed in the prefrontal layer 5b of mouse cortex and loss of $Na_v1.2$ dendritic localization due to ankyrin-B deletion were observed in neocortical neuron cultures [116], we investigated the role of ankyrin-B palmitoylation for $Na_v1.2$ scaffolding in neocortical cultures. To validate that $Na_v1.2$ localized properly at the AIS, where it is canonically scaffolded by ankyrin-G, as well as at dendritic membranes, we transfected DIV2 floxed *Ank2* neocortical neurons with $Na_V1.2$-3x FLAG IRES GFP, fixed at DIV21 (when the $Na_V1.2$ AIS-to-dendrite shift has occurred [117]), and stained with antibodies against FLAG and ankyrin-B. We observed intense $Na_v1.2$-3x FLAG staining at the AIS, consistent with $Na_v1.2$'s role at the AIS in mature neurons (referenced by the white star in **Figure 3.6A**), and $Na_v1.2$-3x FLAG staining at dendritic membranes, as evidenced by the "railroad track" footprint that overlaps with endogenous ankyrin-B staining (**Figure 3.6A**). To validate that deletion of ankyrin-B in neocortical neurons results in loss of $Na_v1.2$-3x FLAG dendritic localization [116], we transfected DIV2 floxed *Ank2* neocortical neurons with $Na_V1.2$-3x FLAG IRES GFP and Cre-2A-BFP to knockout ankyrin-B. As expected, we observed nearly complete reduction in $Na_v1.2$-3x FLAG dendritic immunostaining upon loss of ankyrin-B (**Figure 3.6A-C**). $Na_v1.2$-3x FLAG immunostaining at the AIS remained unchanged, consistent with ankyrin-G-dependent localization of $Na_v1.2$-3x FLAG at the AIS (**Figure**

3.6A,B,D) [191]. While rescue of Cre-mediated deletion of ankyrin-B with WT ankyrin-B-GFP resulted in the re-appearance of membrane-associated $Na_v1.2$-3x FLAG immunostaining specifically at the dendrites, as evidenced by the "railroad track-like" FLAG staining, addition of palmitoylation-dead AAAAA-ankyrin-B-GFP did not rescue loss of $Na_v1.2$-3x FLAG immunostaining at the dendrites in *Ank2* neocortical neurons (**Figure 3.6A-C**). These data suggest that ankyrin-B palmitoylation is required for proper dendritic localization of $Na_v1.2$ in neocortical pyramidal neurons.

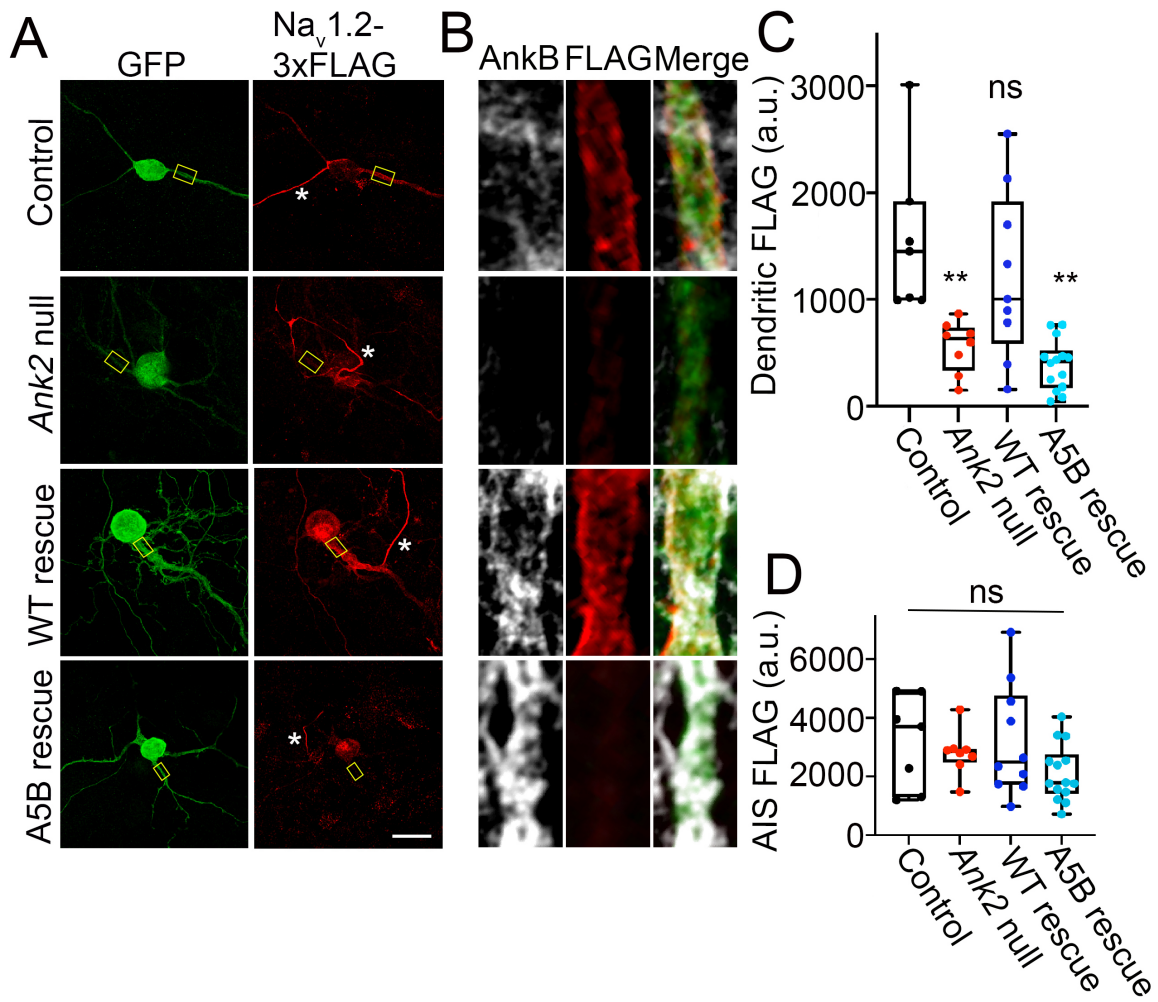

Figure 3.6. Loss of ankyrin-B palmitoylation prevents $Na_v1.2$ from localizing properly at dendritic membranes of cultured neocortical neurons.

A. Representative collapsed *Z*-stacks of DIV21 cultured floxed *Ank2* cortical neurons transfected at DIV2 with $Na_v1.2$-3x FLAG IRES GFP (Control) (*Top*), Cre-2A-BFP and $Na_v1.2$-3x FLAG IRES GFP to generate total ankyrin-B-null neurons (*Second from top*), or Cre-2A-BFP, $Na_v1.2$-3x FLAG IRES GFP, and indicated GFP rescue constructs (*Bottom*). Stars denote axon initial segment. Scale bars 20μm. Neurons stained with anti-GFP shown in green, anti-FLAG shown in red, and anti-ankyrin-B shown in far red. **B**. Zoomed-in single-stack images of selected dendritic compartment from *A* (denoted by square). Anti-FLAG is shown in red, and anti-ankyrin-B is shown in far red. AAAAA-ankyrin-B-cannot rescue the loss of dendritic membrane localization of $Na_v1.2$-3x FLAG induced by Cre-mediated deletion of ankyrin-B, compared to WT ankyrin-B-GFP. **C**. Quantification of mean fluorescence intensity of dendritic $Na_v1.2$-3x FLAG from *A,B*. **P<0.01 relative to Control; one way ANOVA with Tukey's *post-hoc* test, n=7-14 for each group. **D.** Quantification of mean fluorescence intensity of AIS $Na_v1.2$-3x FLAG from *A,B*. There is no change in AIS $Na_v1.2$-3x FLAG localization for any of the conditions. NS (not significant) by one way ANOVA with Tukey's *post-hoc* test, n=7-14 for each group.

Palmitoylation-dead AAAAA-ankyrin-B cannot properly localize to dendritic membranes of neocortical pyramidal neurons.

We reasoned that the inability of palmitoylation-dead ankyrin-B to function in scaffolding Nav1.2 at dendritic membranes may be because palmitoylation-dead ankyrin-B is unable to properly target to dendritic membranes itself. We hypothesized that palmitoylation localizes ankyrin-B at dendritic membranes, where it can then scaffold binding partners like $Na_v1.2$. To investigate whether dendritic localization of ankyrin-B is altered when ankyrin-B is unable to be palmitoylated, we first validated proper dendritic membrane localization of ankyrin-B as observed previously (**Figure 3.6A, B**) [116]. As expected, we observed ankyrin-B membrane localization at the dendritic plasma membrane, as evidenced by the "railroad-track" like appearance of ankyrin-B immunostaining in BFP-transfected control neurons (**Figure 3.7A,B**). We confirmed the efficiency of our knockout by verifying that dendritic membrane ankyrin-B localization was significantly reduced in Cre-2A-BFP-transfected neurons compared to BFP-transfected control neurons (**Figure 3.7A,B**). Rescue of Cre-mediated loss of ankyrin-B with WT 220-kDa ankyrin-B-GFP resulted in the re-appearance of membrane-associated ankyrin-B-GFP staining at the dendrite, as shown by the two green GFP peaks flanking the soluble BFP peak in the plot profile (**Figure 3.7C,D**). Strikingly, rescue of Cre-mediated loss of ankyrin-B with palmitoylation-dead AAAAA-ankyrin-B-GFP resulted in loss of membrane-association of ankyrin-B, as demonstrated by the lack of "railroad-track" like appearance of AAAAA-ankyrin-B-GFP and as shown by the overlapping green GFP and blue soluble BFP peaks (**Figure 3.7C,D**). These data suggest palmitoylation-dead ankyrin-B is not able to associate with dendritic membranes and is instead mainly distributed in the dendrite cytoplasm. This phenotype is consistent with the fate of

palmitoylation-dead neuronal ankyrin-G, C70A ankyrin-G, which is unable to associate specifically with the AIS membrane and instead distributes in a non-polarized fashion throughout the cytoplasm, rendering it non-functional and thus incapable of clustering binding partners such as neurofascin [182]. These data highlight that palmitoylation is required for ankyrin-B dendritic targeting, which is critical for ankyrin-B function in scaffolding $Na_v1.2$ in neocortical pyramidal neurons.

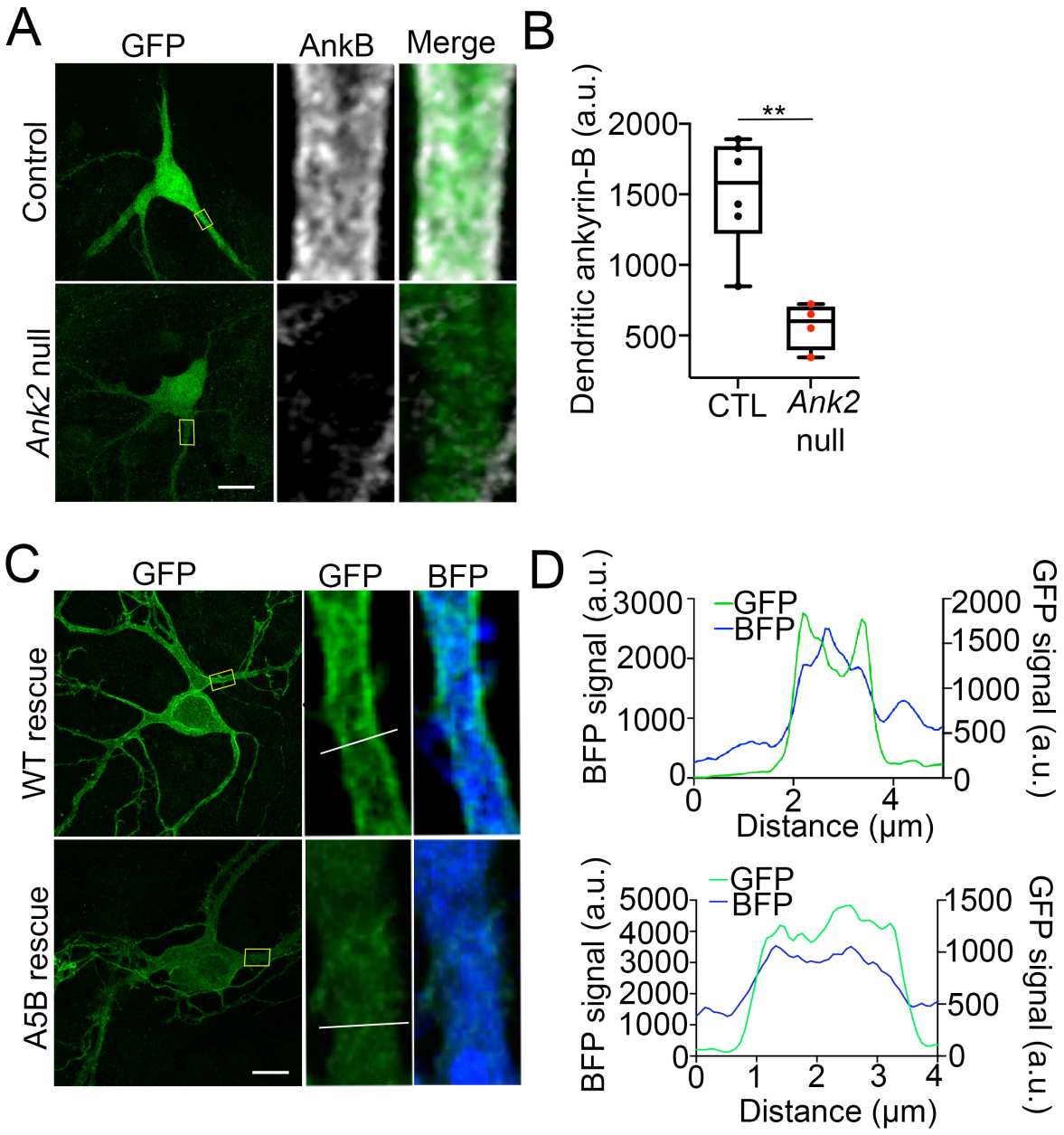

Figure 3.7. Palmitoylation-dead ankyrin-B is unable to target to dendritic membranes in neocortical pyramidal neurons.

A. Representative collapsed *Z*-stack (*left*) and zoomed-in single stack images (*right*) of DIV21 cultured floxed *Ank2* cortical neurons transfected at DIV2 with soluble GFP and BFP (*top*) or soluble GFP and Cre-2A-BFP (*bottom*) to knock-out ankyrin-B. Boxes denote zoomed-in section of the dendrite. Scale bars 20 μm. Neurons stained with anti-GFP shown in green and anti-ankyrin-B shown in white. **B.** Quantification of mean fluorescence intensity of dendritic ankyrin-B from *A*. P**<0.01 relative to Control; student's *t-test* (unpaired), n=4-6 neurons for each group across three independent replicates. **C.** Representative collapsed *Z*-stack (*left*) and zoomed-in single stack images (*right*) of DIV21 cultured floxed *Ank2* cortical neurons transfected at DIV2 both

transfected with Cre-2A-BFP to knock-out ankyrin-B and either rescued with WT ankyrin-B-GFP (*top*) palmitoylation-dead AAAAA-ankyrin-B-GFP (*bottom*) to assess dendritic membrane localization of ankyrin-B. Boxes denote zoomed-in section of the dendrite. White line denotes region of interest across the dendrite used to generate plot profiles outlining membrane versus cytoplasmic ankyrin-B-GFP staining. Scale bars 20 μm. Neurons stained with anti-GFP shown in green. Blue fluorescence comes from transfected Cre-2A-BFP, which fills the cell as soluble BFP. **D.** Plot profile outlining membrane versus cytoplasmic GFP (ankyrin-B) (green) and BFP (blue) staining across dendrite (region of interest denoted by white line on zoomed-in single stack). What appears as plasma-membrane localization of ankyrin-B at dendrites is demonstrated by the two green peaks flanking the soluble BFP peak. The two green peaks in plot profile representing likely membrane-localized ankyrin-B are present in WT ankyrin-B-GFP rescue but not in the palmitoylation-dead ankyrin-B-GFP rescue.

Discussion

Ankyrin-B's functions as a membrane organizer at the axon have been well-characterized. At the axon, ankyrin-B links the dynein/dynactin motor complex to organelles to promote fast axonal cargo transport, scaffolds the cell adhesion molecule L1CAM at the distal axon to repress axonal branching, and assembles a distal axonal cytoskeleton with βII-spectrin and α-II spectrin that restricts ankyrin-G positioning at the AIS [172, 175, 176]. Recently, ankyrin-B, itself highly enriched in dendrites, was revealed to localize the voltage-gated sodium channel $Na_v1.2$ to dendritic membranes to facilitate dendritic excitability [116]. Thus, ankyrin-B plays important roles in ensuring neuronal connectivity, polarization, and excitability. Dysfunction in *ANK2* is highly implicated in ASD, yet it remains unclear how *ANK2*, independently or by converging with high-risk ASD gene *SCN2A* or other ASD-associated genes, contributes to ASD etiology.

Given the strong association between *SCN2A* and *ANK2* in ASD, and the importance of ankyrin-B-mediated scaffolding of $Na_v1.2$ at dendrites for proper dendritic and synaptic function, it is important to understand how ankyrin-B targets to the dendritic membrane to allow for $Na_v1.2$ localization. Previous studies showed other members of the ankyrin family, like ankyrin-R and ankyrin-G, were *S*-palmitoylated and that ankyrin-G palmitoylation was required for proper ankyrin-G localization and function in polarized epithelial cells and in neurons [39, 71, 182, 183]. Here, we extend those findings to show for the first time that ankyrin-B is also *S*-palmitoylated, and relies on palmitoylation for proper localization and function at dendritic membranes in neurons. We also show ankyrin-B palmitoylation does not affect ankyrin-B-mediated axonal cargo transport.

Importantly, this work highlights that ankyrin-B utilizes distinct palmitoylation mechanisms compared to ankyrin-G, which is palmitoylated by functionally redundant zDHHC5 and zDHHC8 at a single cysteine residue, Cys70 [39, 71]. We show that ankyrin-B is capable of being palmitoylated by zDHHC17 in heterologous cells and further validated those findings by demonstrating zDHHC17 is a critical mediator of endogenous ankyrin-B palmitoylation in neurons. In heterologous cells, we observed zDHHC17 recognizes the zDABM domain of ankyrin-B to regulate both ankyrin-B expression levels and ankyrin-B palmitoylation. A previous study demonstrated the ANK domain of zDHHC17 recognizes a specific zDABM signature ((VIAP)(VIT)XXQP (where X is any amino acid)) in its substrate proteins in order to palmitoylate them [46, 50, 187]. Notably, the interaction between the ANK domain of zDHHC17 and the zDABM domain of ankyrin-B observed in this study was previously predicted by a peptide screen that identified the presence of the zDABM protein motif in ankyrins, suggesting our results are consistent with the conserved mechanism zDHHC17 utilizes to recognize and bind its substrates [187]. Consistent with the aforementioned study, we observed that the ability of ankyrin-B to recognize zDHHC17 is required for ankyrin-B palmitoylation, as demonstrated by the loss of ankyrin-B palmitoylation when the substrate binding site of zDHHC17 is ablated with the N100A mutation. Strikingly, loss of zDHHC17-ankyrin-B recognition also drastically reduced ankyrin-B protein levels. Although the enzymatic activity of zDHHC17 was required to regulate ankyrin-B palmitoylation, it was not sufficient to affect ankyrin-B expression levels. These data imply ankyrin-B protein expression is independent of ankyrin-B palmitoylation, even though both protein expression and palmitoylation rely on recognition of ankyrin-B by zDHHC17. The C60A and AAAAA-ankyrin-B-GFP mutants generated in this study to identify ankyrin-B palmitoylation sites also validated our findings that ankyrin-B protein expression was independent from ankyrin-

B palmitoylation. While ankyrin-B palmitoylation was reduced by co-expression of either C60A or AAAAA-ankyrin-B-GFP with zDHHC17, protein expression of these mutant ankyrin-B plasmids was unchanged compared to WT ankyrin-B-GFP (**Figure 3.4B,C,F,G**). We reasoned this was likely because the zDABM in C60A and AAAAA-ankyrin-B-GFP remained intact, such that zDHHC17 is still capable of recognizing mutant ankyrin-B and thereby maintaining its expression. Our cycloheximide chase assays demonstrated that zDHHC17 does not stabilize ankyrin-B in our heterologous cell system with the experimental timepoints used for this assay. Thus, other potential palmitoylation-independent functions of zDHHC17 will need to be investigated to understand how zDHHC17 modulates ankyrin-B expression in heterologous cells. Multiple studies have discussed the possibility of palmitoylation-independent functions of zDHHC17. Only half of the total number of proteins known to interact with zDHHC17 through their zDABM domain are known zDHHC17 substrates, suggesting that a major pool of zDHHC17 interactors rely on zDHHC17 for palmitoylation-independent functions [46]. Furthermore, the zDHHC17 orthologue zDHHC13 also has an ANK repeat domain capable of recognizing zDABM domains in proteins but is not capable of palmitoylating them [50]. The zDABM domain of peripheral membrane protein SNAP25 is capable of interacting with the ANK repeat domains of both zDHHC13 and zDHHC17, but is only capable of being palmitoylated by zDHHC17 and not zDHHC13 in heterologous cells [50]. These data suggest that although zDHHC17-zDABM binding is usually associated with palmitoylation, it can also serve additional substrate recruitment functions independent of zDHHC17 catalytic activity. The biological implications of ANK repeat-zDABM binding outside of zDHHC catalytic activity are only beginning to be uncovered. zDHHC17, by way of its ANK repeat domain, has been hypothesized to act as a hub for protein interaction networks. zDHHC17 is capable of forming large protein complexes by interacting with

proteins involved in neurotransmission, neuronal development, trafficking, signal transduction, and transcriptional regulation, many of which have not been identified as palmitoylated substrates or zDHHC17-specific substrates [192]. However, the functional implications of these interactions are currently unknown. zDHHC17 interacts with c-Jun N terminus kinase (JNK) to activate JNK and promote neuronal cell death in response to pathophysiological triggers like ischemic stroke [193]. zDHHC17 has been shown to promote the TrkA-tubulin complex, which regulates signal transmission in axon growth [194] Thus, our work is consistent with the ability of zDHHC17 to modulate substrates independently of its catalytic zDHHC domain, though this work is the first evidence to our knowledge that zDHHC17-zDABM binding directly regulates protein expression of a substrate in heterologous cells. However, what regulation of ankyrin-B protein levels by zDHHC17 means biologically and in what physiological context this finding is relevant will need to be further investigated.

Consistent with our results in heterologous cells, we observed that a 95% reduction in *Zdhhc17* mRNA in hippocampal neurons resulted in drastic loss of endogenous ankyrin-B palmitoylation. However, ankyrin-B protein levels remained unchanged in the absence of *Zdhhc17* mRNA, suggesting that neurons may have other means of regulating ankyrin-B protein levels independently of zDHHC17. In light of recent work demonstrating zDHHC17 is localized to the somatic golgi [189], ankyrin-B, which is primarily localized to dendrites of mature neurons [116], may not depend on zDHHC17 for maintenance of its protein pool out in the dendrites.

Functional studies with the palmitoylation-dead AAAAA-ankyrin-B-GFP demonstrated that palmitoylation regulates distinct functions of ankyrin-B. Palmitoylation of ankyrin-B was required for ankyrin-B to scaffold $Na_v1.2$ at dendritic membranes of neonatal cortical pyramidal

cells, but was not required for ankyrin-B to mediate axonal cargo transport of synaptotagmin-1. These data suggest there may be two pools of 220-kDa ankyrin-B in neurons, one palmitoylation-dependent pool at the dendrites that promotes $Na_v1.2$ targeting and one palmitoylation-independent pool at the distal axon that promotes cargo transport. Consistent with the hypothesis that some palmitoylated substrates are locally palmitoylated [195], somatic golgi zDHHC17 may be conveniently located to palmitoylate the pool of 220-kDa ankyrin-B destined for dendrites at the soma before ankyrin-B is forward trafficked into dendrites, where it subsequently scaffolds $Na_v1.2$. By contrast, zDHHC17 is specifically excluded from the axon in dorsal root ganglion neurons [189], which may explain why palmitoylation did not contribute to the axonal cargo function of 220-kDa ankyrin-B at the axon: 220-kDa ankyrin-B may simply not be palmitoylated at the axon due to the absence of zDHHC17 there. Interestingly, the pool of 220-kDa ankyrin-B that mediates cargo transport is targeted to vesicles and palmitoylation-independent, while the pool of 220-kDa ankyrin-B that scaffolds $Na_v1.2$ channels at dendrites is plasma-membrane-associated and palmitoylation-dependent. Palmitoylation of the homologous ankyrin-G also drives ankyrin-G targeting at plasma membrane domains of epithelial cells and neurons [39, 71]. It may be that ankyrin palmitoylation defines the precise localization of plasma-membrane-associated pools of ankyrins, such as AIS-localized ankyrin-G and dendritic ankyrin-B, but other mechanisms, posttranslational or otherwise, may drive the specific targeting of intracellular membrane pools of ankyrins such as vesicular ankyrin-B, at the axon. If this is the case, then 440-kDa ankyrin-B, which is targeted to the axonal plasma membrane of neurons to scaffold the cell adhesion molecule L1CAM and repress axonal branching [175] may be likely to rely on palmitoylation for its axonal membrane targeting as well. Our observation that 440-kDa ankyrin-B is palmitoylated both in the brain and in neurons in **Figure 3.1** is consistent with this hypothesis.

Despite the high homology shared between the ankyrin repeat domains of ankyrin-G and ankyrin-B, which harbor their respective palmitoylated cysteine sites, this study revealed non-conserved palmitoylation mechanisms between ankyrin family members. While ankyrin-G is palmitoylated by zDHHC5 and zDHHC8 at one cysteine site Cys70 [39, 71], our study demonstrated that ankyrin-B is palmitoylated by zDHHC17 at multiple cysteine sites (>2). This raises important questions about the biological implications of such distinct palmitoylation mechanisms, and may provide insight the long-standing question about how two highly homologous proteins like ankyrin-G and ankyrin-B target to distinct membrane sites and function in a non-overlapping manner. Numerous studies have shown that divergent domains within ankyrins can confer specificity for ankyrin-B or ankyrin-G localization and function in various cell types, though this has not yet been investigated in neurons. The highly divergent C-terminal domain confers specificity for ankyrin-B function at membranes of the sarcoplasmic reticulum (SR) in neonatal cardiomyocytes [184]. Additionally, the highly divergent short linker peptide between the ankyrin repeat domain and the $ZU5_2$-UPA module inhibits ankyrin-B binding to plasma membrane domains and drives intracellular membrane localization of ankyrin-B in epithelial cells [196]. Given that no consensus has been reached on which domain(s) determine specificity for ankyrin-G or ankyrin-B localization, this work has brought forward the importance of considering palmitoylation as a potential mechanism underlying the distinct localization and functions of ankyrin-B and ankyrin-G.

In light of the recent discoveries highlighting ankyrin-B's role in scaffolding $Na_v1.2$ at dendrites to promote dendritic function [116], it will be of interest to investigate the role of ankyrin-B palmitoylation for dendritic excitability and synaptic plasticity, especially as efforts to

understand the role of ankyrin-B and $Na_v1.2$ in the etiology of ASD continue. Our findings regarding the dendritic pool of ankyrin-B being palmitoylation-dependent and the vesicular pool of ankyrin-B at the distal axon being palmitoylation-independent highlights an opportunity to leverage palmitoylation as a drug target to specifically modulate the dendritic pool of ankyrin-B without affecting the vesicular pool of ankyrin-B at the axon, should the dendritic pool of ankyrin-B be implicated in ASD pathophysiology. It will also be important to investigate the role of $Na_v1.2$ palmitoylation to understand how this may affect the formation and maintenance of the ankyrin-B/$Na_v1.2$ complex at dendritic membranes.

Materials and Methods

Antibodies

The antibodies used for western blotting in this study were chicken anti-GFP antibody (Abcam, 1:2000), rabbit anti-Flotillin-1 antibody (Cell Signaling Technologies, 1:1000), rabbit/mouse anti-HA antibody (Cell Signaling Technologies, 1:1000), and rabbit anti-ankyrin-B C-terminus (custom-made in-house, 1:1000). The specificity of the anti-ankyrin-B antibody has been shown previously by western blotting [172]. LiCor fluorescent secondary antibodies were used: IRDye 800CW donkey anti-rabbit and anti-chicken (for anti-ankyrin-B, anti-HA, anti-Flotillin-1) and IRDye 680RD donkey anti-mouse (for anti-HA) were diluted 1:10,000. The antibodies used for immunofluorescence studies were mouse anti-FLAG M2 (Millipore Sigma, 1:1000), chicken anti-GFP antibody (Abcam, 1:1000), and sheep anti-ankyrin-B C-terminus (custom-made, in-house, 1:1000). Alexa Fluor 488, 568, or 647 secondary antibodies (Fisher scientific) were used at 1:250.

Expression Vectors

The panel (1-24) of mouse zDHHC cDNA constructs subcloned in a pEF-BOS HA backbone were kindly gifted to us by Dr. Masaki Fukata (National Institute of Physiological Sciences, Okazaki, Japan; [34]). The zDHHA17 mutant generated by site-directed mutagenesis was kindly gifted to us by Dr. Luke Chamberlain (University of Strathclyde); [188]). The N100A zDHHC/A17 mutants were generated by our laboratory by site-directed mutagenesis using primers designed by Agilent QuickChange II XL primer design software and using QuickChange II XL site-directed mutagenesis kit (Agilent Technologies), and confirmed by DNA sequencing through Eurofins Genomics (Louisville, KY). Human ankyrin-B-GFP containing the small 220kD splice variant of

ankyrin-B in a pEGFP-N1 vector was previously described [172]. All point mutations generated using the ankyrin-B-GFP cDNA construct were made using site-directed mutagenesis (QuickChange II XL, Agilent Technologies) and confirmed by DNA sequencing through Eurofins Genomics (Louisville, KY). Syt1-TdTomato was generously donated by Drs. Ronald Holz and Arun Anantharam (University of Michigan Medical School, Ann Arbor, MI). CAG-Cre-2A-BFP and CAG-BFP in a pLenti6-V5-DEST viral vector were previously used and described [182].

Animals

Wild type C57Bl/6J (Jackson Laboratories), floxed *Zdhhc17* (on an FVB background [190]), and floxed *Ank2* mice (previously described [197]) were housed in the Unit for Laboratory Animal Medicine at the University of Michigan. All procedures involving animals were performed in accordance with National Institutes of Health guidelines with approval by the Institutional Animal Care and Use Committee (IACUC) of the University of Michigan.

Cell Culture and Transfections

HEK293T cells (gifted to us by Dr. Gareth Thomas, Temple University) were grown in Dulbecco's modified Eagle's high glucose medium with 10% fetal bovine serum, 1% penicillin, and 1% GlutaMax (ThermoFisher) at 37°C, 5% CO_2. For Acyl-RAC experiments, HEK293T cells were plated in 10cm dishes at 80-90% confluency the day before transfection and transfected 16 hours later with 4 µg total DNA (2 µg of each plasmid) using Lipofectamine 3000 (Invitrogen) according to the manufacturer's instructions.

Neuronal Cultures, Transfections, and Viral transductions

Cortical neurons were dissociated from P0 floxed *Zdhhc17* mouse pups and cultured were prepared as previous described [198]. At DIV2, neocortical cultures were transduced with β-galactosidase control adenovirus or Cre recombinase adenovirus, which are previously described [199-201]. Cells were transduced in half of their original media for 6 hours before replacing with the remaining half of their original media and half of fresh, new media. Neurons were left to incubate for 10 days before being processed for RT-PCR or Acyl-RAC analysis.

Hippocampal neurons were dissociated from P0 $Ank2^{f/f}$ mouse pups and cultures were prepared as previously described [198]. For the axonal cargo transport imaging experiments, DIV3 hippocampal neurons were transfected with 1 µg of either CAG-BFP or CAG-Cre-2A-BFP cDNA in combination with 500 ng of the other plasmids (Synaptotagmin-1-TdTomato, WT ankyrin-B-GFP, AAAAA-ankyrin-B-GFP) using Lipofectamine 2000. Briefly, 1 µg or 1.5 µg of cDNA constructs were added to 200 µL of Neurobasal-A medium (Gibco) in an Eppendorf tube. In another tube, 3 µL or 4.5 µL, respectively, of Lipofectamine 2000 were added to 200 µL of Neurobasal-A medium. The two tubes were incubated separately in the hood for 5 minutes before merging, mixing well, and incubating for 20 more minutes. The neuronal growth media on the neurons was collected and saved at 37°C. The transfection mix was then added dropwise to the appropriate dishes of DIV3 neurons and incubated at 37°C for 1 h. The transfection mix was aspirated, cells were washed once with Neurobasal-A medium, and the original growth media was added back onto the neurons. Cells were maintained in culture for 48 h before live imaging.

For the dendritic ankyrin-B function and localization experiments, neocortical neurons were dissociated from P0 floxed *Ank2* mouse pups and cultures were prepared as previously described [198]. DIV2 neurons were transfected with 0.5 μg of each plasmid using Lipofectamine 2000 as described in the above paragraph.

RT-qPCR

RNA was isolated from cultured hippocampal neurons in 6-well dishes (Thermo Fisher) using the RNeasy Mini Kit (QIAGEN). cDNA was prepared using the SuperScript IV First-Strand Synthesis Kit (Invitrogen). Quantitative RT-PCR on the mouse *Zdhhc17* gene using primers spanning exons 1 and 2 (5′-ACCCGGAGGAAATCAAACCACAGA-3′ and 5′-TACATCGTAACCCGCTTCCACCAA-3′) and Sso/Advanced Universal SYBR green supermix (Fisher Scientific) was performed on CFX96 Real Time System (C1000 Touch Thermal Cycler, BioRad) under default conditions. Each sample was run in triplicates. Expression levels for mRNA were normalized to β-actin (5'- CATTGCTGACAGGATGCAGAAGG-3' and 5'-TGCTGGAAGGTGGACAGTGAGG-3').

Acyl Resin Assisted Capture (Acyl-RAC)

Approximately 24h post-transfection, transfected HEK293T cells were lysed in "blocking buffer" containing 100 mM HEPES, 1 mM EDTA, 2.5% SDS, and 4% MMTS (Sigma), adjusted to pH 7.5 and sonicated. Samples were left to simultaneously heat and shake overnight at 40°C and 850 rpm in a Thermal Mixer II (Fisher Scientific). Samples were acetone precipitated with cold acetone (incubated in ice) to remove residual MMTS (previously described [185]) and pellet was re-dissolved in 500 μL of "binding buffer" containing 100 mM HEPES, 1 mM EDTA, and 1% SDS,

pH adjusted to 7.5, in Thermal Mixer II at 40°C and 850 rpm overnight. Protein samples were spun down in standard benchtop centrifuge at maximal speed for 5 minutes to pellet out any non-dissolved protein. Supernatant was then split into three 1.5 mL Eppendorf tubes, one containing 40 µL of unmanipulated starting material, one containing 200 µL of sample for hydroxylamine treatment ("+HA"), and one containing 200 µL of sample for NaCl treatment ("-HA"). 40 µL (1:1) of 5x SDS-PAGE buffer (5% wt/vol SDS, 25% wt/vol sucrose, 50 mM Tris pH 8, 5 mM EDTA, and bromophenol blue) supplemented with 100 mM DTT (Gold Biotechology) was added to the unmanipulated starting material and placed at 65°C for 10 minutes. 50 µL of 1:1 slurry of pre-activated thiopropyl sepharose 6b beads (GE, discontinued) were added to the "+HA" and "-HA" samples (previously described [185]). 40 µL of freshly prepared 2 M hydroxylamine (HA) (Sigma), adjusted to pH 7.5, were added only to the "+HA" designated sample. 40 µL of 2 M NaCl were added to the "-HA" designated sample. Samples treated with HA and beads were left to incubate while rotating at room temperature for 2.5 h before being spun down at 5000 x g for 1 minute and washed 3x with "binding buffer", each time discarding the supernatant and recovering the beads. 40 µL of 5x SDS-PAGE/DTT buffer were used to elute palmitoylated proteins off of the beads and heated for 10 minutes at 65°C. Samples were analyzed by western blotting.

For assessing palmitoylation of proteins from brain tissue or from cultured hippocampal neurons, after overnight MMTS block, samples were transferred to a Slide-A-Lyzer Dialysis Cassette (10,000 MWCO) (Thermo Scientific) for overnight buffer exchange with "Binding buffer". Buffer exchanged samples were recovered from the dialysis cassette and the assay continued as described in the previous paragraph.

Mass Spectrometry (LC-MS/MS)

After subjecting lysates to the Acyl-RAC assay and ensuring sufficient pulldown by western blotting (**Supplementary Fig. 3.3A**), the sample was submitted to the University of Michigan Mass Spectrometry-Based Proteomics Resource Facility (Department of Pathology). There, the thiopropyl sepharose beads (washed without SDS for optimal mass spectrometry analysis) were re-suspended in 50 µL of 8M urea/0.1M ammonium bicarbonate buffer (pH~8). Cysteines (including those holding the previously palmitoylated proteins to the beads) were reduced by adding 50 µL of 10 mM DTT and incubating at 45° C for 30 min. Samples were cooled to room temperature and cysteines were alkylated using 65 mM 2-Chloroacetamide in the dark for 30 minutes at room temperature. Upon diluting the urea to a final concentration of <1 M, sample was incubated with 1 µg sequencing grade, modified trypsin at 37° C overnight. Digestion was stopped by acidification and peptides were desalted using SepPak C18 cartridges using manufacturer's protocol (Waters). Samples were completely dried using vacufuge. To perform the mass spectrometry, trypsinized peptides were dissolved in 9 µL of 0.1% formic acid/2% acetonitrile solution. Two µls of the resulting peptide solution were resolved on a nano-capillary reverse phase column (Acclaim PepMap C18, 2 micron, 50 cm, ThermoScientific) using a 0.1% formic acid/acetonitrile gradient at 300 nl/min over a period of 180 min. Eluent was directly introduced into *Orbitrap Fusion Tribrid* mass spectrometer (Thermo Scientific, San Jose CA) using an EasySpray source. MS1 scans were acquired at 60K resolution (AGC target=$3x10^6$; max IT=50 ms). Data-dependent collision-induced dissociation MS/MS spectra were acquired on 20 most abundant ions following each MS1 scan (NCE ~28%; AGC target $1x10^5$; max IT 45 ms). Proteins were identified by searching the data against *Uniprot protein database* using Proteome Discoverer (v2.4, Thermo Scientific). Search parameters included MS1 mass tolerance of 10 ppm and

fragment tolerance of 0.2 Da. Two missed cleavages were allowed; carbamidomethylation of cysteines (+ 57.021 Da), oxidation of methionine (+ 15.995 Da), deamidation of aspergine and glutamine (+ 0.984 Da), and palmitoylation (+ 238.23 Da) were all considered variable modifications. False discovery rate (FDR) was determined using Percolator and proteins/peptides with an FDR of ≤1% (high confidence) were retained for further analysis.

Western Blotting

Protein lysates, following Acyl-RAC or otherwise, were separated by 3.5-17% gradient gel in 1x Tris buffer, pH 7.4 (40 mM Tris, 20 mM NaOAc, and 2 mM NaEDTA) and 0.2% SDS at 175 Volts for ~4-5 hours. Transfer to a nitrocellulose membrane was performed overnight at 300 mAmps, 4°C in 0.5x Tris buffer and 0.01% SDS. Once transferred, membranes were blocked with 5% Bovine Serum Albumin (BSA) in 1x TBS and rotating overnight at 4°C with primary antibodies diluted at appropriate dilution factor in blocking buffer (5% BSA, 0.1% tween in TBS). Membranes were then washed 3x for 10 minutes each with 1x TBS-T (TBS with 0.1% tween) and incubated for 1 h with LiCor fluorescent antibodies in blocking buffer. Membranes were washed 3x for 10 minutes each in 1x TBS-T before imaging on LiCor Odyssey Clx Imager. Immunoreactive signals were quantified using ImageJ.

Live imaging of hippocampal neurons and image analyses

Live microscopy of neuronal cultures was performed 48 hrs following neuronal transfections using a Zeiss LSM 880 with a 63X NA1.4 Oil/DIC Plan-Apochromat objective with excitation achieved using 405, 488, and 561 nm lasers in fast Airyscan mode. A humidified and temperature-controlled chamber was used to maintain the transfected hippocampal cultures at 37°C and 5% CO_2 in warm

Physiological Saline Solution (130 mM NaCl, 4 mM KCl, 1.5 mM $CaCl_2$, 1 mM $MgCl_2$, 5 mM Glucose, 10 mM HEPES, adjusted to pH 7.4, and filter sterilized). Time-lapse images captured transfected hippocampal neurons in the mid-axon so as to avoid the axon initial segment at a rate 200 ms intervals in fast Airyscan mode. Images were Airyscan-processed using the Zeiss image analysis software (Zen Blue). Kymographs were then generated from each time-lapse image using the KymoToolBox plugin in ImageJ (National Institutes of Health, [202]), as previously described [203]. Briefly, the axon was outlined and traced, from which a kymograph calibrated in space (x-axis in micrometers) and time (y-axis in seconds) was generated. Individual particle movement/trajectory was traced along the kymograph, which the KymoToolBox plugin analyzed in terms of directionality (red for retrograde, green for anterograde, and blue for stationary), directional velocities (μm/seconds), and directional run length for each traced particle.

Fluorescence Labeling of Cortical Neurons and image acquisition

Dissociated cortical neurons at DIV21 (transfected DIV2) were fixed for 15 min at room temperature with 4% formaldehyde, followed by permeabilization with 0.2% triton in PBS for 10 mins at room temperature, and further blocked with blocking buffer (5% BSA, 0.2% Tween 20 in PBS) for one hour. Primary antibodies were diluted in blocking buffer and incubated at 4°C overnight. The next day, cells were washed three times for 10 min with washing buffer (0.2% Tween 20 in PBS) before incubating the cells with secondary antibodies (1:250) diluted in blocking buffer for 1 h at room temperature. Cells were washed three times for 10 min with washing buffer and mounted with prolong gold. Multi-color imaging was performed as previously described using a Zeiss 880 confocal microscope [191]. All images were processed in Adobe Photoshop CS6 and quantified using GraphPad Prism 9.

Statistical Analysis

Statistical analyses for Acyl-RAC experiments were performed with n≥3 for each experiment ((N100A) zDHHC/A17: n=4, *Zdhhc17*/Cre neurons, n=4, C60A: n=7, 120kDa: n=3, for AAAAA: n=5). For the *Zdhhc17*$^{f/f}$ neuron Acyl-RAC, the C60A ankyrin-B Acyl-RAC, and the 120-kDa ankyrin-B Acyl-RAC experiments, a two-tailed student's *t-test* (unpaired) was performed. Data are represented as mean ± SEM. For the Acyl-RACs that included multiple comparisons ((N100A) zDHHC/A17 and AAAAA-ankyrin-B), a one-way ANOVA with multiple comparisons and Tukey's *post-hoc* test was performed. For the cargo transport experiment, four independent experiments were performed. Statistical significance for axonal velocity and run length of Syt1 particles, which included 4-8 axons per condition (n=88-154 particles per condition) was determined with one-way ANOVA with Tukey's *post-hoc* test. To determine statistical significance for percentage of stationary, reversing, or motile Syt1-Tdtomato-positive or ankyrin-B-GFP-positive particles, a two-way ANOVA with multiple comparisons and Tukey's *post-hoc* test was performed. Statistical significance for axonal velocity and run length of ankyrin-B particles, which included 3-7 axons per condition (n=38-76 particles per condition) was determined with a two-tailed student's *t-test* (unpaired). All cargo transport data are represented as mean ± SEM. The $Na_v1.2$-3x FLAG microcopy experiment had an n of 7-14 neurons/condition and was performed in three independent replicates. Mean fluorescence intensity of dendritic FLAG signal and mean fluorescence intensity of AIS FLAG signal were analyzed using one-way ANOVA with multiple comparisons and Tukey's *post-hoc* test. Data are represented as mean ± SEM.

Chapter 4: Discussion and Future Directions

Julie M. Philippe and Paul M. Jenkins, PhD

Summary and Significance

Both studies in this thesis investigated the role of the lipid modification *S*-palmitoylation in regulating the localization and function of two disease-associated substrates, voltage-gated sodium channel β1 subunits and ankyrin-B, which both contribute to neuronal excitability, among a multitude of other roles. One major goal of our research program is to understand the roles of substrates like β1 and ankyrin-B in normal physiology to further highlight how disease-associated mutations or loss-of-function variants in the genes encoding β1 and ankyrin-B contribute to underlying mechanisms of their associated diseases. Variants in *SCN1B,* which encodes β1, are associated with Early Infantile Epileptic Encephalopathy 52 (EIEE52, also called early infantile developmental and epileptic encephalopathy) and Brugada Syndrome [115, 159]. Chapter 2 of this thesis demonstrated the biochemical regulation of β1 by palmitoylation for plasma-membrane localization and subsequent cleavage of β1 by BACE1 and γ-secretase. Understanding the regulatory mechanisms underlying β1 cleavage, a process critical for downstream gene transcription [143], may provide important insight into the etiology of *SCN1B*-associated pathophysiologies like EIEE52 and Brugada Syndrome, and may highlight "druggable" targets for drug development. *ANK2*, which encodes ankyrin-B, has been identified as a high-risk gene for Autism Spectrum Disorders (ASD) [177, 178]. How ankyrin-B is

implicated in ASD etiology is unknown. However, recent discoveries highlighting that ankyrin-B scaffolds Nav1.2 at dendritic membranes of neocortical pyramidal neurons to promote dendritic excitability [116], and that ASD-associated haploinsufficiency of *Scn2a*, which encodes $Na_v1.2$ causes defects in dendritic excitability [117], may represent a novel node of convergence for *ANK2* and *SCN2A* on dendritic excitability that may be important for ASD etiology. Chapter 3 of this thesis investigated the biochemical regulation of ankyrin-B by palmitoylation for ankyrin-B localization and consequently VGSC $Na_v1.2$ targeting to the dendritic plasma membrane, which may be altered in ankyrin-B-associated ASD. Given the multitude of studies demonstrating that defects in palmitoylation are associated with a diverse range of brain diseases [114], and in light of our work showing the critical roles that palmitoylation plays for proper localization and function of β1 and ankyrin-B, this dissertation has provided rationale for further investigating how posttranslational regulatory mechanisms like palmitoylation of β1 and ankyrin-B, and how disease-associated alterations in these regulatory mechanisms, may contribute to EIEE52 and ASD, respectively.

To summarize Chapter 2, using heterologous cells, we demonstrated β1 cell surface localization and subsequent proteolytic cleavage are regulated by *S*-palmitoylation, but not by tyrosine phosphorylation. We show β1 subunits are *S*-palmitoylated in whole mouse brains at a single cysteine residue, C162. Mutating C162 to alanine (β1-p.C162A) abolishes β1 palmitoylation, which reduces cell surface localization of β1 and also decreases the available pool of β1 to undergo cleavage by BACE1 and γ-secretase. This is the first evidence of β1 cleavage occurring at the plasma membrane. We also demonstrate that inhibition of endocytosis restores the cell surface expression of β1-p.C162A, suggesting that palmitoylation likely

stabilizes β1 at the cell surface to oppose the effects of endocytosis. β1 modulation of sodium current (I_{Na}) was not dependent on palmitoylation. This work is particularly important in light of the recent study that demonstrated β1 proteolytic cleavage leads to downstream gene transcription through the generation of a soluble peptide, β1 intracellular domain (β1-ICD) [204]. This work highlights a potentially important regulatory mechanism for gene transcription by the β1-ICD, which should be the focus of future investigation.

To summarize Chapter 3, using both heterologous cells and cultured neurons, we demonstrate ankyrin-B is a substrate for palmitoylation, and promotes the function of ankyrin-B in scaffolding $Na_v1.2$ at neuronal dendrites. We identify the palmitoyl acyl transferase zDHHC17 as a critical mediator of ankyrin-B palmitoylation in heterologous cells and in neurons. Additionally, we found that zDHHC17 regulates ankyrin-B protein levels independently of its *S*-acylation function, through a conserved binding mechanism between the ANK repeat domain of zDHHC17 and the zDHHC ankyrin-repeat binding motif of ankyrin-B. We subsequently identify five cysteines in the N-terminal ankyrin repeat domain of ankyrin-B that are necessary for ankyrin-B palmitoylation. Mutation of these five cysteines to alanines not only abolishes ankyrin-B palmitoylation, but also prevents ankyrin-B from scaffolding $Na_v1.2$ at dendritic membranes of cultured neurons, suggesting palmitoylation is important for function of ankyrin-B at dendrites. Loss of ankyrin-B palmitoylation does not affect ankyrin-B-mediated axonal cargo transport of synaptic vesicle synaptotagmin-1 in cultured neurons. These data imply there may be two pools of ankyrin-B in neurons, one palmitoylation-dependent plasma-membrane pool at the dendrites, and one palmitoylation-independent vesicular pool at the distal axon.

Future Directions

Although this work has answered multiple questions about the regulatory mechanisms that underlie localization and function of the neuronal substrates VGSC β1 subunits and ankyrin-B, it has also raised additional questions, both basic and translational, regarding the implications of neuronal substrate regulation by *S*-palmitoylation, which should be the focus of future research. In the following sections, I will discuss these future directions and provide hypotheses and potential approaches for addressing them, from the perspective of each individual substrate as well as from the point of view of convergent mechanisms between VGSCs, β1 subunits, and ankyrins.

Ankyrins

Determine how differential palmitoylation mechanisms between ankyrin-B and ankyrin-G contribute to localization specificity of ankyrins in diverse cell types.

Chapter 3 of this thesis work demonstrates that palmitoylation of ankyrin-B occurs at distinct cysteine residues and is mediated by different palmitoyl acyl transferases compared to ankyrin-G. This finding provides insight into the long standing question of how two highly homologous proteins like ankyrin-G and ankyrin-B, which are often co-expressed in the same cell types, exhibit such distinct localization and non-overlapping functions. This work also raises questions regarding how two highly homologous proteins can exhibit such differences in palmitoylation mechanisms. The field has long tried to establish how ankyrins achieve specificity in their localization and functions. The family of ankyrin scaffolding proteins consist of three

members, ankyrin-R encoded by *ANK1*, ankyrin-B encoded by *ANK2*, and ankyrin-G encoded by *ANK3*. All three family members generally function as adaptor proteins that target diverse membrane substrates to specialized membrane domains [168]. Vertebrate ankyrins evolved from one single ankyrin gene in the invertebrate urochordate *C. intestinalis*, giving rise to high conservation of both amino acid sequence and structure of their domains [205]. Ankyrins comprise four major domains shared across all three family members: the N-terminal membrane-binding domain composed of 24 consecutive ANK repeats, a spectrin-binding domain consisting of a Zu5 domain that serves as the binding site for spectrin, a second Zu5 domain, a UPA domain, a conserved death domain whose functions are yet to be identified, and an unstructured C-terminal tail [206-208]. Ankyrin-B and ankyrin-G share high homology across all of the aforementioned domains: the membrane-binding domain is 74% homologous, the spectrin-binding domain is 68% homologous, and the death domain is 59% homologous. The only highly divergent domain is the unstructured C-terminal domain, with shares only 11% homology between ankyrin-B and ankyrin-G [184]. One mechanism that has contributed to the diversity in subcellular distribution and function of ankyrins is alternative splicing. Most cell types express 190-kDa ankyrin-G but alternative splicing of the giant 7.8-kB exon produces two additional neuronal isoforms of ankyrin-G, 270- and 480-kDa ankyrin-G. Similarly, *ANK2* leverages similar alternative splicing strategies to generate a ubiquitous 220-kDa isoform and a 440-kDa isoform that is highly expressed in the nervous system [209]. It is important to note that the three major ankyrin domains, the N-terminal ANK repeat domain, the Zu5 domain, and the death/C-terminal domains, are highly conserved across all the higher molecular weight isoforms of ankyrin-G and ankyrin-B; the only difference is the introduction of a giant exon between the Zu5 domain and the death/C-terminal region. Thus, simply identifying the different ankyrin isoforms expressed in the specific

cell types is not sufficient to fully understand the mechanisms underlying specific ankyrin localization and function. In vertebrates, 480kDa-ankyrin-G isoform is localized to the axon initial segment (AIS) and Nodes of Ranvier of myelinated axons, which are regions responsible for the initiation and propagation of the action potential, respectively. At the AIS and nodes, ankyrin-G recruits binding partners such as voltage-gated sodium channels (Na_v family members), KCNQ2/3, the cell adhesion molecule neurofascin, NrCAM, and βIV-spectrin to form this specialized membrane microdomain [209]. More recently, 480kDa-ankyrin-G was also found to localize to somatodendritic membranes, where it forms inhibitory synapses to regulate neuronal excitability and forebrain circuitry [198]. By contrast, both 220-kDa- and 440-kDa ankyrin-B are localized to the distal axon, where the 220-kDa isoform couples the p62 subunit of dynactin to cargoes to facilitate axonal cargo transport and normal axonal growth, and the 440-kDa isoform recruits the cell adhesion molecule L1CAM to repress axonal branching [172, 175]. Ankyrin-B is also localized to dendritic membranes, where it scaffolds the voltage gated sodium channel $Na_v1.2$ to mediate dendritic excitability and synaptic plasticity in mature cortical pyramidal neurons [116]. The isoform specificity of ankyrin-B function at dendrites still remains to be elucidated. Thus, despite high homology and co-expression in neurons, ankyrin-G and ankyrin-B are distinctly localized to allow for unique, non-overlapping functions at these specific cellular compartments. Studies involving gene-specific knockouts have shown that ankyrin-G and ankyrin-B localization and function is so specific that neither one cannot compensate for the loss of the other. For example, knocking out the 480-kDa ankyrin-G *in vivo* results in depletion of ankyrin-G binding partners like Na_vs, neurofascin, KCNQ2, and βIV-spectrin from the AIS despite the unchanged expression of ankyrin-B in this mouse model [191]. Numerous studies have attempted to unravel the basis for such specificity in ankyrin-B and ankyrin-G localization and

function, and have done so by addressing which domains within ankyrin-G and ankyrin-B were capable of conferring specificity. The highly divergent C-terminal domain of 220-kDa ankyrin-B was found to confer specificity for ankyrin-B localization and function at membranes of the sarcoplasmic reticulum (SR) in neonatal cardiomyocytes [184]. Given that 220-kDa ankyrin-B in neonatal cardiomyocytes recruits the ryanodine (RyR) and the IP_3 receptors at the SR to facilitate cardiomyocyte contraction, neonatal cardiomyocytes lacking native ankyrin-B protein exhibit impaired spontaneous contraction rates due to loss of proper SR RyR and IP_3 receptor localization. Rescuing the loss of native ankyrin-B with exogenous WT 190kDa-ankyrin-G cDNA by transient transfection did not restore impaired localization of the IP_3 receptor at the SR or spontaneous contraction rates, but expression of the chimeric 190kDa-ankyrin-G fused to the C-terminal domain of ankyrin-B ($M_GS_GDC_B$) completely restored the localization of ankyrin as well as RyR and IP_3 receptors and restored contraction rates. Similarly, expression of chimeric ankyrin-B fused to the C-terminal domain of ankyrin-G ($M_BS_BDC_G$) was unable to restore impaired contractility due to its inability to rescue loss of proper SR localization of ankyrin, IP_3, and RyR in ankyrin-B-null neonatal cardiomyocytes [184]. These data suggest that the C-terminal domain of ankyrins is an important driver of localization and function specificity between ankyrin-G and ankyrin-B in cardiac muscle [184]. Given that the C-terminal domain of ankyrin-B in this study had little to no activity on its own, the study hypothesized that the ankyrin-B C-terminal region likely interacts with the N-terminal ANK repeat domain to regulate localization and function of ankyrin-B in cardiomyocytes [184]. Further work showed that an amphipathic alpha helix specific to the C-terminal domain of ankyrin-B is required for ankyrin-B-mediated recruitment and scaffolding of Na^+/Ca^{2+} exchanger and Na^+/K^+ ATPase at the T-tubules, and IP_3 receptor at the SR through association of this ankyrin-B helix with molecular chaperone Hdj1/Hsp40 [210]. These data

suggest yet another level of specificity within the C-terminal domain that drives ankyrin-B function in cardiomyocytes. Whether or not these studies translate to neuronal isoforms of ankyrins has not yet been investigated. Another important domain that confers specificity is a highly divergent short linker peptide between the N-terminal ankyrin repeat domain and the first $Zu5_2$-UPA module in 220-kDa ankyrin-B. This linker inhibits ankyrin-B binding to the plasma membrane of polarized epithelial cells and neurons [196]. The ankyrin-B specific linker is encoded by a small exon that is conserved within the ankyrin-B lineage but divergent across other ankyrin family members [196]. Using antibodies towards endogenous ankyrins as well as by exogenous transfection of cDNAs, previous work showed that 190-kDa ankyrin-G is localized specifically to the lateral membrane whereas 220-kDa ankyrin-B is localized to intracellular vesicles in polarized epithelial cells. Using a chimeric approach, ankyrin-B can be re-localized to the plasma membrane of polarized epithelial cells when its aforementioned linker domain is replaced with the linker domain of ankyrin-G. Interestingly, N-terminal ANK repeat domains of ankyrin-G and ankyrin-B are both able to target to the lateral membrane, but fusion of the short linker peptide of ankyrin-B to the ANK repeat domain of ankyrin-B drives intracellular targeting of ankyrin-B and inhibits plasma membrane association of its ANK repeat domain. The authors argued this was due to an autoinhibitory mechanism of the ankyrin-B linker, whereby the linker of ankyrin-B interacts directly with the ANK repeat to suppress localization to the plasma membrane and prevent association of the ANK repeat domain with binding partners such as neurofascin and E-cadherin at the plasma membrane [196].

Though a multitude of divergent domains in 220-kDa ankyrin-B have shown to be important for the specificity of ankyrin-B localization and function in diverse cell types, this work has brought forward the importance of considering palmitoylation as a potential mechanism

underlying the distinct localization and functions of ankyrin-B and ankyrin-G, which should be the focus of future work. Previous work demonstrated 190-kDa ankyrin-G is *S*-palmitoylated at one single cysteine in the ANK repeat domain, cysteine 70 [71]. Palmitoylation is required for proper localization of the 190-kDa ankyrin-G to the lateral membrane of polarized epithelial cells, which subsequently promotes membrane biogenesis and length [71]. Palmitoylation also directs the specific targeting of 480-kDa ankyrin-G at the AIS of neurons, necessary for ankyrin-G-mediated recruitment of voltage-gated sodium channels and neurofascin at the AIS [71, 182]. 190-kDa ankyrin-G palmitoylation is mediated by zDHHC5 and zDHHC8, and simultaneous knockdown of these two enzymes using shRNAs recapitulates the localization and functional defects of the palmitoylation-dead ankyrin-G, C70A ankyrin-G, in polarized epithelial cells [39]. Despite the fact that Cys70 is highly conserved across all three ankyrin family members, this work demonstrated a lack of conservation in ankyrin palmitoylation mechanisms: whereas 190-kDa ankyrin-G is palmitoylated at a single cysteine by zDHHC5 and zDHHC8, we showed 220-kDa ankyrin-B has multiple palmitoylated cysteines, including the homologous Cys70 (Cys60), and is palmitoylated by zDHHC17, which differs from ankyrin-G. Given this work only showed zDHHC17's critical role for ankyrin-B palmitoylation, future work will need to verify that deletion of zDHHC5 and/or zDHHC8 (using floxed zDHHC5 and zDHHC8 mouse lines our laboratory recently generated) does not affect ankyrin-B palmitoylation, and that deletion of zDHHC17 does not in turn affect ankyrin-G palmitoylation. Perhaps more intriguingly, we demonstrated palmitoylation selectively regulates ankyrin-B functions, such that ankyrin-B palmitoylation was required for dendritic $Na_v1.2$ scaffolding but was not important for axonal cargo transport. By contrast, palmitoylation was required for all the known functions of ankyrin-G in polarized epithelial cells and in neurons known at the time the studies were published.

Whether palmitoylation plays roles for the novel functions of ankyrin-G such as formation of inhibitory synapses or stabilization of dendritic spines in neurons remains unknown [198, 211]. Future work should investigate whether the aforementioned differences in palmitoylation mechanisms between ankyrin-G and ankyrin-B contribute to establishing their unique subcellular distributions in polarized epithelial cells and in neurons. For example, in polarized epithelial cells where 190-kDa ankyrin-G localizes to the plasma membrane but 220-kDa ankyrin-B localizes to intracellular membranes due to the its divergent linker [196], does ankyrin-B rely on more palmitoylation sites than ankyrin-G because the ankyrin-B linker folds over Cys60 in the ANK repeat domain and prevents its complete palmitoylation? Furthermore, does the ankyrin-B linker folding over the ANK repeat domain preclude recognition of ankyrin-B by plasma membrane-localized zDHHC5 and zDHHC8, such that ankyrin-B instead gets recognized and palmitoylated by Golgi-localized zDHHC17 and subsequently targeted to intracellular membranes? It will be important to test whether we can alter recognition and palmitoylation by different zDHHC enzymes to drive distinct subcellular ankyrin localization depending on the identity of the linker domain. One approach would be to investigate whether chimeric ankyrin-B fused to the linker of ankyrin-G, which re-localizes to the plasma membrane of polarized epithelial cells, can be palmitoylated by zDHHC5 and zDHHC8 instead of zDHHC17. These results would demonstrate how post-translational mechanisms like palmitoylation leverage divergent domains within ankyrins to drive unique ankyrin localization patterns, and would provide a tunable means of exogenously regulating ankyrin localization and function. This would also further establish the idea that local palmitoylation, whereby substrates need to be in the same subcellular compartments as their zDHHCs to be palmitoylated, is an important aspect of ankyrin palmitoylation mechanisms [195].

Why ankyrin-G and ankyrin-B are palmitoylated by a distinct set of enzymes despite high homology needs to be further investigated. One potential hypothesis is that ankyrins are locally palmitoylated and therefore localized to the site where their respective zDHHC enzymes already are [195]. Although much of the synaptic localization of zDHHC5 and zDHHC8 has been covered in Chapter 1, a recent study demonstrated that overexpressed zDHHC5 and zDHHC8 were specifically enriched in axons of dorsal root ganglion (DRG) neurons, compared to the remaining 21 zDHHC PATs [212]. Further staining with an antibody towards endogenous zDHHC5 as well shRNA-induced knockdowns of *Zdhhc5* in these DRG cultures confirmed the axonal distribution of zDHHC5 [212]. Though it is the 190-kDa isoform of ankyrin-G that was shown to be palmitoylated by zDHHC5 and zDHHC8 [39], axonal zDHHC5 seems conveniently located to palmitoylate AIS-localized 480-kDa ankyrin-G. zDHHC5 and zDHHC8 are also localized to dendritic spines and would be well-positioned to palmitoylate spine-localized 190-kDa ankyrin-G as well [195, 198]. In light of recent work that demonstrated zDHHC17 is detected specifically at the soma and excluded from axons of DRG neurons [189], somatic zDHHC17 also appears to be conveniently located to palmitoylate ankyrin-B at neuronal somatodendritic compartments. Since zDHHC17 was found to be in the somatic Golgi [189], perhaps ankyrin-B is palmitoylated in the somatic Golgi before being forward trafficked out into the dendrites. Exclusion of zDHHC17 from the axon could also explain why palmitoylation did not contribute to the axonal cargo function of ankyrin-B at the axon: ankyrin-B may simply not be palmitoylated at the axon. If that is the case, that would suggest that palmitoylation is not the only mechanism defining specific localization of different pools of ankyrins in neurons. One interesting (observable) difference between axonal ankyrin-B and dendritic ankyrin-B is that endogenous dendritic ankyrin-B is highly plasma-membrane-associated (as evidenced by the railroad-track-like staining

observed with antibodies towards endogenous ankyrin-B [116]), while the pool of ankyrin-B that mediates axonal cargo transport (overexpressed 220-kDa ankyrin-B) is targeted to vesicles and transported with cargoes on motile axonal vesicles [172]. That is not to say there is not any plasma-membrane-associated ankyrin-B at the axon as endogenous 440-kDa ankyrin-B at the distal axon appears plasma-membrane associated [172], but our work showed the vesicular pool of 220-kDa ankyrin-B, which mediates axonal cargo transport, is targeted to the distal axon and functions in a palmitoylation-independent manner. Thus, it may be that local palmitoylation by distinct zDHHC PATs defines the precise localization of plasma-membrane-associated pools of ankyrins, such as AIS-localized ankyrin-G and dendritic ankyrin-B, but other mechanisms, posttranslational or otherwise, may drive the specific targeting of vesicular pools of ankyrin-B at the axon. This must be investigated further.

Additionally, it will be necessary to understand how zDHHC specificity is achieved between the homologous ankyrin-G and ankyrin-B beyond the possibility of local palmitoylation. Why does zDHHC17 fail to recognize ankyrin-G and is instead primarily palmitoylated by zDHHC5 and zDHHC8? Our deletion studies in primary neuronal cultures demonstrated zDHHC17 mediates the majority of ankyrin-B palmitoylation in neurons (**Figure 3.3**). Why is ankyrin-B primarily recognized by zDHHC17? How does such specificity arise especially when considering that the N-terminal ANK repeat domain harboring the palmitoylated cysteines in both ankyrin-G and ankyrin-B is so homologous? zDHHC5 and zDHHC8 have long C-terminal tails that contain PDZ-binding motifs, which for some substrates like PDZ-containing PLM, explains how zDHHC5 and zDHHC8 recognize their substrates for palmitoylation [195]. However, ankyrins do not have canonical PDZ domains. Therefore, ankyrin-G is likely dependent on local palmitoylation by plasma-membrane-localized zDHHC5 and zDHHC8. Though direct interaction

between ankyrin-G and zDHHC5 or zDHHC8 has never been investigated, zDHHC5 and zDHHC8 do not necessarily require direct interaction with their substrates for palmitoylation [195]. By contrast, many studies have shown that zDHHC17-mediated palmitoylation is highly dependent on the ANK domain of zDHHC17 directly interacting with its substrate [46, 186]. zDHHC17 has been characterized as a "high-selectivity/low activity enzyme" as it contains seven ankyrin (ANK) repeats at its N-terminus which recognizes a conserved (VIAP)(VIT)XXQP (X is any amino acid) sequence (zDABM) in the substrates it palmitoylates [46, 50, 186]. Mutating the highly conserved proline residue in the zDABM or deleting the ANK domain in zDHHC17 prevents zDHHC17 from being able to interact with its substrates and subsequently impedes palmitoylation [50]. Additionally, mutating zDHHC17 at asparagine 100 to an alanine (zDHHC17-N100A) results in tremendous loss of affinity between the ANK domain of zDHHC17 and zDABM-containing substrates [186, 189]. As mentioned in Chapter 3, the zDABM domain was identified in the ankyrin family using a peptide array [187]. Our work has shown zDHHC17 recognition to the zDABM of ankyrin-B is required for ankyrin-B palmitoylation and for modulation of ankyrin-B protein levels (**Figure 3.2**). Although the peptide screen identified all members of the ankyrin family as having zDABM-bearing consensus sequences, the study also identified amino acid preferences within the zDABM sequence, specific to each substrate, that enhanced affinity for zDHHC17 due to better contact [187]. However, zDABM sequences with less favorable amino acids at those positions still bound to zDHHC17, just less strongly [187]. This amino acid "favoritism" within ankyrin zDABM domains could explain the specificity of zDHHC17 for ankyrin-B compared to ankyrin-G. It is plausible that ankyrin-B contains "preferred" amino acids within its zDABM sequence as well as other favorable surrounding amino acids, which could enhance its interaction with zDHHC17 and allow for efficient palmitoylation.

By contrast, ankyrin-G may contain the more "non-favorable" amino acids within its zDABM sequence without any favorable surrounding amino acids, thereby dampening its affinity for zDHHC17 to such an extent that it cannot palmitoylate ankyrin-G. Additionally, serine and threonine phosphorylation in zDABM domains has been postulated to regulate zDABM-AR domain binding [46]. Serine phosphorylation in the zDABM domain of HDAC4 impaired binding to AR domain of ANKRA2 [213]. However, it is plausible that phosphorylation positively or negatively regulates the binding of zDABM motifs to the AR domain of zDHHC17. The peptide array identified one zDABM sequence within ankyrin-G (one with a proline at position 1207), and two zDABM sequences within ankyrin-B (one with a proline at position 1224 present in 220- and 440-kDa ankyrin-B located in the second ZU5 domain and the other containing a proline at position 2691 which is only present in the giant exon of 440-kDa ankyrin-B) [187]. The zDABM sequence identified in ankyrin-B where the proline is positioned at amino acid 1224 has a serine and threonine residue that are completely conserved with those of ankyrin-G. However, based on phosphosite database predictions, the threonine in the ankyrin-B zDABM sequence is predicted to be phosphorylated, but not the threonine in the ankyrin-G zDABM sequence [187]. This suggests that the phosphorylated threonine in ankyrin-B may positively regulate binding to zDHHC17 and establish specificity for zDHHC17 binding between ankyrin-G and ankyrin-B. The phosphorylation states of the zDABM domain may represent another level of regulation underlying zDHHC17 specificity for ankyrin-B, and are worth investigating in the future. The effect of flanking amino acids on the zDABM motif's ability to interact with zDHHC17 ANK domain should not be dismissed, as a previous study demonstrated that solely abolishing the interaction between zDHHC17 ANK domain and zDABM-containing substrate NMNAT2 using the zDHHC17-N100A mutant did not completely reduce palmitoylation of NMNAT2. It was the

combined effect of abolishing zDHHC17's ability to recognize zDABM of NMNAT2 through zDHHC17-N100A and mutation of three basic residues surrounding NMNAT2's zDABM sequence that abolished NMNAT2 palmitoylation [189]. Thus, it may be that 190-kDa ankyrin-G is locally palmitoylated by zDHHC5 and zDHHC8 just by nature of their shared subcellular distribution, but 220-kDa ankyrin-B by contrast depends on direct and specific interaction with zDHHC17 for its palmitoylation. How such specificity is achieved should be investigated in the future.

Determine whether palmitoylation mechanisms are conserved across other neuronal ankyrin isoforms.

Our work demonstrates that all neuronal isoforms of ankyrin-G (190-kDa, 270-kDa, and 480-kDa), and those of ankyrin-B (220-kDa and 440-kDa) are palmitoylated (**Figure 3.1**). Previous work also demonstrated that the 190-kDa isoform of ankyrin-G is palmitoylated by zDHHC5 and zDHHC8 in epithelial cells [39], and we showed zDHHC17 palmitoylates ankyrin-B in neurons (**Figure 3.3**). Whether zDHHC5 and zDHHC8 are capable of palmitoylating all neuronal isoforms of ankyrin-G, 190-kDa, 270-kDa and 480-kDa ankyrin-G, remains unknown. Similarly, whether zDHHC17 is capable of palmitoylating 440-kDa ankyrin-B is unknown. Given that the palmitoylated cysteine sites in both ankyrin-G and ankyrin-B are conserved within all major splice variants, it would be expected that zDHHC PATs would also be conserved. However, the local palmitoylation hypothesis instead supports a model where different ankyrin splice variants may rely on zDHHC enzymes that already targeted to the subcellular compartments these ankyrins isoforms need to go to. Future studies will need to investigate whether zDHHC5 and

zDHHC8, which are known to be localized to dendritic spines [195], palmitoylate 190-kDa ankyrin-G to target it to dendritic spines in neurons [198, 211]. Our laboratory has recently generated floxed *Zdhhc5* and *Zdhhc8* mouse lines to answer these questions. Cre cDNA can be transiently transfected in neuronal cultures of double floxed *Zdhhc5* and *Zdhhc8* mice to knock-out *Zdhhc5* and *Zdhhc8* simultaneously to see if ankyrin-G is still capable of accumulating in dendritic spines and form nanodomain structures within the spine head and neck after 21 days in culture when spine formation is complete. I hypothesize that simultaneous deletion of *Zdhhc5* and *Zdhhc8* would lead to loss of ankyrin-G palmitoylation and thus recapitulate the decrease in dendritic spine length, width, and density seen with RNAi-mediated knockdown of *Ank3*, which encodes ankyrin-G, in mature cortical neuron cultures [211]. Since there is no antibody specific to 190-kDa ankyrin-G because the antibodies are custom generated to the C-terminal death domain present in all three neuronal isoforms of ankyrin-G, this experiment in double floxed *Zdhhc5* and *Zdhhc8* neurons could also be performed with overexpressed WT 190-kDa ankyrin-G-GFP to ensure that the dendritic spine effects seen are 190-kDa ankyrin-G-dependent, and not dependent on 270- or 480-kDa ankyrin-G. Although palmitoylation is required for 480-kD ankyrin-G to localize to and scaffold its binding partners at the AIS [182], which zDHHC enzymes palmitoylate 480-kDa ankyrin-G are unknown. Given the recent study showing zDHHC5 localizes to the axon in DRG neurons [212], zDHHC5 might be uniquely positioned to locally palmitoylate 480-kDa ankyrin-G at the AIS. Using the same experimental approach as described above, I hypothesize that if 480-kDa ankyrin-G is locally palmitoylated at the axon, then deleting *Zdhhc5* in floxed *Zdhhc5* cortical neurons would be sufficient for 480-kDa ankyrin-G to lose its specific AIS localization. This effect could be verified using a specific 480-kDa ankyrin-G antibody designed to ensure AIS effects with *Zdhhc5* deletion are 480-kDa ankyrin-G-dependent. Palmitoylation of

480-kDa ankyrin-G by zDHHC5 would need to be verified biochemically by Acyl-RAC using these floxed *Zdhhc5* cortical neurons. However, given that the palmitoylation site of 190-kDa ankyrin-G, Cys70, is conserved across all neuronal isoforms of ankyrin-G [71], it is also possible both zDHHC5 and zDHHC8 palmitoylate 480-kDa ankyrin-G in a functionally redundant manner. If neither zDHHC5 or zDHHC8 palmitoylate 480-kDa ankyrin-G in neurons, it will be important to screen through the library of zDHHC PATs in heterologous cells to identify other PATs capable of palmitoylating 480-kDa ankyrin-G-GFP.

As for 440-kDa ankyrin-B, it appears to be the dominant isoform localized to axons and scaffolds L1CAM to repress axonal branching at the axon [175]. As mentioned in the previous section, zDHHC17 was shown to be excluded from axons of DRG neurons [189]. Assuming that DRG and hippocampal neurons exhibit similar distributions of zDHHC enzymes, I hypothesize that zDHHC17 will still be *capable* of palmitoylating 440-kDa ankyrin-B-GFP in heterologous cells, but will not mediate local palmitoylation of endogenous 440-kDa ankyrin-B given zDHHC17's absence from the axon. Interestingly, the two zDABM sequences (one with proline at position 1224 and the other at position 2691) identified in ankyrin-B from the peptide array [187] are both present in the 440-kDa ankyrin-B, which suggests that zDHHC17 could theoretically recognize, bind, and palmitoylate 440-kDa ankyrin-B in an overexpression system in heterologous cells, but might not be able to in polarized neuronal cells where zDHHC17 is not at the axon. Using the same experimental approach as described above, this question can be answered using Cre-transfected floxed *Zdhhc17* neurons to see if 440-kDa ankyrin-B targets to the distal axon properly (using our 440-kDa specific antibody). This also highlights the limitations of using heterologous cells as a model for identifying zDHHC enzyme-substrate pairs: observing that an overexpressed enzyme is capable of palmitoylating an overexpressed substrate does not

necessarily translate to more physiological cell types, where there is no overexpression and where subcellular distribution matters. *Just because it can does not mean it will.*

However, if zDHHC17 is not capable of recognizing and palmitoylating 440-kDa ankyrin-B even in a heterologous system, despite having two zDABM predicted domains [187], this could be explained by the fact that the zDABM sequence with proline at position 2691, which is specific to 440-kDa ankyrin-B, does not include any serine or threonine residues for phosphorylation. If phosphorylation of serines or threonines in ankyrin zDABM domains is a driver for zDHHC17 binding, then the lack of a phosphorylatable serine/threonine in the 440-kDa ankyrin-B-specific zDABM motif could explain lack of zDHHC17 recognition.

Understanding which zDHHC enzymes palmitoylate major ankyrin splice variants may highlight means to selectively target specific ankyrin isoforms without affecting others depending on their specific involvement in distinct processes and associations with neuropathophysiologies.

Test the local palmitoylation hypothesis directly for ankyrin-G and ankyrin-B palmitoylation.

As mentioned in chapter 1 as well as throughout this discussion chapter, multiple lines of evidence support the local palmitoylation of ankyrin-G and ankyrin-B for proper targeting to their respective subcellular compartments in the neuron. However, this has never been tested directly. If we arrest ankyrin-G in a subcellular compartment, like the ER or the Golgi, such that ankyrin-G never "sees" zDHHC5 and zDHHC8 at the plasma membrane, then is ankyrin-G able to get palmitoylated at all? Presumably, the subcellular compartment that ankyrin-G will be arrested in also has zDHHC enzymes of its own and should be capable of palmitoylating ankyrin-G if the local hypothesis holds true. Although zDHHC17 is appropriately positioned at the neuronal soma

to locally palmitoylate 220-kDa ankyrin-B and target it to somatodendritic compartments, zDHHC17 requires direct interaction with its substrates through their zDABM domain [46, 187]. Thus, it is likely that arresting ankyrin-B in a subcellular compartment like the ER where zDHHC17 does not reside would preclude ankyrin-B from getting palmitoylated. One approach to investigating this would be employing the Retention Using Selective Hook (RUSH) System. This assay relies on a hook, stably expressed in a "donor compartment", and a "reporter" protein of interest fused to streptavidin binding protein (SBP). The SBP-fused reporter protein is retained in the donor compartment via its interaction with the hook, which is itself fused to core streptavidin. The reporter can be released and trafficked to its original "acceptor" compartment by addition of biotin [214, 215]. Thus, this system could be re-engineered such that SBP-fused full length GFP-tagged human ankyrin-G transfected into stably-expressing Golgi (Streptavidin-HA-Golgin84) or ER (Streptavidin-HA-Ii) hook HEK293T cells would be arrested into the Golgi or ER and evaluated for its ability to be palmitoylated. If ankyrin-G is still capable of being palmitoylated regardless of its localization in the ER, in the Golgi, or at the plasma-membrane, these data would support a model of palmitoylation being a local phenomenon. The same approach could be employed for ankyrin-B but given zDHHC17 is Golgi-localized in HEK cells, the RUSH system would be used to arrest ankyrin-B in ER hook or plasma-membrane hook cells and assess its palmitoylation there. While it is very plausible that ankyrin-G would remain palmitoylated regardless of its localization at the ER, Golgi, or plasma-membrane, I hypothesize ankyrin-B would not be palmitoylated when arrested in the ER or at the plasma membrane as those compartments lack zDHHC17.

Determine the depalmitoylation mechanisms for ankyrins.

S-palmitoylation is a reversible process, thereby allowing for the fine-tuning of substrate localization and function in response to dynamic extracellular stimuli. Thus far, this work has covered the *S*-palmitoylation side of the equilibrium, but whether ankyrins undergo depalmitoylation will be necessary to fully understand the role of this posttranslational regulatory mechanism for ankyrin localization and function, and subsequent downstream effects for neuronal homeostasis (or dysregulation in pathological states associated with altered neuronal excitability). Depalmitoylating enzymes mediate the hydrolysis of *S*-palmitoylated cysteine residues to release palmitoylated substrates from their membrane domains. Enzymologically, depalmitoylating enzymes belong to a superfamily of serine hydrolases. Thus far, the 21 identified depalmitoylating serine hydrolases contain a α/β-hydrolase fold domain as a catalytic domain, can be blocked by the depalmitoylation inhibitor hexadecylfluorophosphonate (HDFP), and include protein thioesterases (such as PPT1) and the related ABHD proteins [216, 217]. The molecular consequences ensued by depalmitoylation of the abundant postsynaptic scaffolding protein PSD-95 highlight the value of investigating depalmitoylation as an important regulatory process for neuronal function, especially in the context of altered neuronal excitability. Increasing depalmitoylation activity by overexpression of the serine hydrolase ABHD17 or inhibiting global palmitoylation using the "dirty" palmitoylation inhibitor 2-bromopalmitate in neurons reduced palmitoylation levels of PSD-95, and subsequently reduced synaptic clustering of PSD-95 and AMPA receptors, suggesting shifts in the palmitoylation/depalmitoylation equilibrium have important effects on synaptic structure and plasticity [218]. Whether ankyrins undergo palmitoylation/depalmitoylation cycling and which serine hydrolases depalmitoylate ankyrin-G

and ankyrin-B in neurons needs to be investigated. Previous work from our laboratory has shown that 190-kDa ankyrin-G is sensitive to changes in neuronal excitability. In a mouse model of hyperexcitability where a mutation in ankyrin-G abolishes the ability of ankyrin-G to form GABAergic synapses on forebrain pyramidal neurons, 190-kDa ankyrin-G levels are reduced and subsequently, palmitoylation of 190-kDa ankyrin-G is also reduced by 65% [198, 219]. The study hypothesized that decreases in 190-kDa ankyrin-G levels are compensatory to offset the devastating effects of loss of inhibitory input. These findings suggest that 190-kDa ankyrin-G is likely depalmitoylated to regulate its protein levels (and perhaps localization as well) in response to changes in neuronal excitability. Our results showing a drastic reduction of ankyrin-B palmitoylation upon loss of *Zdhhc17* mRNA suggests that ankyrin-B is capable of being depalmitoylated. Whether the ankyrin-B palmitoylation/depalmitoylation equilibrium is shifted in response to changes in neuronal excitability warrants further investigation, especially in light of ankyrin-B's critical role in mediating dendritic excitability. It will be necessary to investigate whether ankyrin-B palmitoylation/depalmitoylation changes under conditions of altered dendritic excitability by way of impaired dendritic backpropagation of action potentials, impaired calcium dynamics at synapses, impaired LTP/LTD, or morphologically immature dendritic spines, or even in mouse models with learning and social behavior deficits. Given our findings showing that palmitoylation is required for ankyrin-B-mediated scaffolding of $Na_v1.2$ at dendrites in cortical pyramidal neurons, I hypothesize that abnormal and pathological reductions in dendritic excitability and synaptic plasticity would lead to an increase in ankyrin-B depalmitoylation to reduce ankyrin-B localization at the dendrites and subsequently reduce $Na_v1.2$ targeting at the dendrites. Palmitoylation/depalmitoylation cycles may be an important means of regulating ankyrin membrane targeting and protein levels. Understanding how the

palmitoylation/depalmitoylation equilibrium may be shifted under conditions of altered neuronal excitability will provide important insights into mechanisms of ankyrin-associated neuropathologies.

Determine the role of ankyrin-B palmitoylation for dendritic excitability and synaptic plasticity in vivo.

Canonically, the voltage gated sodium channel $Na_v1.2$ was thought to be scaffolded by ankyrin-G at the AIS, thereby promoting the initiation of action potentials in response to neuronal depolarization [191]. Recently, $Na_v1.2$ was found capable of translocating to distal dendrites of neocortical pyramidal neurons late in development to promote dendritic excitability and synaptic function. In fact, haploinsufficiency of *Scn2a*, the gene that encodes $Na_v1.2$, lead to reduced action potential backpropagation into dendrites, thereby impairing synaptic plasticity and synaptic strength, and causing defects in learning and sociability consistent with autism-related behaviors [117]. Here, we define dendritic excitability as action potentials back-propagating into dendrites to induce long-term potentiation (LTP) or long-term depression (LTD) at synapses, necessary processes for memory formation. Backpropagating action potentials (bAP) that travel down the dendrite increase dendritic calcium levels necessary to depolarize and relieve the magnesium block at NMDA receptors at synapses, which subsequently induces LTP and LTD depending on the magnitude of change in the dendritic membrane voltage induced by the bAP [220]. Recent work from our laboratory in collaboration with the Bender laboratory at UCSF revealed that $Na_v1.2$ is scaffolded at the dendrites by ankyrin-B, which is conveniently localized to the dendritic membrane. Interestingly, haploinsufficiency of *Ank2*, the gene that encodes

ankyrin-B, exhibits deficits in dendritic excitability and synaptic plasticity that phenocopy those observed with *Scn2a* heterozygosity, suggesting that ankyrin-B plays an important role in mediating synapse function through its scaffolding of dendritic $Na_v1.2$ [116]. Furthermore, part of my thesis work implicated palmitoylation as a critical regulator of ankyrin-B's function in scaffolding $Na_v1.2$ at dendrites. *In vitro*, we observed that exogenous addition of the palmitoylation-dead 220-kDa ankyrin-B after Cre-mediated knock-out of ankyrin-B in floxed *Ank2* cortical neurons impaired rescue of FLAG-tagged $Na_v1.2$ localization to dendritic membranes, suggesting that ankyrin-B palmitoylation is required for ankyrin-B to promote proper dendritic membrane targeting of $Na_v1.2$ (**Figure 3.6**). Palmitoylation drives the membrane association of ankyrin-B at the dendrites, so that ankyrin-B can in turn scaffold $Na_v1.2$ at the dendritic membrane. Interestingly, preliminary data in cortices of early and mature WT mice demonstrated that palmitoylation of ankyrin-B trends upwards throughout development, suggesting that palmitoylation is a mechanism ankyrin-B employs to ensure its own localization at the dendritic membrane as the need to scaffold sodium channels at the dendrite increases throughout development (**Figure 4.1**).

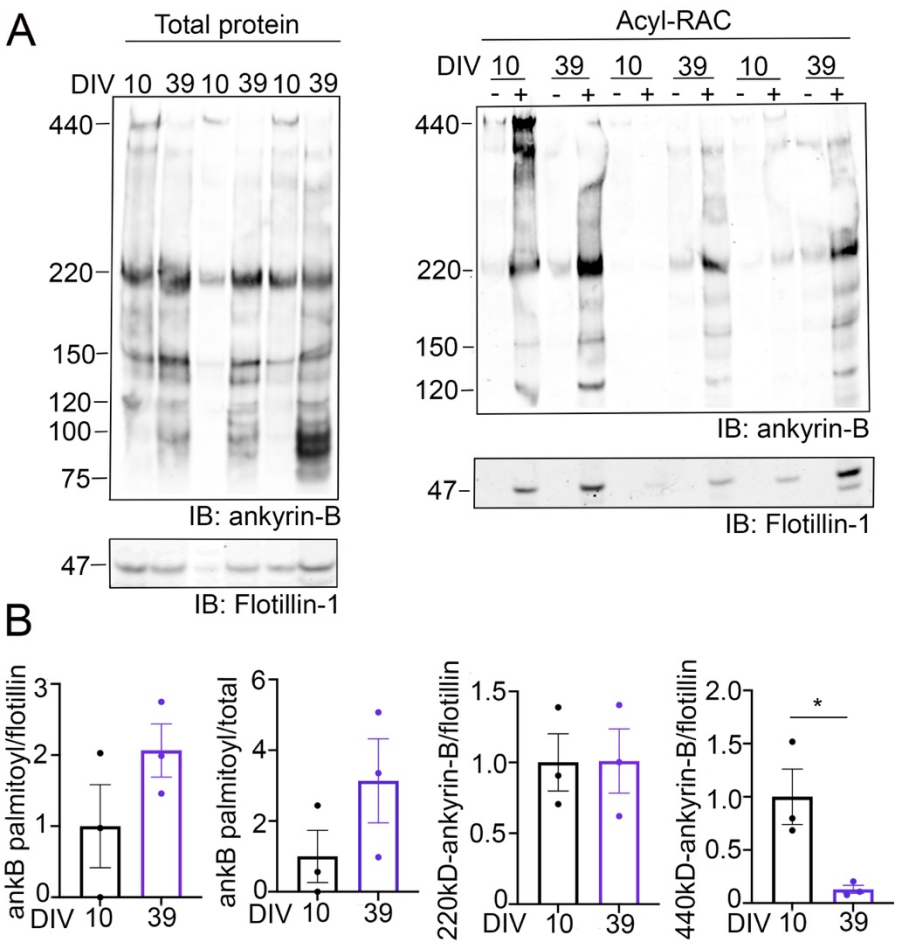

Figure 4.1. Ankyrin-B S-palmitoylation increases throughout the course of development.

A. Representative western blot showing total protein levels of endogenous ankyrin-B (*left*) and palmitoylation levels of ankyrin-B (*right*) from DIV10 and DIV39 cortices subjected to the Acyl-RAC assay. Ankyrin-B protein expression and palmitoylation are detected with an antibody towards against the C-terminal domain of ankyrin-B. Palmitoylation of 220-kDa ankyrin-B (*right blot*) is trending upwards at DIV39 compared to DIV10, while 220-kDa ankyrin-B expression remains fairly similar between DIV10 and DIV39 (*right blot*). **B.** Quantified *S*-palmitoylation normalized to palmitoylated flotillin or total protein and protein levels of ankyrin-B normalized to input flotillin signal from n=3 independent replicates per condition. A student's *t-test* was performed to determine significance, though neither 220-kDa ankyrin-B palmitoylation nor protein expression were statistically different at DIV10 versus DIV39. However, ankyrin-B palmitoylation at DIV39 appears to be trending upwards compared to DIV10, and more individual replicates may be needed to better power the experiment. 440-kDa ankyrin-B protein expression significantly decreases at DIV39 compared to DIV10. *P<0.05; Student's *t-test* (unpaired).

If ankyrin-B relies on palmitoylation to scaffold $Na_v1.2$ channels to pyramidal neuron dendrites *in vivo*, then loss of ankyrin-B palmitoylation should lead to similar deficits in dendritic excitability and synaptic plasticity as those observed in haploinsufficient *Scn2a* and *Ank2* mice. Thus, future work should investigate dendritic excitability and synaptic function in a mouse model that lacks 50% of palmitoylatable ankyrin-B (heterozygous for 220-kDa AAAAA-ankyrin-B). This mouse could be engineered using CRISPR/Cas9 to knock-in the appropriate nucleotide changes (tgt/c → gct/c) that encode the five cysteines in the N-terminal ankyrin repeat domain in one of the two floxed *Ank2* alleles to allow for spatial and temporal control of mutant expression. In this model, it will be important to investigate whether measures of intrinsic neuronal excitability, such as AP generation/waveforms, burst-evoked calcium transients (to assess backpropagation and thus dendritic excitability), mEPSC frequency, AMPA/NMDA ratio, and paired-pulse ratios (to assess postsynaptic function), and AP-evoked sodium influx are different between WT and heterozygous AAAAA ankyrin-B mice, while making direct comparisons between the haploinsufficient *Scn2a* and *Ank2* mice [116, 117]. If our hypothesis regarding there being two pools of ankyrin-B, dendritic ankyrin-B being palmitoylation-dependent, the heterozygous palmitoylation-dead ankyrin-B mouse model would allow us to specifically investigate the dendritic pool of ankyrin-B without confounding effects of axonal pools of ankyrin-B, which is not regulated by palmitoylation according to our work. These studies would provide a feasible "druggable" mechanistic target for brain diseases like ASD associated with dysfunction of ankyrin-B and $Na_v1.2$.

Determine whether ASD-associated variants in ANK2 lead to altered palmitoylation to affect localization and function of the ankyrin-B/ $Na_v1.2$ complex at dendritic membranes.

Autism spectrum disorder (ASD) is a neurodevelopmental disorder that affects developmental milestones starting around the age of two, particularly of social and language nature, with lasting deficits in social behavior [179]. It has been reported that those with ASD may be hyper- or hypo-sensitive to certain stimuli such as temperature, noise, texture, and/or light. The gene that encodes $Na_v1.2$, *SCN2A*, is recognized as a high susceptibility gene for neurodevelopmental disorders, including autism spectrum disorder (ASD) [179]. In fact, loss-of-function in *SCN2A* is one of the strongest, if not the strongest, risk factor for ASD based on exome sequencing [180, 181]. Mutations in *SCN2A* account for 7.5 cases of ASD per 100,000 births [221, 222]. Interestingly, *ANK2*, which encodes ankyrin-B, is also a high confidence gene for ASD, and with *SCN2A,* falls within the top 20 most common disrupted genes in ASD [177, 178]. Although many ASD risk-factor genes can be broadly characterized as chromatin modifiers and synaptic function regulators, $Na_v1.2$ and ankyrin-B interacting to mediate dendritic excitability provides strong rationale that deficits in dendritic excitability may be a common point of convergence for two strong ASD risk genes like *SCN2A* and *ANK2.* Exome sequencing has enabled the identification of a number of new ASD-associated *ANK2* variants [178, 223, 224]. One well characterized ASD-associated variant causes a frameshift that specifically and exclusively affects the 440-kDa isoform of ankyrin-B, thereby causing increased axonal branching through loss of axonal scaffolding of L1CAM, increased axonal connectivity, and behavioral impairments in mice reminiscent of social and communicative deficits seen in human ASD patients [175]. However, ASD-associated variants more commonly cause protein-

truncation and nonsense mediated decay and affect both the 220- and the 440-kDa isoforms of ankyrin-B [178]. Several missense variants and protein-truncating variants have been identified in *ANK2* as well as in the regions of *SCN2A* that encode the Na_v 1.2 II-III loop domain, which is the predicted binding interface for ankyrins. Although the functional effects of these variants still need to be investigated, we predict that missense variants in *ANK2* or within the aforementioned *SCN2A* region where binding between ankyrin-B and $Na_v1.2$ is abolished might result in reduced ankyrin-B-mediated dendritic $Na_v1.2$ targeting and deficits in dendritic excitability and synaptic plasticity. Furthermore, future work will need to test whether ASD-associated missense variants in *ANK2*, for instance L384R (c.114177051 T>G) (Stephen Sanders, unpublished), affect ankyrin-B's ability to be palmitoylated, and impair proper targeting of $Na_v1.2$ at dendrites and reduce dendritic excitability. Firstly, it will be important to verify that these *ANK2* variants express normally as it will be impossible to study palmitoylation if mutant ankyrin-B is degraded. One could envision "screening" these ASD-associated missense mutations *in vitro* by overexpressing mutant ankyrin-B-GFP like the L384R ankyrin-B-GFP cDNA in HEK293T cells with zDHHC17 to test its ability to be palmitoylated relative to WT ankyrin-B-GFP. Additionally, ASD-associated ankyrin-B-GFP mutants could be used to rescue Cre-mediated knockout of ankyrin-B in *Ank2* flox/flox cortical neurons to see if the mutant ankyrin-B can rescue FLAG-tagged $Na_v1.2$ localization at dendritic membranes in cortical neuron cultures. Provided that mutants are unable to be palmitoylated *in vitro* and cannot rescue dendritic $Na_v1.2$ localization in cultured neurons, then *in utero* electroporation can be employed to induce expression of the mutant ankyrin-B in E10 embryos for later electrophysiological studies of dendritic excitability. It is rational to hypothesize that point mutations in the ankyrin-B N-terminus, particularly around the cysteine rich region containing the potentially palmitoylated

cysteine residues (C305, C347, C375, C406) could disrupt the local electrostatic environment sufficiently to affect ankyrin-B palmitoylation. Given that both the membrane as well as acyl-coenzyme A (palmitic acid) are largely negatively charged, polybasic or positively charged amino acids around the cysteine-rich region of palmitoylated proteins are generally thought to increase a protein's ability to anchor ("electrostatic anchoring") at the membrane so it can be palmitoylated. This hypothesis was highlighted in a study where addition of negatively charged residues in the cysteine-rich region of the SNARE protein SNAP25 caused less palmitoylation and less SNAP25 targeting to the plasma membrane compared to WT SNAP25 in neuroendocrine PC12 cells [225]. Fewer positive charges are thought to decrease the binding affinity for palmitate and/or may change the geometry of the contact between the protein and the membrane. In contrast, addition of additional positively charged residues near the palmitoylated cysteine cluster of SNAP25 lead to higher plasma membrane affinity in a palmitoylation-independent manner, suggesting that pure protein electrostatics are sufficient to facilitate anchoring of the protein to the membrane and facilitate further palmitoylation. Interestingly, the study also showed that not all SNAP25 mutants with increased positive charge showed increased membrane targeting, which demonstrates that some mutations that add too much positive charge can cause protein-membrane contacts to become so tight that attachment of the palmitate becomes unfavorable [225]. Assuming that ankyrin-B relies on electrostatic anchoring preceding palmitoylation in a similar fashion as SNAP25 (which is unknown), one could imagine the ASD-associated mutation in ankyrin-B, L384R, which just so happens to be between two potentially cysteine residues C375 and C406, could either enhance or decrease palmitoylation: the switch from a non-polar amino acid like leucine to a positively charged amino acid like arginine could increase the positive charge of the local electrostatic environment to increase the affinity of ankyrin-B for the

membrane, thereby increasing its ability to be palmitoylated. In contrast, the addition of this positive charge could also increase membrane affinity to such a great extent that addition of the palmitate is geometrically unfavorable, leading to less initial plasma membrane contacts and less palmitoylation at the plasma membrane. Thus, it will be important to determine how these variants affect ankyrin-B's ability to be palmitoylated and determine the downstream effects on $Na_v1.2$ scaffolding and dendritic excitability. Interestingly, many of the variants identified both in *ANK2* and in the ankyrin binding interface of *SCN2A* are associated with a broad range of disorders, including ASD, developmental delay, and epilepsy. In fact, many of these variants can be characterized as gain-of-function variants, which are common in children suffering from early-onset epilepsy, or loss-of-function variants, which are common in children diagnosed with ASD and/or developmental delay [179, 181]. Thus, it will be worth investigating whether missense variants that alter palmitoylation increase or decrease ankyrin-B's ability to target dendritic $Na_v1.2$. Increases in dendritic excitability by increased ankyrin-B palmitoylation may correlate with epilepsy phenotypes, whereas decreases in dendritic excitability by decreased ankyrin-B palmitoylation may correlate with ASD and/or intellectual delays. Such studies would directly implicate dysfunctional ankyrin-B palmitoylation as a mechanism underlying ASD or epilepsy etiology, and would position palmitoylation as a targetable means to restore changes in $Na_v1.2$ localization and function for patients with ASD, developmental delays, or epilepsy.

Understanding the role of palmitoylation for $Na_v1.2$ channels and its implications for the $Na_v1.2$/ankyrin-B complex at the dendritic membrane.

The work demonstrated in Chapter 3 demonstrated that palmitoylation of ankyrin-B is required to scaffold $Na_v1.2$ at the dendritic membrane in cultured neocortical pyramidal neurons. Much evidence points to $Na_v1.2$ itself being capable of undergoing palmitoylation to regulate channel gating, yet how $Na_v1.2$ palmitoylation impacts formation of the $Na_v1.2$-ankyrin-B complex has not yet been investigated. The cardiac sodium channel $Na_v1.5$ is post-translationally modified by palmitoylation to increase channel availability and modulates sodium currents, thereby leading to enhanced cardiac excitability and prolonged action potential duration in cultured cardiomyocytes from neonatal rats [226]. Inhibition of palmitoylation resulted in faster close-state inactivation and reduced channel availability, while increasing palmitoylation through palmitic acid prolonged action potential duration and induced early after depolarizations. These data suggest palmitoylation of $Na_v1.5$ tightly regulates channel inactivation properties to ensure fine-tuning of cardiac excitability [226]. Multiple studies have demonstrated that voltage-gated sodium channels (VGSCs) in the brain are also subject to palmitoylation [226-229]. Na_v channels rely on palmitoylation for their biosynthesis and processing as they traffic to the membrane [228]. Furthermore, integrating a palmitoylation site in place of a glycine residue (G1079C) within the II-III loop of the rat $Na_v1.2a$ alters the pharmacological properties (the mutant channel exhibits enhanced sensitivity to tarantula toxins) and causes the channel to activate at more negative voltages compared to WT rat $Na_v1.2a$ [229]. Although the study demonstrated that rat $Na_v1.2$ palmitoylation can alter gating properties and pharmacological sensitivities of the channel, it did so by way of 2-bromopalmitate as a palmitoylation inhibitor which is considered by the field as

a “dirty”, nonspecific inhibitor and only identified predicted palmitoylation sites but failed to show actual palmitoylation changes by biochemistry [229]. Thus, it is critical that future studies utilize the Acyl-RAC assay to demonstrate whether $Na_v1.2$ is palmitoylated in mouse brain and show loss of $Na_v1.2$ palmitoylation when a single or a combination of the predicted palmitoylation sites (I-II loop C650, II-III loop C1053, II-III loop C1182) are mutated to alanines by biochemistry. If $Na_v1.2$ is palmitoylated, it may be that ankyrin-B relies on palmitoylation to target itself to the dendritic membrane so as to scaffold $Na_v1.2$ at the dendrites, and $Na_v1.2$ may be subsequently palmitoylated to modulate $Na_v1.2$ gating properties, consistent with what was observed with rat $Na_v1.2$ and cardiac $Na_v1.5$. Numerous studies have also shown different ways in which palmitoylation can modify transmembrane substrates like sodium channels. For example, palmitoylation can induce conformational tilting of transmembrane domains, promote substrate association with lipid rafts to facilitate protein-protein interactions or segregate proteins under specific circumstances, regulates protein complex interactions, and can modulate other posttranslational modifications [12]. Interestingly, the most likely predicted palmitoylation site (C1182) in $Na_v1.2$ resides in the intracellular II-III loop, where the nine-amino acid (aa 1105-1113) ankyrin-binding motif is located [160, 229]. C1182 is near a sequence of glutamate and serine CK2-mediated phosphorylation sites (E1111, S1112, S1123, S1124, S1126) that regulate the interaction between the Na_v1 ankyrin-binding motif and the membrane binding domain of ankyrins [230]. Thus, it is possible that palmitoylation of $Na_v1.2$ at C1182 promotes phosphorylation-dependent binding of $Na_v1.2$ to the membrane binding domain of ankyrin-B or ankyrin-G. Given that the sequence of phosphorylated residues in $Na_v1.2$ II-III loop are well conserved in $Na_v1.1$, 1.2, and 1.6, and that the ankyrin binding domain where sodium channels bind is also well-conserved among ankyrin-B and ankyrin-G [160], it may be that ankyrin-B

palmitoylation drives the specificity of ankyrin-B-$Na_v1.2$ localization at the dendrites in mature neurons, but that palmitoylation of $Na_v1.2$ promotes phosphorylation of $Na_v1.2$ II-III loop residues to enhance affinity of whichever ankyrin happens to be where $Na_v1.2$ is. Lastly, assuming that $Na_v1.2$ is palmitoylated, it will be important to determine whether $Na_v1.2$ palmitoylation regulates its ability to interact with β1 subunits, which modulate trafficking, gating, and kinetics of the Na_v alpha subunits [115]. To test this, one could co-express WT or palmitoylation-dead $Na_V1.2$-3x FLAG IRES GFP with Na_V β1-2A-mCherry in HEK cells and measure current density (as a measure of how many channels are at the cell surface), gating, and kinetics in the presence or absence of Na_V β1-2A-mCherry. Understanding how $Na_v1.2$ palmitoylation contributes to the dendritic $Na_v1.2$-ankyrin-B-β1 complex will provide mechanistic insights into ways ASD-associated *SCN2A* variants affect formation or maintenance of this complex in a palmitoylation-dependent manner.

It will also be equally important to determine the role of zDHHC17 for the formation and localization of the $Na_v1.2$-ankyrin-B complex. If $Na_v1.2$ is palmitoylated, it will be important to determine whether zDHHC17 mediates its palmitoylation, using Cre-transduced floxed *Zdhhc17* neurons subjected to Acyl-RAC. If zDHHC17 is not a candidate enzyme for $Na_v1.2$, then a screening approach will need to be employed in heterologous cells to determine which other zDHHC enzymes are capable of palmitoylating $Na_v1.2$. If $Na_v1.2$ is not palmitoylated, further work should investigate the role of the zDHHC17-ankyrin-B substrate pair for $Na_v1.2$ localization at dendritic membranes. For example, in the absence of zDHHC17 in floxed *Zdhhc17* neurons transfected with Cre, where presumably ankyrin-B cannot be palmitoylated, I hypothesize $Na_v1.2$ would not be able to localize to the dendritic membrane, similar to the effects observed with the palmitoylation-dead ankyrin-B rescue in floxed *Ank2* cortical neurons (**Figure**

3.6).

β1 subunits

Determine whether β1 palmitoylation affects gene transcription

Chapter 2 of this thesis showed that β1 palmitoylation regulates β1 localization at the plasma membrane, and consequently its intramembrane proteolytic cleavage (RIP). Recent work demonstrated that β1 RIP by BACE1 and γ-secretase generates a soluble intracellular domain of β1, known as the β1-ICD, which gets translocated to the cell nucleus to modulate gene transcription. β1-ICD overexpression in heterologous cells resulted in downregulation of genes involved in cell adhesion, the immune response, cellular proliferation, and calcium ion binding. By contrast, cardiac ventricles from *Scn1b* null P10 mice, which lack the β1-ICD signaling pathway, exhibited upregulation of the aforementioned genes families involved in the immune response, proliferation, and calcium ion binding pathways [204]. These data suggest that the β1-ICD may act as a molecular brake on gene expression in the heart *in vivo*, and potentially implicates β1 RIP-regulated gene expression as a disease mechanism to be investigated for loss of function *SCN1B* variants [204]. Given our work showing β1 RIP is also regulated by palmitoylation, future work should focus on understanding the role of palmitoylation for β1 RIP-mediated gene transcription. Proof-of-principle experiments could be performed in heterologous cells to see if overexpressed palmitoylation-dead β1-p.C162A-V5-2AeGFP downregulates gene expression by RNA-sequencing compared to WT β1-V5-2AeGFP, similarly to the β1-ICD. If β1

C162A instead upregulates gene expression similarly to cardiac ventricles from *Scn1b* null P10 mice, then β1 C162A in vivo would provide a means to investigate downstream effects on cleavage and gene transcription without affecting β1's ability to modulate alpha subunit gating and kinetics [185]. It will also be important to identify human variants in *SCN1B* that prevent palmitoylation and test their effects on RIP and subsequently gene expression. Interestingly, a Brugada Syndrome 5 patient variant in *SCN1B*, p.C162Y is predicted to prevent β1 palmitoylation as it abolishes β1's only palmitoylated cysteine (ClinVar). Lastly, it will be important to understand whether palmitoylation regulates β1 RIP in response to changes in neuronal or heart activity. As Chapter 1 highlighted, zDHHC enzymes sense changing neuronal excitability to enhance or reduce palmitoylation to alter targeting of specific substrates. zDHHC2 translocates to the plasma membrane to increase palmitoylation and accumulation of PSD95 at the synaptic membrane in response to decreases in neuronal activity [36]. It may be that altered levels of palmitoylation in response to changes in extracellular stimuli is a means for β1 to adapt cleavage and changes in gene expression and cellular excitability accordingly, which future work should assess.

Overall Conclusions

Taken together, this thesis describes the regulation of localization and function of two important neuronal substrates, VGSC β1 subunits and ankyrin-B, by palmitoylation. VGSC β1 is lipid-modified by *S*-palmitoylation to regulate its cell surface localization and subsequently its proteolytic cleavage in heterologous cells. When β1 cannot be palmitoylated, it is less retained at the plasma membrane, and therefore a smaller pool is available to be cleaved by the proteolytic

enzymes BACE1 and γ-secretase. We resolved for the first time in this work that β1 proteolytic cleavage occurred at the plasma membrane. This work provides a new mechanism to regulate β1 cleavage by BACE1 and γ-secretase, which has important consequences for downstream cellular excitability as β1 proteolytic cleavage modulates gene transcription [115]. We also show in this thesis that the dendritic pool of ankyrin-B is lipid-modified by *S*-palmitoylation to scaffold $Na_v1.2$ channels at dendritic membranes. By contrast, the pool of ankyrin-B on vesicles responsible for mediating axonal cargo transport is not dependent on palmitoylation for its function. This work highlights a new regulatory mechanism underlying ankyrin-B's functions at dendritic membranes, which has important implications for dendritic excitability and synaptic plasticity. Based on this work, we hypothesize that specific disease-linked variants in *SCN1B*, which encodes β1, may disrupt β1 palmitoylation and thereby impair downstream cleavage and gene transcription, ultimately contributing to onset and/or progression of *SCN1B*-linked disease states like EIEE52. Likewise, we hypothesize that specific disease-linked variants in *ANK2*, which encodes ankyrin-B, may disrupt ankyrin-B palmitoylation and thereby prevent proper scaffolding of $Na_v1.2$ at dendritic membranes to cause impaired dendritic excitability, processes that are likely relevant in ASD etiology. As previously mentioned, though β1 and ankyrin-B are not inherently related substrates, this work has been made especially relevant in light of the recently discovered convergent mechanisms between voltage gated sodium channels and ankyrin-B. VGSC α subunits depend on the non-covalent association of β1 subunits for modulation of their biophysical properties and surface expression. Therefore, we cannot consider our findings about β1 and ankyrin-B palmitoylation in a vacuum- as we continue to elucidate the role of the $Na_v1.2$-ankyrin-B complex in mediating dendritic excitability in neurons, we must not forget the very critical role that β1 subunits play for Na_v function and how β1 palmitoylation may be a critical component of

$Na_v1.2$/ankyrin-B-mediated dendritic excitability. Future work will examine detailed mechanisms by which disease-linked disruptions in palmitoylation of β1 or ankyrin-B contribute to the underlying mechanisms of their associated diseases, EIEE52 and ASD respectively, and whether palmitoylation may be a feasible drug target to restore potentially affected processes such as loss of β1-ICD-mediated gene transcription, or ankyrin-B-mediated dendritic excitability. Additionally, it will be important to determine how ASD variants that disrupt ankyrin-B palmitoylation also disrupt $Na_v1.2$ localization and dendritic excitability, and the role of β1 in the formation and maintenance of this macromolecular complex.

Bibliography

1. Linder, M.E. and R.J. Deschenes, *Palmitoylation: policing protein stability and traffic.* Nat Rev Mol Cell Biol, 2007. **8**(1): p. 74-84.
2. Fukata, Y. and M. Fukata, *Protein palmitoylation in neuronal development and synaptic plasticity.* Nat Rev Neurosci, 2010. **11**(3): p. 161-75.
3. Holland, S.M. and G.M. Thomas, *Roles of palmitoylation in axon growth, degeneration and regeneration.* J Neurosci Res, 2017. **95**(8): p. 1528-1539.
4. Mitchell, D.A., et al., *Protein palmitoylation by a family of DHHC protein S-acyltransferases.* J Lipid Res, 2006. **47**(6): p. 1118-27.
5. Mitchell, D.A., et al., *Mutational analysis of Saccharomyces cerevisiae Erf2 reveals a two-step reaction mechanism for protein palmitoylation by DHHC enzymes.* J Biol Chem, 2010. **285**(49): p. 38104-14.
6. Putilina, T., P. Wong, and S. Gentleman, *The DHHC domain: a new highly conserved cysteine-rich motif.* Mol Cell Biochem, 1999. **195**(1-2): p. 219-26.
7. Rana, M.S., C.J. Lee, and A. Banerjee, *The molecular mechanism of DHHC protein acyltransferases.* Biochem Soc Trans, 2019. **47**(1): p. 157-167.
8. Politis, E.G., A.F. Roth, and N.G. Davis, *Transmembrane topology of the protein palmitoyl transferase Akr1.* J Biol Chem, 2005. **280**(11): p. 10156-63.
9. Guan, X. and C.A. Fierke, *Understanding Protein Palmitoylation: Biological Significance and Enzymology.* Sci China Chem, 2011. **54**(12): p. 1888-1897.
10. Iwanaga, T., et al., *Dynamic protein palmitoylation in cellular signaling.* Prog Lipid Res, 2009. **48**(3-4): p. 117-27.
11. Nadolski, M.J. and M.E. Linder, *Protein lipidation.* FEBS J, 2007. **274**(20): p. 5202-10.
12. Blaskovic, S., M. Blanc, and F.G. van der Goot, *What does S-palmitoylation do to membrane proteins?* FEBS J, 2013. **280**(12): p. 2766-74.
13. Sanders, S.S., et al., *Curation of the Mammalian Palmitoylome Indicates a Pivotal Role for Palmitoylation in Diseases and Disorders of the Nervous System and Cancers.* PLoS Comput Biol, 2015. **11**(8): p. e1004405.
14. Blanc, M., et al., *SwissPalm: Protein Palmitoylation database.* F1000Res, 2015. **4**: p. 261.
15. Mukai, J., et al., *Evidence that the gene encoding ZDHHC8 contributes to the risk of schizophrenia.* Nat Genet, 2004. **36**(7): p. 725-31.
16. Woodin, M., et al., *Neuropsychological profile of children and adolescents with the 22q11.2 microdeletion.* Genet Med, 2001. **3**(1): p. 34-9.
17. Mukai, J., et al., *Palmitoylation-dependent neurodevelopmental deficits in a mouse model of 22q11 microdeletion.* Nat Neurosci, 2008. **11**(11): p. 1302-10.
18. Masurel-Paulet, A., et al., *Expanding the clinical phenotype of patients with a ZDHHC9 mutation.* Am J Med Genet A, 2014. **164A**(3): p. 789-95.

19. Raymond, F.L., et al., *Mutations in ZDHHC9, which encodes a palmitoyltransferase of NRAS and HRAS, cause X-linked mental retardation associated with a Marfanoid habitus.* Am J Hum Genet, 2007. **80**(5): p. 982-7.
20. Sutton, L.M., et al., *Hip14l-deficient mice develop neuropathological and behavioural features of Huntington disease.* Hum Mol Genet, 2013. **22**(3): p. 452-65.
21. Greaves, J. and L.H. Chamberlain, *New links between S-acylation and cancer.* J Pathol, 2014. **233**(1): p. 4-6.
22. Sobocinska, J., et al., *Protein Palmitoylation and Its Role in Bacterial and Viral Infections.* Front Immunol, 2017. **8**: p. 2003.
23. Roth, A.F., et al., *Global analysis of protein palmitoylation in yeast.* Cell, 2006. **125**(5): p. 1003-13.
24. Lobo, S., et al., *Identification of a Ras palmitoyltransferase in Saccharomyces cerevisiae.* J Biol Chem, 2002. **277**(43): p. 41268-73.
25. Bartels, D.J., et al., *Erf2, a novel gene product that affects the localization and palmitoylation of Ras2 in Saccharomyces cerevisiae.* Mol Cell Biol, 1999. **19**(10): p. 6775-87.
26. Roth, A.F., et al., *The yeast DHHC cysteine-rich domain protein Akr1p is a palmitoyl transferase.* J Cell Biol, 2002. **159**(1): p. 23-8.
27. Babu, P., R.J. Deschenes, and L.C. Robinson, *Akr1p-dependent palmitoylation of Yck2p yeast casein kinase 1 is necessary and sufficient for plasma membrane targeting.* J Biol Chem, 2004. **279**(26): p. 27138-47.
28. Valdez-Taubas, J. and H. Pelham, *Swf1-dependent palmitoylation of the SNARE Tlg1 prevents its ubiquitination and degradation.* EMBO J, 2005. **24**(14): p. 2524-32.
29. Lam, K.K., et al., *Palmitoylation by the DHHC protein Pfa4 regulates the ER exit of Chs3.* J Cell Biol, 2006. **174**(1): p. 19-25.
30. Ohno, Y., et al., *Analysis of substrate specificity of human DHHC protein acyltransferases using a yeast expression system.* Mol Biol Cell, 2012. **23**(23): p. 4543-51.
31. Hou, H., et al., *The DHHC protein Pfa3 affects vacuole-associated palmitoylation of the fusion factor Vac8.* Proc Natl Acad Sci U S A, 2005. **102**(48): p. 17366-71.
32. Smotrys, J.E., et al., *The vacuolar DHHC-CRD protein Pfa3p is a protein acyltransferase for Vac8p.* J Cell Biol, 2005. **170**(7): p. 1091-9.
33. Hou, H., et al., *Analysis of DHHC acyltransferases implies overlapping substrate specificity and a two-step reaction mechanism.* Traffic, 2009. **10**(8): p. 1061-73.
34. Fukata, M., et al., *Identification of PSD-95 palmitoylating enzymes.* Neuron, 2004. **44**(6): p. 987-96.
35. Jeyifous, O., et al., *Palmitoylation regulates glutamate receptor distributions in postsynaptic densities through control of PSD95 conformation and orientation.* Proc Natl Acad Sci U S A, 2016. **113**(52): p. E8482-E8491.
36. Noritake, J., et al., *Mobile DHHC palmitoylating enzyme mediates activity-sensitive synaptic targeting of PSD-95.* J Cell Biol, 2009. **186**(1): p. 147-60.
37. Tian, L., et al., *Multiple palmitoyltransferases are required for palmitoylation-dependent regulation of large conductance calcium- and voltage-activated potassium channels.* J Biol Chem, 2010. **285**(31): p. 23954-62.
38. Fernandez-Hernando, C., et al., *Identification of Golgi-localized acyl transferases that palmitoylate and regulate endothelial nitric oxide synthase.* J Cell Biol, 2006. **174**(3): p. 369-77.

39. He, M., K.M. Abdi, and V. Bennett, *Ankyrin-G palmitoylation and betaII-spectrin binding to phosphoinositide lipids drive lateral membrane assembly.* J Cell Biol, 2014. **206**(2): p. 273-88.
40. Greaves, J., et al., *Palmitoylation and membrane interactions of the neuroprotective chaperone cysteine-string protein.* J Biol Chem, 2008. **283**(36): p. 25014-26.
41. Greaves, J., et al., *Palmitoylation of the SNAP25 protein family: specificity and regulation by DHHC palmitoyl transferases.* J Biol Chem, 2010. **285**(32): p. 24629-38.
42. Tsutsumi, R., et al., *Identification of G protein alpha subunit-palmitoylating enzyme.* Mol Cell Biol, 2009. **29**(2): p. 435-47.
43. Shmueli, A., et al., *Ndel1 palmitoylation: a new mean to regulate cytoplasmic dynein activity.* EMBO J, 2010. **29**(1): p. 107-19.
44. Lemonidis, K., et al., *Substrate selectivity in the zDHHC family of S-acyltransferases.* Biochem Soc Trans, 2017. **45**(3): p. 751-758.
45. Huang, K., et al., *Neuronal palmitoyl acyl transferases exhibit distinct substrate specificity.* FASEB J, 2009. **23**(8): p. 2605-15.
46. Lemonidis, K., M.C. Sanchez-Perez, and L.H. Chamberlain, *Identification of a Novel Sequence Motif Recognized by the Ankyrin Repeat Domain of zDHHC17/13 S-Acyltransferases.* J Biol Chem, 2015. **290**(36): p. 21939-50.
47. Gorleku, O.A., et al., *Endoplasmic reticulum localization of DHHC palmitoyltransferases mediated by lysine-based sorting signals.* J Biol Chem, 2011. **286**(45): p. 39573-84.
48. Salaun, C., J. Greaves, and L.H. Chamberlain, *The intracellular dynamic of protein palmitoylation.* J Cell Biol, 2010. **191**(7): p. 1229-38.
49. Nadolski, M.J. and M.E. Linder, *Molecular recognition of the palmitoylation substrate Vac8 by its palmitoyltransferase Pfa3.* J Biol Chem, 2009. **284**(26): p. 17720-30.
50. Lemonidis, K., et al., *The Golgi S-acylation machinery comprises zDHHC enzymes with major differences in substrate affinity and S-acylation activity.* Mol Biol Cell, 2014. **25**(24): p. 3870-83.
51. Plain, F., et al., *An amphipathic alpha-helix directs palmitoylation of the large intracellular loop of the sodium/calcium exchanger.* J Biol Chem, 2017. **292**(25): p. 10745-10752.
52. Rodenburg, R.N.P., et al., *Stochastic palmitoylation of accessible cysteines in membrane proteins revealed by native mass spectrometry.* Nat Commun, 2017. **8**(1): p. 1280.
53. Ernst, A.M., D. Toomre, and J.S. Bogan, *Acylation - A New Means to Control Traffic Through the Golgi.* Front Cell Dev Biol, 2019. **7**: p. 109.
54. Fukata, Y., et al., *Local palmitoylation cycles define activity-regulated postsynaptic subdomains.* J Cell Biol, 2013. **202**(1): p. 145-61.
55. Ohno, Y., et al., *Intracellular localization and tissue-specific distribution of human and yeast DHHC cysteine-rich domain-containing proteins.* Biochim Biophys Acta, 2006. **1761**(4): p. 474-83.
56. Rocks, O., et al., *The palmitoylation machinery is a spatially organizing system for peripheral membrane proteins.* Cell, 2010. **141**(3): p. 458-71.
57. Ernst, A.M., et al., *S-Palmitoylation Sorts Membrane Cargo for Anterograde Transport in the Golgi.* Dev Cell, 2018. **47**(4): p. 479-493 e7.
58. Rocks, O., et al., *An acylation cycle regulates localization and activity of palmitoylated Ras isoforms.* Science, 2005. **307**(5716): p. 1746-52.

59. Swarthout, J.T., et al., *DHHC9 and GCP16 constitute a human protein fatty acyltransferase with specificity for H- and N-Ras.* J Biol Chem, 2005. **280**(35): p. 31141-8.
60. Kanaani, J., et al., *A combination of three distinct trafficking signals mediates axonal targeting and presynaptic clustering of GAD65.* J Cell Biol, 2002. **158**(7): p. 1229-38.
61. Kanaani, J., et al., *A palmitoylation cycle dynamically regulates partitioning of the GABA-synthesizing enzyme GAD65 between ER-Golgi and post-Golgi membranes.* J Cell Sci, 2008. **121**(Pt 4): p. 437-49.
62. Rush, D.B., et al., *Palmitoylation and trafficking of GAD65 are impaired in a cellular model of Huntington's disease.* Biochem J, 2012. **442**(1): p. 39-48.
63. Greaves, J. and L.H. Chamberlain, *Palmitoylation-dependent protein sorting.* J Cell Biol, 2007. **176**(3): p. 249-54.
64. Globa, A.K. and S.X. Bamji, *Protein palmitoylation in the development and plasticity of neuronal connections.* Curr Opin Neurobiol, 2017. **45**: p. 210-220.
65. Brigidi, G.S., et al., *Activity-regulated trafficking of the palmitoyl-acyl transferase DHHC5.* Nat Commun, 2015. **6**: p. 8200.
66. Thomas, G.M., et al., *Palmitoylation by DHHC5/8 targets GRIP1 to dendritic endosomes to regulate AMPA-R trafficking.* Neuron, 2012. **73**(3): p. 482-96.
67. Howie, J., et al., *Substrate recognition by the cell surface palmitoyl transferase DHHC5.* Proc Natl Acad Sci U S A, 2014. **111**(49): p. 17534-9.
68. Setou, M., et al., *Glutamate-receptor-interacting protein GRIP1 directly steers kinesin to dendrites.* Nature, 2002. **417**(6884): p. 83-7.
69. Moutin, E., et al., *Palmitoylation of cdc42 Promotes Spine Stabilization and Rescues Spine Density Deficit in a Mouse Model of 22q11.2 Deletion Syndrome.* Cereb Cortex, 2017. **27**(7): p. 3618-3629.
70. Thomas, G.M., et al., *DHHC8-dependent PICK1 palmitoylation is required for induction of cerebellar long-term synaptic depression.* J Neurosci, 2013. **33**(39): p. 15401-7.
71. He, M., P. Jenkins, and V. Bennett, *Cysteine 70 of ankyrin-G is S-palmitoylated and is required for function of ankyrin-G in membrane domain assembly.* J Biol Chem, 2012. **287**(52): p. 43995-4005.
72. Jenkins, P.M., M. He, and V. Bennett, *Dynamic spectrin/ankyrin-G microdomains promote lateral membrane assembly by opposing endocytosis.* Sci Adv, 2015. **1**(8): p. e1500301.
73. Lin, M.J., et al., *Massive palmitoylation-dependent endocytosis during reoxygenation of anoxic cardiac muscle.* Elife, 2013. **2**: p. e01295.
74. Tulloch, L.B., et al., *The inhibitory effect of phospholemman on the sodium pump requires its palmitoylation.* J Biol Chem, 2011. **286**(41): p. 36020-31.
75. Greaves, J., J.A. Carmichael, and L.H. Chamberlain, *The palmitoyl transferase DHHC2 targets a dynamic membrane cycling pathway: regulation by a C-terminal domain.* Mol Biol Cell, 2011. **22**(11): p. 1887-95.
76. Chen, X., et al., *PSD-95 is required to sustain the molecular organization of the postsynaptic density.* J Neurosci, 2011. **31**(17): p. 6329-38.
77. El-Husseini Ael, D., et al., *Synaptic strength regulated by palmitate cycling on PSD-95.* Cell, 2002. **108**(6): p. 849-63.
78. Gold, M.G., et al., *Architecture and dynamics of an A-kinase anchoring protein 79 (AKAP79) signaling complex.* Proc Natl Acad Sci U S A, 2011. **108**(16): p. 6426-31.

79. Sanderson, J.L. and M.L. Dell'Acqua, *AKAP signaling complexes in regulation of excitatory synaptic plasticity.* Neuroscientist, 2011. **17**(3): p. 321-36.
80. Sanderson, J.L., et al., *AKAP150-anchored calcineurin regulates synaptic plasticity by limiting synaptic incorporation of Ca2+-permeable AMPA receptors.* J Neurosci, 2012. **32**(43): p. 15036-52.
81. Park, M., et al., *Plasticity-induced growth of dendritic spines by exocytic trafficking from recycling endosomes.* Neuron, 2006. **52**(5): p. 817-30.
82. Park, M., et al., *Recycling endosomes supply AMPA receptors for LTP.* Science, 2004. **305**(5692): p. 1972-5.
83. Keith, D.J., et al., *Palmitoylation of A-kinase anchoring protein 79/150 regulates dendritic endosomal targeting and synaptic plasticity mechanisms.* J Neurosci, 2012. **32**(21): p. 7119-36.
84. Tavalin, S.J., et al., *Regulation of GluR1 by the A-kinase anchoring protein 79 (AKAP79) signaling complex shares properties with long-term depression.* J Neurosci, 2002. **22**(8): p. 3044-51.
85. Smith, K.E., E.S. Gibson, and M.L. Dell'Acqua, *cAMP-dependent protein kinase postsynaptic localization regulated by NMDA receptor activation through translocation of an A-kinase anchoring protein scaffold protein.* J Neurosci, 2006. **26**(9): p. 2391-402.
86. Jurado, S., V. Biou, and R.C. Malenka, *A calcineurin/AKAP complex is required for NMDA receptor-dependent long-term depression.* Nat Neurosci, 2010. **13**(9): p. 1053-5.
87. Woolfrey, K.M., J.L. Sanderson, and M.L. Dell'Acqua, *The palmitoyl acyltransferase DHHC2 regulates recycling endosome exocytosis and synaptic potentiation through palmitoylation of AKAP79/150.* J Neurosci, 2015. **35**(2): p. 442-56.
88. Hayashi, T., G. Rumbaugh, and R.L. Huganir, *Differential regulation of AMPA receptor subunit trafficking by palmitoylation of two distinct sites.* Neuron, 2005. **47**(5): p. 709-23.
89. Brigidi, G.S., et al., *Palmitoylation of delta-catenin by DHHC5 mediates activity-induced synapse plasticity.* Nat Neurosci, 2014. **17**(4): p. 522-32.
90. Salaun, C., et al., *The C-terminal domain of zDHHC2 contains distinct sorting signals that regulate intracellular localisation in neurons and neuroendocrine cells.* Mol Cell Neurosci, 2017. **85**: p. 235-246.
91. Siddoway, B., et al., *Synaptic activity bidirectionally regulates a novel sequence-specific S-Q phosphoproteome in neurons.* J Neurochem, 2014. **128**(6): p. 841-51.
92. Lundby, A., et al., *In vivo phosphoproteomics analysis reveals the cardiac targets of beta-adrenergic receptor signaling.* Sci Signal, 2013. **6**(278): p. rs11.
93. Lievens, P.M., et al., *ZDHHC3 Tyrosine Phosphorylation Regulates Neural Cell Adhesion Molecule Palmitoylation.* Mol Cell Biol, 2016. **36**(17): p. 2208-25.
94. Traub, L.M. and J.S. Bonifacino, *Cargo recognition in clathrin-mediated endocytosis.* Cold Spring Harb Perspect Biol, 2013. **5**(11): p. a016790.
95. Kim, E. and M. Sheng, *PDZ domain proteins of synapses.* Nat Rev Neurosci, 2004. **5**(10): p. 771-81.
96. Hata, Y., H. Nakanishi, and Y. Takai, *Synaptic PDZ domain-containing proteins.* Neurosci Res, 1998. **32**(1): p. 1-7.
97. Feng, W. and M. Zhang, *Organization and dynamics of PDZ-domain-related supramodules in the postsynaptic density.* Nat Rev Neurosci, 2009. **10**(2): p. 87-99.
98. Yuan, L., et al., *delta-Catenin Regulates Spine Architecture via Cadherin and PDZ-dependent Interactions.* J Biol Chem, 2015. **290**(17): p. 10947-57.

99. Lakkaraju, A.K., et al., *Palmitoylated calnexin is a key component of the ribosome-translocon complex.* EMBO J, 2012. **31**(7): p. 1823-35.
100. Fairbank, M., et al., *RING finger palmitoylation of the endoplasmic reticulum Gp78 E3 ubiquitin ligase.* FEBS Lett, 2012. **586**(16): p. 2488-93.
101. Fredericks, G.J., et al., *Stable expression and function of the inositol 1,4,5-triphosphate receptor requires palmitoylation by a DHHC6/selenoprotein K complex.* Proc Natl Acad Sci U S A, 2014. **111**(46): p. 16478-83.
102. Abrami, L., et al., *Palmitoylation and ubiquitination regulate exit of the Wnt signaling protein LRP6 from the endoplasmic reticulum.* Proc Natl Acad Sci U S A, 2008. **105**(14): p. 5384-9.
103. Perrody, E., et al., *Ubiquitin-dependent folding of the Wnt signaling coreceptor LRP6.* Elife, 2016. **5**.
104. Mitchell, D.A., et al., *Mutations in the X-linked intellectual disability gene, zDHHC9, alter autopalmitoylation activity by distinct mechanisms.* J Biol Chem, 2014. **289**(26): p. 18582-92.
105. Tzschach, A., et al., *Next-generation sequencing in X-linked intellectual disability.* Eur J Hum Genet, 2015. **23**(11): p. 1513-8.
106. Han, J.Y., et al., *The first patient with sporadic X-linked intellectual disability with de novo ZDHHC9 mutation identified by targeted next-generation sequencing.* Eur J Med Genet, 2017. **60**(10): p. 499-503.
107. Baker, K., et al., *Epilepsy, cognitive deficits and neuroanatomy in males with ZDHHC9 mutations.* Ann Clin Transl Neurol, 2015. **2**(5): p. 559-69.
108. Shimell, J.J., et al., *The X-Linked Intellectual Disability Gene Zdhhc9 Is Essential for Dendrite Outgrowth and Inhibitory Synapse Formation.* Cell Rep, 2019. **29**(8): p. 2422-2437 e8.
109. Fallin, M.D., et al., *Genomewide linkage scan for bipolar-disorder susceptibility loci among Ashkenazi Jewish families.* Am J Hum Genet, 2004. **75**(2): p. 204-19.
110. Schizophrenia Working Group of the Psychiatric Genomics, C., *Biological insights from 108 schizophrenia-associated genetic loci.* Nature, 2014. **511**(7510): p. 421-7.
111. Fromer, M., et al., *De novo mutations in schizophrenia implicate synaptic networks.* Nature, 2014. **506**(7487): p. 179-84.
112. Mukai, J., et al., *Molecular substrates of altered axonal growth and brain connectivity in a mouse model of schizophrenia.* Neuron, 2015. **86**(3): p. 680-95.
113. Pinner, A.L., et al., *Decreased protein S-palmitoylation in dorsolateral prefrontal cortex in schizophrenia.* Schizophr Res, 2016. **177**(1-3): p. 78-87.
114. Zareba-Koziol, M., et al., *Insights Into Protein S-Palmitoylation in Synaptic Plasticity and Neurological Disorders: Potential and Limitations of Methods for Detection and Analysis.* Front Mol Neurosci, 2018. **11**: p. 175.
115. Bouza, A.A. and L.L. Isom, *Voltage-Gated Sodium Channel beta Subunits and Their Related Diseases.* Handb Exp Pharmacol, 2018. **246**: p. 423-450.
116. Nelson, A.D., *Convergent mechanisms for two neurodevelopmental disorder genes, ANK2 and SCN2A*.
117. Spratt, P.W.E., et al., *The Autism-Associated Gene Scn2a Contributes to Dendritic Excitability and Synaptic Function in the Prefrontal Cortex.* Neuron, 2019. **103**(4): p. 673-685 e5.

118. O'Malley, H.A. and L.L. Isom, *Sodium channel beta subunits: emerging targets in channelopathies.* Annu Rev Physiol, 2015. **77**: p. 481-504.
119. Hull, J.M. and L.L. Isom, *Voltage-gated sodium channel beta subunits: The power outside the pore in brain development and disease.* Neuropharmacology, 2018. **132**: p. 43-57.
120. Isom, L.L., et al., *Primary structure and functional expression of the beta 1 subunit of the rat brain sodium channel.* Science, 1992. **256**(5058): p. 839-42.
121. Isom, L.L., et al., *Structure and function of the beta 2 subunit of brain sodium channels, a transmembrane glycoprotein with a CAM motif.* Cell, 1995. **83**(3): p. 433-42.
122. Brackenbury, W.J., et al., *Abnormal neuronal patterning occurs during early postnatal brain development of Scn1b-null mice and precedes hyperexcitability.* Proc Natl Acad Sci U S A, 2013. **110**(3): p. 1089-94.
123. Brackenbury, W.J., et al., *Functional reciprocity between Na+ channel Nav1.6 and beta1 subunits in the coordinated regulation of excitability and neurite outgrowth.* Proc Natl Acad Sci U S A, 2010. **107**(5): p. 2283-8.
124. Brackenbury, W.J., et al., *Voltage-gated Na+ channel beta1 subunit-mediated neurite outgrowth requires Fyn kinase and contributes to postnatal CNS development in vivo.* J Neurosci, 2008. **28**(12): p. 3246-56.
125. Malhotra, J.D., et al., *Sodium channel beta subunits mediate homophilic cell adhesion and recruit ankyrin to points of cell-cell contact.* J Biol Chem, 2000. **275**(15): p. 11383-8.
126. Malhotra, J.D., et al., *Tyrosine-phosphorylated and nonphosphorylated sodium channel beta1 subunits are differentially localized in cardiac myocytes.* J Biol Chem, 2004. **279**(39): p. 40748-54.
127. Marionneau, C., et al., *The sodium channel accessory subunit Navbeta1 regulates neuronal excitability through modulation of repolarizing voltage-gated K(+) channels.* J Neurosci, 2012. **32**(17): p. 5716-27.
128. Veeraraghavan, R., et al., *The adhesion function of the sodium channel beta subunit (beta1) contributes to cardiac action potential propagation.* Elife, 2018. **7**.
129. Malhotra, J.D., et al., *Structural requirements for interaction of sodium channel beta 1 subunits with ankyrin.* J Biol Chem, 2002. **277**(29): p. 26681-8.
130. McEwen, D.P., et al., *Sodium channel beta1 subunit-mediated modulation of Nav1.2 currents and cell surface density is dependent on interactions with contactin and ankyrin.* J Biol Chem, 2004. **279**(16): p. 16044-9.
131. Xiao, Z.C., et al., *Tenascin-R is a functional modulator of sodium channel beta subunits.* J Biol Chem, 1999. **274**(37): p. 26511-7.
132. McEwen, D.P. and L.L. Isom, *Heterophilic interactions of sodium channel beta1 subunits with axonal and glial cell adhesion molecules.* J Biol Chem, 2004. **279**(50): p. 52744-52.
133. Aeby, A., et al., *SCN1B-linked early infantile developmental and epileptic encephalopathy.* Ann Clin Transl Neurol, 2019. **6**(12): p. 2354-2367.
134. Chen, C., et al., *Mice lacking sodium channel beta1 subunits display defects in neuronal excitability, sodium channel expression, and nodal architecture.* J Neurosci, 2004. **24**(16): p. 4030-42.
135. Lin, X., et al., *Scn1b deletion leads to increased tetrodotoxin-sensitive sodium current, altered intracellular calcium homeostasis and arrhythmias in murine hearts.* J Physiol, 2015. **593**(6): p. 1389-407.
136. Lopez-Santiago, L.F., et al., *Sodium channel Scn1b null mice exhibit prolonged QT and RR intervals.* J Mol Cell Cardiol, 2007. **43**(5): p. 636-47.

137. Gray, B., et al., *Lack of genotype-phenotype correlation in Brugada Syndrome and Sudden Arrhythmic Death Syndrome families with reported pathogenic SCN1B variants.* Heart Rhythm, 2018. **15**(7): p. 1051-1057.
138. Ricci, M.T., et al., *SCN1B gene variants in Brugada Syndrome: a study of 145 SCN5A-negative patients.* Sci Rep, 2014. **4**: p. 6470.
139. Watanabe, H., et al., *Sodium channel beta1 subunit mutations associated with Brugada syndrome and cardiac conduction disease in humans.* J Clin Invest, 2008. **118**(6): p. 2260-8.
140. Watanabe, H., et al., *Mutations in sodium channel beta1- and beta2-subunits associated with atrial fibrillation.* Circ Arrhythm Electrophysiol, 2009. **2**(3): p. 268-75.
141. Olesen, M.S., et al., *SCN1Bb R214Q found in 3 patients: 1 with Brugada syndrome and 2 with lone atrial fibrillation.* Heart Rhythm, 2012. **9**(5): p. 770-3.
142. Wong, H.K., et al., *beta Subunits of voltage-gated sodium channels are novel substrates of beta-site amyloid precursor protein-cleaving enzyme (BACE1) and gamma-secretase.* J Biol Chem, 2005. **280**(24): p. 23009-17.
143. Bouza, A.A., Nnamdi Edokobi, Alexa M. Pinsky, James Offord, Lin Piao, Anatoli N. Lopatin, Luis F. Lopez-Santiago, Lori L. Isom *Voltage-gated sodium channel B1 subunits mediate excitation-transcription coupling through regulated intramembrane proteolysis* In Review, 2020.
144. Patino, G.A., et al., *Voltage-gated Na+ channel beta1B: a secreted cell adhesion molecule involved in human epilepsy.* J Neurosci, 2011. **31**(41): p. 14577-91.
145. Davis, T.H., C. Chen, and L.L. Isom, *Sodium channel beta1 subunits promote neurite outgrowth in cerebellar granule neurons.* J Biol Chem, 2004. **279**(49): p. 51424-32.
146. Haapasalo, A. and D.M. Kovacs, *The many substrates of presenilin/gamma-secretase.* J Alzheimers Dis, 2011. **25**(1): p. 3-28.
147. Brackenbury, W.J. and L.L. Isom, *Na Channel beta Subunits: Overachievers of the Ion Channel Family.* Front Pharmacol, 2011. **2**: p. 53.
148. Kim, D.Y., et al., *Presenilin/gamma-secretase-mediated cleavage of the voltage-gated sodium channel beta2-subunit regulates cell adhesion and migration.* J Biol Chem, 2005. **280**(24): p. 23251-61.
149. Bhattacharyya, R., C. Barren, and D.M. Kovacs, *Palmitoylation of amyloid precursor protein regulates amyloidogenic processing in lipid rafts.* J Neurosci, 2013. **33**(27): p. 11169-83.
150. Zhang, S., et al., *BACE1 Cleavage Site Selection Critical for Amyloidogenesis and Alzheimer's Pathogenesis.* J Neurosci, 2017. **37**(29): p. 6915-6925.
151. Cole, S.L. and R. Vassar, *The Alzheimer's disease beta-secretase enzyme, BACE1.* Mol Neurodegener, 2007. **2**: p. 22.
152. Forrester, M.T., et al., *Site-specific analysis of protein S-acylation by resin-assisted capture.* J Lipid Res, 2011. **52**(2): p. 393-8.
153. Giri, B., et al., *CXCL12-induced partitioning of flotillin-1 with lipid rafts plays a role in CXCR4 function.* Eur J Immunol, 2007. **37**(8): p. 2104-16.
154. Percher, A., et al., *Mass-tag labeling reveals site-specific and endogenous levels of protein S-fatty acylation.* Proc Natl Acad Sci U S A, 2016. **113**(16): p. 4302-7.
155. Bharadwaj, M. and O.A. Bizzozero, *Myelin P0 glycoprotein and a synthetic peptide containing the palmitoylation site are both autoacylated.* J Neurochem, 1995. **65**(4): p. 1805-15.

156. Kruger, L.C., et al., *beta1-C121W Is Down But Not Out: Epilepsy-Associated Scn1b-C121W Results in a Deleterious Gain-of-Function.* J Neurosci, 2016. **36**(23): p. 6213-24.
157. Pischedda, F., et al., *A cell surface biotinylation assay to reveal membrane-associated neuronal cues: Negr1 regulates dendritic arborization.* Mol Cell Proteomics, 2014. **13**(3): p. 733-48.
158. Levental, I., et al., *Palmitoylation regulates raft affinity for the majority of integral raft proteins.* Proc Natl Acad Sci U S A, 2010. **107**(51): p. 22050-4.
159. Calhoun, J.D. and L.L. Isom, *The role of non-pore-forming beta subunits in physiology and pathophysiology of voltage-gated sodium channels.* Handb Exp Pharmacol, 2014. **221**: p. 51-89.
160. Lemaillet, G., B. Walker, and S. Lambert, *Identification of a conserved ankyrin-binding motif in the family of sodium channel alpha subunits.* J Biol Chem, 2003. **278**(30): p. 27333-9.
161. Srinivasan, Y., M. Lewallen, and K.J. Angelides, *Mapping the binding site on ankyrin for the voltage-dependent sodium channel from brain.* J Biol Chem, 1992. **267**(11): p. 7483-9.
162. Xing, D., et al., *Expression of neonatal Nav1.5 in human brain astrocytoma and its effect on proliferation, invasion and apoptosis of astrocytoma cells.* Oncol Rep, 2014. **31**(6): p. 2692-700.
163. Wang, J., et al., *Molecular expression of multiple Nav1.5 splice variants in the frontal lobe of the human brain.* Int J Mol Med, 2018. **41**(2): p. 915-923.
164. Wang, J., et al., *Multiple Nav1.5 isoforms are functionally expressed in the brain and present distinct expression patterns compared with cardiac Nav1.5.* Mol Med Rep, 2017. **16**(1): p. 719-729.
165. Abriel, H., *Cardiac sodium channel Na(v)1.5 and interacting proteins: Physiology and pathophysiology.* J Mol Cell Cardiol, 2010. **48**(1): p. 2-11.
166. Patino, G.A., et al., *A functional null mutation of SCN1B in a patient with Dravet syndrome.* J Neurosci, 2009. **29**(34): p. 10764-78.
167. Reverter, M., et al., *Cholesterol transport from late endosomes to the Golgi regulates t-SNARE trafficking, assembly, and function.* Mol Biol Cell, 2011. **22**(21): p. 4108-23.
168. Bennett, V. and D.N. Lorenzo, *Spectrin- and ankyrin-based membrane domains and the evolution of vertebrates.* Curr Top Membr, 2013. **72**: p. 1-37.
169. Ayalon, G., et al., *An ankyrin-based mechanism for functional organization of dystrophin and dystroglycan.* Cell, 2008. **135**(7): p. 1189-200.
170. Ayalon, G., et al., *Ankyrin-B interactions with spectrin and dynactin-4 are required for dystrophin-based protection of skeletal muscle from exercise injury.* J Biol Chem, 2011. **286**(9): p. 7370-8.
171. Sucharski, H.C., et al., *Mechanisms and Alterations of Cardiac Ion Channels Leading to Disease: Role of Ankyrin-B in Cardiac Function.* Biomolecules, 2020. **10**(2).
172. Lorenzo, D.N., et al., *A PIK3C3-ankyrin-B-dynactin pathway promotes axonal growth and multiorganelle transport.* J Cell Biol, 2014. **207**(6): p. 735-52.
173. Lorenzo, D.N., *Cargo hold and delivery: Ankyrins, spectrins, and their functional patterning of neurons.* Cytoskeleton (Hoboken), 2020.
174. Lorenzo, D.N. and V. Bennett, *Cell-autonomous adiposity through increased cell surface GLUT4 due to ankyrin-B deficiency.* Proc Natl Acad Sci U S A, 2017. **114**(48): p. 12743-12748.

175. Yang, R., et al., *ANK2 autism mutation targeting giant ankyrin-B promotes axon branching and ectopic connectivity.* Proc Natl Acad Sci U S A, 2019. **116**(30): p. 15262-15271.
176. Galiano, M.R., et al., *A distal axonal cytoskeleton forms an intra-axonal boundary that controls axon initial segment assembly.* Cell, 2012. **149**(5): p. 1125-39.
177. Stessman, H.A., et al., *Targeted sequencing identifies 91 neurodevelopmental-disorder risk genes with autism and developmental-disability biases.* Nat Genet, 2017. **49**(4): p. 515-526.
178. Satterstrom, F.K., et al., *Large-Scale Exome Sequencing Study Implicates Both Developmental and Functional Changes in the Neurobiology of Autism.* Cell, 2020. **180**(3): p. 568-584 e23.
179. Sanders, S.J., et al., *Progress in Understanding and Treating SCN2A-Mediated Disorders.* Trends Neurosci, 2018. **41**(7): p. 442-456.
180. Sanders, S.J., et al., *Insights into Autism Spectrum Disorder Genomic Architecture and Biology from 71 Risk Loci.* Neuron, 2015. **87**(6): p. 1215-1233.
181. Ben-Shalom, R., et al., *Opposing Effects on NaV1.2 Function Underlie Differences Between SCN2A Variants Observed in Individuals With Autism Spectrum Disorder or Infantile Seizures.* Biol Psychiatry, 2017. **82**(3): p. 224-232.
182. Tseng, W.C., et al., *Giant ankyrin-G stabilizes somatodendritic GABAergic synapses through opposing endocytosis of GABAA receptors.* Proc Natl Acad Sci U S A, 2015. **112**(4): p. 1214-9.
183. Staufenbiel, M., *Ankyrin-bound fatty acid turns over rapidly at the erythrocyte plasma membrane.* Mol Cell Biol, 1987. **7**(8): p. 2981-4.
184. Mohler, P.J., A.O. Gramolini, and V. Bennett, *The ankyrin-B C-terminal domain determines activity of ankyrin-B/G chimeras in rescue of abnormal inositol 1,4,5-trisphosphate and ryanodine receptor distribution in ankyrin-B (-/-) neonatal cardiomyocytes.* J Biol Chem, 2002. **277**(12): p. 10599-607.
185. Bouza, A.A., et al., *Sodium channel beta1 subunits are post-translationally modified by tyrosine phosphorylation, S-palmitoylation, and regulated intramembrane proteolysis.* J Biol Chem, 2020. **295**(30): p. 10380-10393.
186. Verardi, R., et al., *Structural Basis for Substrate Recognition by the Ankyrin Repeat Domain of Human DHHC17 Palmitoyltransferase.* Structure, 2017. **25**(9): p. 1337-1347 e6.
187. Lemonidis, K., et al., *Peptide array-based screening reveals a large number of proteins interacting with the ankyrin-repeat domain of the zDHHC17 S-acyltransferase.* J Biol Chem, 2017. **292**(42): p. 17190-17202.
188. Locatelli, C., et al., *Identification of key features required for efficient S-acylation and plasma membrane targeting of sprouty-2.* J Cell Sci, 2020. **133**(21).
189. Niu, J., et al., *Coupled Control of Distal Axon Integrity and Somal Responses to Axonal Damage by the Palmitoyl Acyltransferase ZDHHC17.* Cell Rep, 2020. **33**(7): p. 108365.
190. Sanders, S.S., et al., *Sudden death due to paralysis and synaptic and behavioral deficits when Hip14/Zdhhc17 is deleted in adult mice.* BMC Biol, 2016. **14**(1): p. 108.
191. Jenkins, P.M., et al., *Giant ankyrin-G: a critical innovation in vertebrate evolution of fast and integrated neuronal signaling.* Proc Natl Acad Sci U S A, 2015. **112**(4): p. 957-64.
192. Butland, S.L., et al., *The palmitoyl acyltransferase HIP14 shares a high proportion of interactors with huntingtin: implications for a role in the pathogenesis of Huntington's disease.* Hum Mol Genet, 2014. **23**(15): p. 4142-60.

193. Yang, G. and M.S. Cynader, *Palmitoyl acyltransferase zD17 mediates neuronal responses in acute ischemic brain injury by regulating JNK activation in a signaling module.* J Neurosci, 2011. **31**(33): p. 11980-91.
194. Shi, W., et al., *ZDHHC17 promotes axon outgrowth by regulating TrkA-tubulin complex formation.* Mol Cell Neurosci, 2015. **68**: p. 194-202.
195. Philippe, J.M. and P.M. Jenkins, *Spatial organization of palmitoyl acyl transferases governs substrate localization and function.* Mol Membr Biol, 2019. **35**(1): p. 60-75.
196. He, M., W.C. Tseng, and V. Bennett, *A single divergent exon inhibits ankyrin-B association with the plasma membrane.* J Biol Chem, 2013. **288**(21): p. 14769-79.
197. Chang, K.J., et al., *Glial ankyrins facilitate paranodal axoglial junction assembly.* Nat Neurosci, 2014. **17**(12): p. 1673-81.
198. Nelson, A.D., et al., *Ankyrin-G regulates forebrain connectivity and network synchronization via interaction with GABARAP*. Mol Psychiatry, 2018.
199. Brody, M.J., et al., *Dissection of Thrombospondin-4 Domains Involved in Intracellular Adaptive Endoplasmic Reticulum Stress-Responsive Signaling.* Mol Cell Biol, 2016. **36**(1): p. 2-12.
200. Brody, M.J., et al., *Defective Flux of Thrombospondin-4 through the Secretory Pathway Impairs Cardiomyocyte Membrane Stability and Causes Cardiomyopathy.* Mol Cell Biol, 2018. **38**(14).
201. Davis, J., et al., *MBNL1-mediated regulation of differentiation RNAs promotes myofibroblast transformation and the fibrotic response.* Nat Commun, 2015. **6**: p. 10084.
202. Schindelin, J., et al., *Fiji: an open-source platform for biological-image analysis.* Nat Methods, 2012. **9**(7): p. 676-82.
203. Zala, D., et al., *Vesicular glycolysis provides on-board energy for fast axonal transport.* Cell, 2013. **152**(3): p. 479-91.
204. Bouza, A.A., et al., *Sodium channel beta1 subunits participate in regulated intramembrane proteolysis-excitation coupling.* JCI Insight, 2021. **6**(3).
205. Cai, X. and Y. Zhang, *Molecular evolution of the ankyrin gene family.* Mol Biol Evol, 2006. **23**(3): p. 550-8.
206. Bennett, V. and J. Healy, *Membrane domains based on ankyrin and spectrin associated with cell-cell interactions.* Cold Spring Harb Perspect Biol, 2009. **1**(6): p. a003012.
207. Davis, L., et al., *Localization and structure of the ankyrin-binding site on beta2-spectrin.* J Biol Chem, 2009. **284**(11): p. 6982-7.
208. Wang, C., et al., *Structure of the ZU5-ZU5-UPA-DD tandem of ankyrin-B reveals interaction surfaces necessary for ankyrin function.* Proc Natl Acad Sci U S A, 2012. **109**(13): p. 4822-7.
209. Nelson, A.D. and P.M. Jenkins, *Axonal Membranes and Their Domains: Assembly and Function of the Axon Initial Segment and Node of Ranvier.* Front Cell Neurosci, 2017. **11**: p. 136.
210. Mohler, P.J., et al., *Isoform specificity among ankyrins. An amphipathic alpha-helix in the divergent regulatory domain of ankyrin-b interacts with the molecular co-chaperone Hdj1/Hsp40.* J Biol Chem, 2004. **279**(24): p. 25798-804.
211. Smith, K.R., et al., *Psychiatric risk factor ANK3/ankyrin-G nanodomains regulate the structure and function of glutamatergic synapses.* Neuron, 2014. **84**(2): p. 399-415.

212. Collura, K.M., et al., *The palmitoyl acyltransferases ZDHHC5 and ZDHHC8 are uniquely present in DRG axons and control retrograde signaling via the Gp130/JAK/STAT3 pathway.* J Biol Chem, 2020. **295**(46): p. 15427-15437.
213. Xu, C., et al., *Sequence-specific recognition of a PxLPxI/L motif by an ankyrin repeat tumbler lock.* Sci Signal, 2012. **5**(226): p. ra39.
214. Boncompain, G., et al., *Synchronization of secretory protein traffic in populations of cells.* Nat Methods, 2012. **9**(5): p. 493-8.
215. Gok C, M.A., Gao X, Kerekes Z, Plain F, Kuo C-Wen, Robertson AD, Fraser NJ, Fuller W, *Insights into the Molecular Basis of the Palmitoylation and Depalmitoylation of NCX1*. Cell Calcium, 2021.
216. Martin, B.R., et al., *Global profiling of dynamic protein palmitoylation.* Nat Methods, 2011. **9**(1): p. 84-9.
217. Lord, C.C., G. Thomas, and J.M. Brown, *Mammalian alpha beta hydrolase domain (ABHD) proteins: Lipid metabolizing enzymes at the interface of cell signaling and energy metabolism.* Biochim Biophys Acta, 2013. **1831**(4): p. 792-802.
218. Yokoi, N., et al., *Identification of PSD-95 Depalmitoylating Enzymes.* J Neurosci, 2016. **36**(24): p. 6431-44.
219. Nelson, A.D., *Understanding the Role of Ankyrin-G in Synaptic Biology*, in *Pharmacology*. 2019, University of Michigan. p. 179.
220. Nestor, M.W. and D.A. Hoffman, *Aberrant dendritic excitability: a common pathophysiology in CNS disorders affecting memory?* Mol Neurobiol, 2012. **45**(3): p. 478-87.
221. Kamiya, K., et al., *A nonsense mutation of the sodium channel gene SCN2A in a patient with intractable epilepsy and mental decline.* J Neurosci, 2004. **24**(11): p. 2690-8.
222. Buxbaum, J.D., et al., *The autism sequencing consortium: large-scale, high-throughput sequencing in autism spectrum disorders.* Neuron, 2012. **76**(6): p. 1052-6.
223. De Rubeis, S., et al., *Synaptic, transcriptional and chromatin genes disrupted in autism.* Nature, 2014. **515**(7526): p. 209-15.
224. Sanders, S.J., et al., *De novo mutations revealed by whole-exome sequencing are strongly associated with autism.* Nature, 2012. **485**(7397): p. 237-41.
225. Weber, P., et al., *Electrostatic anchoring precedes stable membrane attachment of SNAP25/SNAP23 to the plasma membrane.* Elife, 2017. **6**.
226. Pei, Z., et al., *Cardiac sodium channel palmitoylation regulates channel availability and myocyte excitability with implications for arrhythmia generation.* Nat Commun, 2016. **7**: p. 12035.
227. Kang, R., et al., *Neural palmitoyl-proteomics reveals dynamic synaptic palmitoylation.* Nature, 2008. **456**(7224): p. 904-9.
228. Schmidt, J.W. and W.A. Catterall, *Palmitylation, sulfation, and glycosylation of the alpha subunit of the sodium channel. Role of post-translational modifications in channel assembly.* J Biol Chem, 1987. **262**(28): p. 13713-23.
229. Bosmans, F., M. Milescu, and K.J. Swartz, *Palmitoylation influences the function and pharmacology of sodium channels.* Proc Natl Acad Sci U S A, 2011. **108**(50): p. 20213-8.
230. Brechet, A., et al., *Protein kinase CK2 contributes to the organization of sodium channels in axonal membranes by regulating their interactions with ankyrin G.* J Cell Biol, 2008. **183**(6): p. 1101-14.